Effectiveness of Ion Exchange, Reverse Osmosis and Coagulation and filtration in the removal of Radioactivity from Acid Mine Drainage

TC Dlamini

orcid.org 0000-0002-0172-904

Thesis submitted in fulfilment of the requirements for the degree *Doctor of Philosophy in Physics* at the North-West University

Promoter: Prof VM Tshivhase

Co-promoter: Dr PP Maleka

Graduation: April 2019

Student number: 23915919

Declaration

I hereby declare that this research thesis entitled, “Effectiveness of Ion Exchange, Reverse Osmosis and Coagulation and filtration in the removal of Radioactivity from Acid Mine Drainage” is my own work, carried out at the Centre for Applied Radiation Science and Technology (CARST) at the North-West University, South Africa, between August 2015 and June 2018 under the guidance and supervision of Prof. V.M. Tshivhase and Dr PP Maleka for the degree of Doctor of Philosophy in Physics. This thesis has not been submitted for any degree at any other university or institution before, and all the sources of data used, have been fully indicated and duly acknowledged by means of complete references.

Full name: Thulani Criswell Dlamini Date: June 2018

Signed: 

Key words

Gross alpha/beta activity; Acid Mine Drainage; mine waste treatment; Witwatersrand basin; radioactivity; naturally occurring radioactive materials; radionuclide speciation

Acknowledgements

I would like to thank God for being with me throughout the research. I take this opportunity to express my sincere gratitude to the supervisors of this study Prof. VM Tshivhase and Dr PP Maleka for their immense support and guidance, without their guidance and supervision this work would not have been completed. I thank my family for their emotional and financial support during this research work.

The financial assistance of the National Research Foundation (NRF) towards this research is hereby acknowledged by the corresponding student author. Opinions expressed and conclusions arrived at, are those of the author and are not necessarily to be attributed to the NRF.

I would also like to express my gratitude to the Centre for Applied Radiation Science and Technology, North-West University, for allowing me the opportunity to do my research within their facilities and the personnel, both students and stuff for their assistance. My thanks also go out to Mr M Mashaba for his assistance during gross alpha and gross beta analysis. The Eco-Analytica Laboratory of the North-West University, is also acknowledged for their assistance in the ICP-MS and anion analysis of samples. Purolite is also acknowledged for supplying the ion exchange resins used in this study.

Abstract

The aim of the study is to assess the effectiveness of ion exchange, reverse osmosis and coagulation filtration, three of the best available treatment methods, in the removal of radioactivity and heavy metals from Acid Mine Drainage (AMD) and make recommendations on the most appropriate method among the three that South Africa can employ in the treatment of AMD.

Mine shaft AMD samples were collected from an AMD pumping station in the central basin of the Witwatersrand region. Another set of samples were collected from an AMD dam that has developed from abandoned gold mining operations. Temperature, pH, conductivity and Total Dissolved Solids were measured in the field during sampling. The samples were then analyzed for gross alpha and gross beta activity, metal concentration, anions and radionuclides. After analysis the samples were then treated using ion exchange, reverse osmosis and coagulation & filtration. Treated samples were then analyzed for gross alpha and gross beta activity and metal concentration.

For treated mine shaft AMD the average gross alpha activity concentrations were 0.895±0.347 Bq/L, 0.045±0.035 Bq/L and 0.310±0.066 Bq/L for reverse osmosis, ion exchange and coagulation & filtration respectively. The gross beta activity concentrations were 0.083±0.004 Bq/L, 0.116±0.071 Bq/L and 0.696±0.105 Bq/L for reverse osmosis, ion exchange and coagulation & filtration respectively. The average gross alpha removal rates for reverse osmosis, ion exchange and coagulation & filtration were 77.87%, 98.03% and 87.80% respectively. The average gross beta removal rates for reverse osmosis, ion exchange and coagulation & filtration were 95.58%, 94.68% and 76.86% respectively.

For treated surface AMD the average gross alpha activity concentrations were 2.346±0.347 Bq/L, 0.065±0.0375 Bq/L and 2.717±0.124 Bq/L for reverse osmosis, ion exchange and coagulation & filtration respectively. The gross beta activity concentrations were 0.186±0.014 Bq/L, 3.798±0.212 Bq/L and 5.847±0.267 Bq/L for reverse osmosis, ion exchange and coagulation & filtration respectively. The average gross alpha removal rates for reverse osmosis, ion exchange and coagulation & filtration were 96.24%, 99.90% and 95.63% respectively. The average gross beta removal rates for reverse osmosis, ion exchange and coagulation & filtration were

99.68%, 93.84% and 89.99% respectively. The World Health Organization guidance limits for gross alpha and gross beta activity in portable water are 0.5 Bq/L and 1 Bq/L respectively. According to the findings of this study ion exchange is the best method for the removal of both radioactivity and heavy metals from AMD, producing small amounts of solid waste and high radioactivity and metal removal rates.

Table of Contents

List of Figures

List of Tables

List of Annexures

List of Abbreviations

AMD	Acid Mine Drainage
BAS	Basis Species
CARST	Centre for Applied Radiation Science and Technology
CGS	Committee for GeoScience
DSA	Digital Spectrum Analyser
DSP	Digital Spectrum Processing
ERPM	East Rand Propriety Mines
GEM	Generalized Equilibrium Modelling
HPGe	High Purity Germanium
IAEA	International Atomic Energy Agency
ICP-MS	Inductively Coupled Plasma Mass Spectroscopy
ICRP	International Commission of Radiological Protection
JESS	Joint Expert Speciation System
JHT	JESS Thermodynamic Database
LabSOCS	Laboratory Sourceless Object Calibration Software
LLD	Lower Limit of Detection
LSC	Liquid Scintillation Counting
MBU	Mass Balance Units
MCA	Multi-channel Analyser
NNR	National Nuclear Regulator
NORM	Naturally Occurring Radioactive Material
PMT	Photo Multiplier Tube
PSA	Pulse Shape Analyser
QED	Quasi Equilibrium Determination
SPQ(E)	Spectral Quench Parameter of the External standard
SUB	Sub-database
TDS	Total Dissolved Solids
TFC	Thin-film Composite
USEPA	United States Environmental Protection Agency
WHO	World Health Organisation
WRC	Water Research Commission

Chapter 1: Introduction

1.1 Background literature

South Africa has been a mining country for over a century and even though the minerals being mined have changed in quantities over that period, mining is still a major part of the South African economy. Gold mining has been the major mining activity in South Africa, especially in the Witwatersrand Basin. Gold mining began in the general area of Johannesburg 1886 (Werdmüller, 1986). The gold occurred in 1 to 2 m thick tabular conglomerate layers of the Witwatersrand Super-group, which extends in an east–west direction over a strike length of about 45 km (Naicker et al., 2003). Mining activities led to the formation of a large conurbation centred on Johannesburg, which as of 2011 holds a population of 4.3 Million people (Statistics SA, 2016).

In the beginning of the mining operations the mercury amalgam, method was used for the extraction of Gold. As the mining operation continued over time, deeper ores were mined. These deeper ores were un-oxidized and contained pyrite (FeS_2), which made the mercury amalgam method unsuitable for extraction. At about this time, the MacArthur-Forrest process of gold extraction, which used cyanide, was developed and successfully applied to the deeper un-oxidized Witwatersrand ores. This method of extraction started being used during the 1890s. Mining operations in the Johannesburg area continued until the early 1960s, reaching final depths of about 2500m below the surface. At this depths, the concentration of gold was usually low and therefore it became uneconomical to continue with the mining operations (Naicker et al., 2003).

The Witwatersrand conglomerates consist of quartz pebbles of about 1–3 cm in diameter, normally occurring in a matrix of quartz sand. This quartz matrix normally contains about 3% pyrite and smaller amounts of a wide variety of other sulphide and oxide minerals, in addition to gold. According to Feather and Koen (1975) at least 70 different ore minerals have been identified in the conglomerates the most abundant of which are uraninite (UO_2), brannerite ($UO_3Ti_2O_4$), arsenopyrite (FeAsS), cobaltite (CoAsS), galena (PbS), pyrrhotite (FeS), gersdofite (NiAsS) and chromite ($FeCr_2O_4$).

During the mining operations, ore mined underground was brought to the surface, where it was milled to a fine sand, during and after which it was exposed to a film of

mercury spread on copper plates (Feather and Koen, 1975). To recover the gold, these plates would be removed after a specific processed volume and the mercury-gold amalgam would be removed and distilled to recover the gold. All the tailings were then removed from the extraction plant to designated areas of disposal. These places were called mine dumps. For the cyanide process the ore had to be finer than in the mercury amalgam method. After the fine milling, the ore was then mixed with a solution containing cyanide which selectively dissolved the gold. The pH of the chemical system needed to be controlled and therefore, lime was usually used for that purpose. The solution was then separated for further processing, while the tailings were pumped to large dumps, known as ‘‘slimes dumps’’. Both recovery processes are highly selective for gold; therefore the other minerals in the ore were never extracted and were disposed of in the tailings dumps.

Even though the methods were very selective, they didn’t extract all of the gold from the ore, with around 0.5 g/t remaining in the tailings (Naicker et al., 2003). Over time the methods of gold extraction have drastically improved and therefore it has become economically viable to reprocess the tailings from the early mining operations to recover some of the gold that was left behind. In the current operations there is usually a co-extraction of the gold with pyrite. Most of the tailings from these new operations were being dumped towards the south of the city of Johannesburg. Even though there have been some operations in other tailings dams, others have been virtually undisturbed ever since the early mining operations in the region. For decades these mine dumps have been exposed to oxygenated water in the form of rainwater, causing oxidation of the pyrite as well as other sulphide materials which were previously un-oxidized. The mine dumps, being just piles of sand have had the most oxidation due the high permeability and therefore most of these mine dumps are oxidized to greater depths. The slimes dams on the other hand are more compact resulting in lower permeability and therefore slower bulk oxidation rate (Marsden, 1986).

Uranium is a radioactive heavy element, with average natural background concentrations that range from <2 to 4 mg/kg (Turekian and Wedepohl, 1961). However, in the gold deposits of the Witwatersrand basin, uranium is enriched to levels of up to 1 000 mg/kg (0.1 %). Compared to uranium ores with grades of about 0.3 - 6 % (3 000 - > 60 000 mg/kg) mined in Canada and Australia, this is considered as low-grade ore and therefore not economically viable to mine outright (McLEAN, 1994,

Wilson and Anhaeusser, 1998). Due to the low grade, the uranium that occurred with the gold in the Witwatersrand basin was mined as a byproduct of the gold mining enterprise. This was a method that was used to offset some of the mining costs associated with the gold and therefore improve profits. The first uranium recovery plant was commissioned in 1952. The recovery of uranium during the gold mining went on until the early 1990s, at which point over 170 000 tons of U_3O_8 were recovered and sold (Ford, 1993, Wymer, 2001). Around the early 1980s the price of uranium in the world market steadily declined, reaching a point where it was no longer economically sound to recover uranium from the tailings anymore (Venter, 2001). This therefore led to a steady decline in the recovery of uranium from gold mining operations (Wendle, 1998, Wilson and Anhaeusser, 1998). Initially there were 26 mines, feeding 18 Uranium recovery plants, but only three mines and four plants were left by 1995, producing about 1 500 tons of U_3O_8 per year (Wilson and Anhaeusser, 1998). That figure was reduced further to less than 1 000 tons per year in 2001 (Venter, 2001).

The Witwatersrand ores contain much higher concentrations of uranium compared to the metal of interest which is gold, with gold-uranium ratios ranging from about 1:10 to 1:100. Without recovery therefore, there is a relatively large amount of uranium that is brought to the surface by gold mining. The uranium recovery process, which used sulfuric acid, was able to remove 90% of the uranium in the ore leaving only 10% in the mine dumps (Ford, 1993, Wendle, 1998). This means that mine dumps which were created from operations where there was no uranium recovery contain about 10 times more uranium than those from operations where uranium was recovered. There were some mines in which even during the period when uranium recovery was being done and was economically good, no recovery was being done. This was due to the fact that in some of the mines, the concentration was too low for any economic value and therefore the recovery was never done. Nowadays there are therefore two classifications of mine dumps in terms of uranium concentrations, those which were leached and those which were never leached. The ones that were never leached are therefore expected to have elevated concentrations of uranium than those which were leached. Around 2002, there was still a lot of uranium being disposed into mine dumps (about 6 000 tons of uranium per year) from gold mining in South Africa (Winde and de Villiers, 2002).

Since the beginning of the mining operations in the Witwatersrand basin, more than six billion tons of tailings have been produced (Janisch, 1986, Robb and Robb, 1998, Robb et al., 1998, Wymer, 2001). The average uranium concentration in these tailings is about 100 mg/kg, translating to over 600 000 tons of uranium oxide being exposed to the open environment. This estimation doesn't even take into account the amount of uranium in slimes dams, which contain even higher concentrations of uranium that the mine dumps (Winde and de Villiers, 2002). Mine dumps and slimes dumps cover an estimated surface area in the Witwatersrand of about 400 km². This value just go to show the extent of environmental scare that gold mining has left in the region and the scale of rehabilitation work that still needs to be done (Robb and Robb, 1998).

Initially radioactive pollution from gold mining was never considered a problem because the amount of radiation and radioactive material were probably considered insignificant. From the inception of an independent regulatory body, the National Nuclear Regulator (NNR) in 1990, radiological hazards associated with mining operations were being regulated. In 1995 the Department of Water Affairs conducted country-wide surveys and identified several "hot spots" of radioactive water pollution (Winde et al., 2004). Guideline limits for radioactive pollution in water are expressed as radioactivity concentrations, measured as the number of nuclear disintegrations per second (Bq) in one liter of water (Bq/L). The effect that radiation has on the human body is expressed as an effective dose per year (mSv/year). These measurements can be related to the uranium mass concentration (g/L) (WHO, 2006). In terms of water quality, the uranium, radium and radon nuclides are of practical importance.

1.2 Motivation and problem statement

Transport of dissolved uranium from mine dumps and slimes dams is a major pathway for environmental contamination of stream water, groundwater and sediments (Hobbs and Cobbing, 2007). In contrast to erosion of uranium bearing particles, where uranium concentration in the sink is lowered by dilution into unpolluted matrix; solute transport is associated with chemical re-concentration of uranium in the environment. The mining voids that were left behind from mining are filling up with water and it is estimated that in the central groundwater basin in the Witwatersrand, the water level within the voids is rising at a rate of 12m per month (McCarthy, 2011). The level was projected to reach an environmental critical level mid-year 2012 and decanting was

estimated to start occurring in the central sections of Boksburg shortly after that period (Coetzee et al., 2010).

Studies have been conducted to monitor the amount of uranium in streams next to tailing dams and mine dumps. There have been studies in the physicochemical properties of acid mine water, hence the need for the rehabilitation of the mine water in the Gauteng region. The government needs to urgently put up the structures and plans to deal with acid mine drainage. East Rand Propriety Mines (ERPM) was the last company that has been pumping water from the tunnels but have stopped operating and now the acid mine water is rising rapidly and this requires remedial action (Coetzee et al., 2010, Van Tonder et al., 2008). The acid mine water is radioactive and the radioactivity levels will have to be reduced drastically as one of the remediation practices (Coetzee et al., 2006, Tutu et al., 2008). Even after the remediation processes, thorough tests must be done to ensure that the treated water is safe either for use or for release into the environment (Coetzee et al., 2010).

There is potential for water supply from the Witwatersrand goldfield alone, with an estimated 350 ML/day. This is 10% of the potable water supplied daily by Rand Water at a cost of R3/kL (R3 000/ML) to different municipalities for urban distribution in Gauteng and surrounding areas. This volume of water and the potential economic value that it represents is not just good for the environment, but also for the communities in terms of the potential for adequate water supply and also in an economic point of view, for job creation and other businesses associated with the treated mine water. One of the first entities to try and take advantage of this situation has been the Western Utilities Corporation (WUC), which has initiated the immediate construction of a mine water treatment plant (Turton, 2010) with a potential to produce industrial grade “process” water (60 ML/day) and potable water (15 ML/day).

Although approximately 38 WRC-funded projects have been completed on mine water, with another 16 continuing in 2010. These projects are focussed on specific research questions, ranging from the development of treatment technologies to the characteristics of mine dumps (Coetzee et al., 2010). Most of the studies that have been completed have not been specialist studies and therefore detailed knowledge into any aspect of the acid mine water is still lacking, such as the status of the geo-hydrological regime, the amount and range of contamination, preferential pathways

and modelling to predict long term migratory patterns. The treatment of AMD and the potential to generate valuable by-products from it has received the most attention of all WRC subject areas. Around 40 reports on this matter have been produced. A major benefit of by-product recovery is a reduction in the overall volume of sludge, as well as a reduction in the hazard rating of the sludge produced. Several WRC projects focussed on the treatment technologies available and the development of new technologies. Both international and national best practice guidelines exist for AMD treatment methods, and South African inventions and developments abound within those guidelines. Source identification, quantification and characterisation of mine related pollutants, and the assessment of environmental risks (seismic, subsidence**,** radiation, dust, noise, aesthetics and risky openings) have been identified by the CGS as some of the key research gaps in the study on AMD (Coetzee et al., 2010). Even if all the measures described to limit water ingress into mine voids and prevent pollution are taken, some water will be polluted and some AMD will be generated. This will need to be treated to a quality suitable for discharge or use.

None of the studies conducted so far concentrated on the radiological aspect of AMD, which is a specialist field of research. This study will fill in the knowledge gap in the concentration of the radionuclides in the acid mine drainage, the effectiveness of treatment methodologies in the removal of radionuclides and the potential impact on humans that can arise from use of treated water in terms of dose rates. The study will attempt to evaluate the best treatment method to be used in the removal of the radionuclides from AMD. If the water can be treated, it could be used domestically, subsidizing the cost of the treatment process. The study will answer questions about the best method for treatment, the cost of removing radionuclides from acid mine drainage, the dose rate of acid mine drainage and the dose rate of treated AMD. Because the recorded water qualities of the different basins vary so much, it is not possible to recommend one single treatment method suitable for all types of mine water. Mine water varies widely in terms of its pH, concentrations of metals, the concentration of sulphate and sulphate containing minerals. The treatment method to be used is very much determined by some of these characteristics, whose effect is also dependant on the method of treatment to be used (Coetzee et al., 2010, Coetzee et al., 2007). This study will look at the concentration of radionuclides in the acid mine drainage and also look at the chemical properties of the water. The decision on the

best method will be based on the cost of the method, the level of skill it requires, the waste streams produced and available waste disposal facilities.

1.3 Aim and Objectives of the study

The aim of the study is to assess the effectiveness of ion exchange, reverse osmosis and coagulation filtration, three of the best available treatment methods, in the removal of radioactivity and heavy metals from Acid Mine Drainage water and make recommendations on the most appropriate method among the three that South Africa can employ in the treatment of AMD.

The objectives of the study are to:

- measure physical and chemical parameters of AMD and investigate if there is a correlation between specific parameters and the concentration of metal contaminants,
- measure the activity concentration of NORM nuclides in untreated AMD water,
- measure gross alpha and gross beta counts in untreated AMD water,
- model the chemical speciation of uranium, thorium and radium in AMD under reducing and oxidizing conditions using Visual Minteq and Joint Expert Speciation System,
- treat AMD using ion exchange, Reverse Osmosis and Coagulation & filtration,
- evaluate the efficiency of heavy metal and radioactivity removal by the three methods of treatment.

Chapter 2: Literature Study

2.1 Water in Gauteng

Freshwater is considered as one of the limited resources in South Africa because of the seasonal distribution and unpredictability of rainfall and also the high population that depends on this resource (Department of Environmental Affairs and Tourism, 2008). In the water cycle surface water which is usually from rain seeps and infiltrates into underground water reservoirs. The underground water then interacts with surface water through springs which might form part of the water supply of a river system. Lower lying river valleys and wetlands are actually groundwater that breaks onto the surface through some fissures in the surface rock. The Gauteng province of South Africa lacks major water sources originating within the province, depending mainly on water originating from other provinces especially the Vaal River Catchment (Carden and Armitage, 2013).

The quality and quantity of available water in Gauteng is influenced by a number of factors. The demand for different types of water in terms of quality has a huge influence. An increase in industrial operations, including mining operations will lead to an increase in the need for industrial grade water (Dawson, 2008). Food processing industries will draw a lot on the portable water resources of the province. Domestic water will cause the largest draw in portable water resource which is also used for sanitation purposes in urban arears. Urban development also leads to an increased demand on different types of water quality. Growth in the population due to natural and migratory reasons will lead to increased pressure on the water resources. Agriculture is also one of the major activities in the province which draws a lot on the water resource. An increase in the water demand and therefore use within the province will lead to the generation of more liquid waste which will lead to the pollution of water bodies and the environment (Varis et al., 2006). Natural water channels will be modified to supply water for uses where it is needed. An example of this is the construction of dams and small water storage reservoirs along river channels especially for agriculture. The increase and misuse of water resources will also lead to the loss of wetlands. Mining activities in the province have produced a new pollution problem in the form of Acid Mine Drainage (AMD) (Adler et al., 2007). AMD has a hugely negative impact on the province's groundwater resources. About 11% of the

country's water is used in the Gauteng province. Most of this water (about 80%) is consumed by the urban sector, with about 9% being utilized by the mining sector and industrial operations. Agriculture, especially irrigation, consumes 6% of the province's water resource (Holtzhausen, 2006). Most of the formal and informal housing sectors have access to potable water and sanitation services (Holtzhausen, 2006). The Water Services National Information System (WSNIS) states that Johannesburg has the largest sanitary waste as well as waste water from portable water supply (Carden and Armitage, 2013). Mining activities in the region have had a huge influence on the supply, use and management of water sources in the province. Mining activities throughout history were not usually located next to a major supply of water. Therefore, as they developed, water had to be supplied from other locations. Formal and informal settlements also developed next to the different mining operations leading to increased demands on water supply as well as increased generation of sanitary waste. Other land uses also developed with the new communities including crop and stock farming both at a subsistence level and on a larger scale. Urbanisation and the associated migration of people into the region most likely led to a degradation in the water management practices especially at domestic levels which exerts pressure on water use management. Due to the increasing levels of unemployment in the country and the perception amongst the population that Johannesburg still offers a lot of job opportunities, the pressure has not decreased but increased over time and will most likely continue to increase.

2.2 Gold mining and Acid Mine Drainage

Acid mine drainage is associated mainly with gold and coal mining, where pyrite is oxidised due to bacterial action to produce sulphuric acid. Acid mine drainage is associated with increased salinity, reduced pH, increased metals concentration (Maree et al., 2006) and has a major, multidimensional impact on water resources. The National Water Act (1998), in Chapter 3, Part 4, deals with pollution prevention, particularly resulting from land-based activities, and accompanying regulations deal specifically with pollution of water resources due to mining activities (Winde et al., 2004).

Acid Mine Drainage (AMD) is produced when material that has sulphide is exposed to water and an oxidizing agent, usually oxygen. AMD is mainly observed in rocks that

have a lot of sulphide compounds (sulphide aggregates). Acid mine drainage occurs in nature but at a slower rate. Activities like mining increase the rate of AMD generation by exposing most of the sulphide aggregates to oxygen and water. Undisturbed rock material provides very little surface area for the oxidation of the sulphide aggregates. Certain bacteria that occur in nature do increase the rate of AMD formation by facilitating the breakdown of sulphide containing minerals (Akcil and Koldas, 2006). Acid mine drainage is also referred to as acid rock drainage (ARD). Most of the characteristics of AMD are determined by the properties of the local rock material as well as the abundance or lack of water and oxygen (Akcil and Koldas, 2006). Acid mine drainage usually has very low pH and generally a high concentration of heavy metals. Because of these characteristics, it can cause severe contamination of both surface and ground water as well as surrounding soils depending on the migratory patterns (Peppas et al., 2000).

The ore properties of a mine are dependent on the formation and geology of the mineral deposits. Different deposits were formed in different ways and therefore the compositions are different. The formation and chemistry of deposits are dependent on a number of climatic and physical factors (Blowes et al., 2003). Therefore, the severity of the problem of AMD varies widely from one mining region to another. Dealing with the issue of AMD must begin with recognition that there are AMD hazards at individual sites, and that they give rise to risks specific to that particular site. There are areas where mining has taken place and the issue of AMD is inevitable. In these areas the first step, even before the issue comes up, it is important to do a site specific research since not all AMD problems are the same (Johnson and Hallberg, 2005). In mining regions where AMD has yet to be formed, research must be conducted not only to avoid its formation but also to be ready to deal with it if it is finally formed. The site specific research will be able to inform mine planners and managers of means to reduce or eliminate the chances of AMD formation from their mining operations. It will also help them to device means of reducing the impact of AMD on humans and their environment (Morrissey, 2003).

There are many types of sulphide minerals. Iron sulphides are the main culprits in the formation of AMD but other metal sulphide minerals may also contribute to the production of AMD. Exposing these sulphide minerals to an oxidizing agent, usually oxygen in the air, and water, an acidic, sulphate rich drainage is formed. The level of

metal contamination associated with AMD is highly dependent on the chemistry of the ore material in terms of the different metals present as well as their concentration and the amount of sulphide mineral that was oxidized. There are a number of reactions that are responsible for the oxidation of the sulphide minerals leading to the formation of the acidic drainage. The primary components needed for acid generation are: (1) presence of sulphide minerals; (2) water or humid conditions; and (3) an oxidising agent, usually oxygen from the atmosphere or from chemical sources. As discussed already, certain bacteria play a major role in the formation of acid drainage and therefore any method that can be used to inhibit the activity of these bacteria can lead to a reduction in the rate of AMD formation (Akcil and Koldas, 2006).

Decant, which the uncontrolled discharge of contaminated mine water into the environment, is one of the most important environmental problems associated with abandoned mining operations around the world (Pulles et al., 2005). Widely known as acid mine drainage, it is responsible for expensive environmental and socio-economic impacts. South Africa has made a lot of progress in amending policy frameworks to address mine closure and the management of mine water as well as realising a change in the mining industry's practices to conform to new legislation and regulations. There are still a lot of weaknesses in the current management system. AMD is characterized by high levels of acidity, high salinity levels, high concentrations of sulphate, iron, aluminium and manganese, elevated levels of toxic heavy metals such as cadmium, cobalt, copper, molybdenum and zinc, and some naturally occurring radionuclides such as uranium and thorium. Due to the acidity, the mine water has a high ability to dissolve salts and mobilize previously immobile heavy metals from mine shafts as well as mine dumps. Acid mine drainage water is usually dark brown in colour due to the oxidation of iron(II), with pH values as low as 1.8 (Akcil and Koldas, 2006). AMD is responsible for surface and groundwater pollution as well as the degradation of soil quality, contamination of aquatic habitats and for facilitating the transportation of toxic heavy metals from mine workings to the immediate environment (Adler and Rascher, 2007). One of the most difficult things in dealing with AMD is the fact that it is very difficult to eliminate completely once the problem has started, it therefore requires constant control over decades which is expensive.

2.3 Radioactivity

Most of the radiation that is received by humans come from ^{238}U and ^{232}Th series and from ^{40}K which exist at different concentrations in the soil and the environment. The level of exposure to natural radiation is strongly dependant on the geology and geography of their particular area. To be more specific, the type of rock from which the soil of that area originates, will determine most of the radioactivity parameters of the soil (Momčilović et al., 2010).

Radionuclides are by definition nuclides that exhibit radioactivity (Berg, 2004). A nuclide is a distinct atom with a specific atomic number (number of protons) and atomic mass (number of protons and neutrons). A distinct nuclides is one that is able to exist for a measurable lifetime ($>10^{-10}$ s). Radioactive decay is a random occurrence whereby an unstable nuclide spontaneously disintegrates and is transformed into another nuclide which is more stable than itself. There might be one or more product nuclides, which might be radioactive or stable. Usually a nuclear decay is accompanied by one of the three following processes (Hu et al., 2010):

- Emission of mass and energy from the nucleus;
- Nuclear capture or ejection of orbital electrons; or
- Nuclear fission.

There are three main classes of ionizing radiation resulting from the decay of unstable nuclides: alpha (α), beta (β), and gamma-ray (γ). Alpha decay is the emission of a helium nucleus (two protons and two neutrons) from the radioactive nuclide. The alpha particle relative to other nuclear emissions has a large mass and it is usually emitted with high energies. Beta decay is the emission of an electron (negative electron) from the nucleus. It is common in nuclides which are neutron rich, which in order to reduce the number of neutrons convert a neutron into a proton and an electron and the electron is ejected from the nucleus. The energy of the electron varies largely and in some cases it can be quite high. The beta particle has the mass of an electron and it is therefore lighter than an alpha particle. Gamma emissions are not nuclear decay events like alpha or beta decay, but they are the emission of excess energy after nuclear decay. The unstable nuclide resulting from α and β emissions gives off a γ photon and drops to a lower, more stable energy state (Aichinger et al., 2012).

There is natural radioactivity on earth which comes from two classes of radioactive nuclides. These are the primordial radionuclides, which are basically those radionuclides which have existed since the formation of the earth and cosmogenic radionuclides which are created through the interaction of cosmic waves with the earth's atmosphere. Radioactive decay is a random or spontaneous process via which unstable nuclei attempt to attain stability. Radionuclides undergo radioactive decay by emitting subatomic particles (α-particles and β-particles). After most radioactive decay events, the product or daughter nuclide is left in an excited energy state and usually releases that energy in the form of high energy photons (γ-rays and X-rays) (Eckerman et al., 2013, Tykva and Sabol, 1995). Radioactive decay is also called a nuclear transition. Radioactive decay occurs because nuclei are seeking more stability. Henri Becquerel is the man who discovered radioactivity back in 1896. He was actually performing research on phosphor materials, in which experiment he used a uranium salt. He couldn't expose the material to sunlight because of the weather but he decided to develop the film anyway. He discovered that the material was actually releasing ionizing photons spontaneously and that is how radioactivity was discovered (Eisenbud and Gesell, 1997). Decay series of the NORM nuclides (^{238}U and ^{232}Th) is shown in annexures 1 and 2, along with major gamma emission lines.

Radioactive equilibrium is a steady state that is reached between a radioactive nuclide and its daughter nuclide. It is usually used in a decay chain series to describe the radioactive decay rate of parent and daughter nuclides. It is generally a state in which radioactive elements in a decay chain series decay at some constant rate, that is, the rate of production equals the rate of decay (Prince, 1979). There are two states of radioactive equilibrium that can be established within a decay chain and these are secular equilibrium and transient equilibrium. The state of equilibrium reached is dependent on the half-lives of both the parent and the daughter nuclides. Secular equilibrium is a useful state of equilibrium in NORM studies due to its dominance in the three main natural decay series. Secular equilibrium occurs in a case where the half-life of the parent radionuclide is far greater than that of the daughter nuclides and therefore the rate of its decay becomes the limiting factor in the whole decay chain. That leads to all the daughter nuclides in the decay chain to decay at the same rate as the parent radionuclide (Burcham, 1973, Cember and Johnson, 2009, Faires and Boswell, 1981). Figure 1 shows the secular equilibrium between ^{226}Ra and its daughter

nuclide ^{222}Rn. The activity of daughter nuclei in a decay chain series is given by equation (1) (Lapp and Andrews, 1972, Lilley, 2013);

$$N_D(t) = N_P(t_0)\frac{\lambda_P}{\lambda_D - \lambda_P}(e^{-\lambda_P t} - e^{-\lambda_D t}). \quad (1)$$

In secular equilibrium this equation can be simplified into (Lapp and Andrews, 1972);

$$N_D(t) = N_P(t_0)\frac{\lambda_P}{\lambda_D}(1 - e^{-\lambda_D t}), \quad (2)$$

with time the $e^{-\lambda_D t}$ term will become negligible and the number of daughter nuclei will decay at a constant rate (Cember and Johnson, 2009, Lapp and Andrews, 1972, Turner, 2007a):

$$N_D(t) = N_P(t_0)\frac{\lambda_P}{\lambda_D}. \quad (3)$$

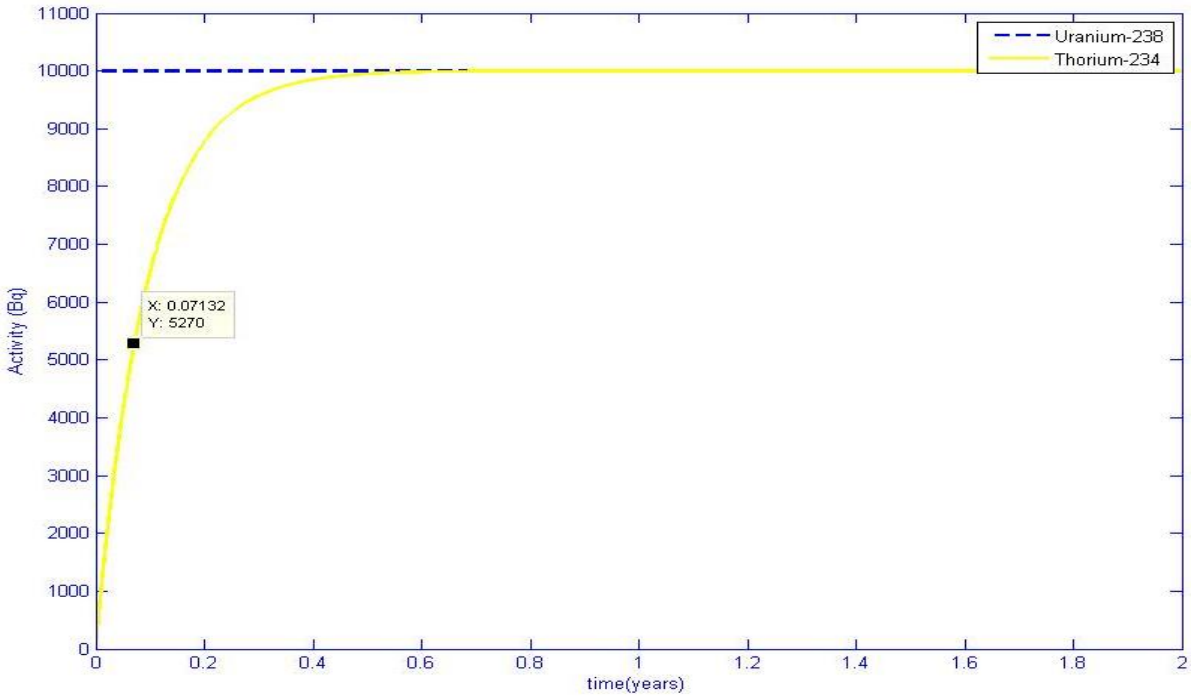

Figure 1: Secular equilibrium between a short-lived daughter and a long-lived parent nuclide.

At a state of secular equilibrium the daughter and parent have the same activities;

$$N_D\lambda_D = N_P\lambda_P. \quad (4)$$

2.4 Radioactivity detection

2.4.1 Interaction of photons with matter

Photons interact with matter in three different ways; photo-electric effect, Compton scattering and Pair production (Aichinger et al., 2012). Photons are extremely penetrating in matter and generally their energy is not degraded as they pass through matter, only their intensity is affected. The reason for such penetration is due to the zero mass and neutral charge of the photons. This means unlike charged particles which undergo electrostatic interactions with atoms, gamma photons only interact via absorption or scattering (Barrett et al., 1995).

2.4.1.1 Photo-electric effect

Photoelectric interactions usually occur with electrons that are firmly bound to the atom, that is, those with a relatively high binding energy. In the photoelectric interaction, a photon transfers all its energy to an atomic shell electron. The electron is ejected (ionization) from the atom by this energy and begins to pass through the surrounding matter. The electron will then lose all of its energy in a short distance from where it was ejected. The photon's energy is, therefore, deposited in the matter close to the site of the photoelectric interaction (Cohen-Tannoudji et al., 1998). Photoelectric interactions are most likely when the binding energy of the electron is slightly less than the energy of the incoming photon. If the binding energy is more than the energy of the photon, a photoelectric interaction cannot occur (Peterson, 2015).

The photon's energy is lost in two different ways during the interaction. Part of the photons energy is used to overcome the electrostatic forces which are keeping the electron in orbit around the atom. This is the most useful interaction for the detection of photons in gamma spectroscopy. The energy level of the electron involved in the photo-electric event can be a K-shell electron, depending on the energy of the incoming photon. Excitation of a K-shell- electron leaves the atom in an excited state and it may de-excite either via Auger electron emission or X-ray fluorescence. In Auger electron emission, the ‘hole’ left by the ejection of the K-electron is filled up by a higher energy level electron, and its place is also taken up in a similar way. As the electrons go to lower energy levels, they release their energy in the form of photons. These low energy photons have enough energy to excite a shell-electron, which will be ejected

from the atom. The result is a number of low energy electrons being ejected from the atom, and these electrons are called auger electrons. In X-ray fluorescence an outer shell electron fills the vacancy in an inner shell releasing characteristic X-rays (Knoll, 2000).

2.4.1.2 Compton Scattering

Compton scattering is an interaction of a photon with an almost unbound electron (Podgoršak, 2009). The photon scatters at an angle with the electron and it loses some of its energy. The amount of energy that is lost by the photon depends chiefly on the scattering angle. Since there is a change in photon direction, this type of interaction is classified as a scattering process. This is sometimes important not just as a method of energy loss but also from the aspect of secondary radiation production. The material within the primary gamma or X-ray beam becomes a secondary radiation source. The scattered radiation may cause interferences with equipment such as gamma detectors, by interfering with the low energy region of a spectrum. The photon continues on an altered path after the interaction with a different energy. The electron will gain kinetic energy equal to the amount of energy that is lost by the photon (Turner, 2007b). Figure 2 demonstrates the concept of Compton scattering;

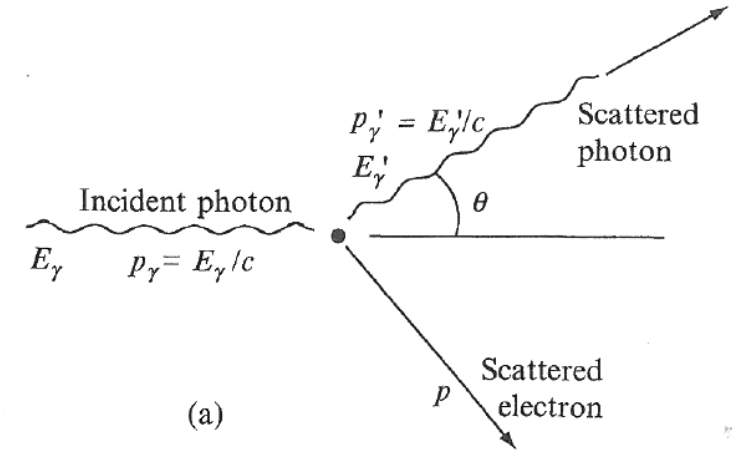

Figure 2: Compton scattering (Peterson, 2015).

Compton interactions can occur with low binding-energy electrons. All electrons in low-Z materials and the majority of electrons in high-Z materials have low binding energies. Compton scattering is mainly affected by the density of electrons in the attenuating material. If the electron density is high, the chances of a Compton scattering event is also high due to the increased probability of interaction. The number of atoms in a

gram of material, is almost similar, except for hydrogen. Unlike the photo-electric effect where the probability of an interaction is proportional to the atomic number, in Compton scattering it is only proportional to the physical density of the attenuating material. This is because the concentration of electrons in a given volume is proportional to the density, since the higher the mass you have per unit volume, the more electrons there will be per unit volume. Materials with a high proportion of hydrogen have slightly enhanced probabilities for Compton scattering due to the increased electron density. The probability of a Compton interaction is proportional to the photon energy and decreases with a decreasing photon energy. The rate of decrease in interaction probability is not as dramatic as in the photo-electric effect, where it varies as the inverse cube of the photon energy (Cember and Johnson, 2009, Knoll, 2010).

2.4.1.3 Pair Production

Pair production is an interaction between matter and a photon (Ting, 1972). There is a threshold energy for this kind of photon interaction to occur, as only photons with energies above 1022 keV can undergo this kind of interaction. In pair-production, the photon interacts with the nucleus. This high energy interaction converts the incoming photon into two electrons, a positive electron called a positron and a negative electron. The two particles have the same mass, which is equivalent to the rest energy of the electron (511 keV). If the incoming photon had more than the threshold energy, the excess energy is distributed between the positron and negatron equally as their kinetic energy. Therefore higher energy photons produce, energetic electron-positron pairs. The electron and positron each continue in different paths and interact with atomic electrons. The electron will eventually be absorbed by an atom and the positron finally combines with an orbital electron to produce two gamma photons of equal energy (Cember and Johnson, 2009, Knoll, 2000, Knoll, 2010).

A fundamental feature of nuclear processes is that the energy released is larger than the binding energies of atomic electrons. Any emitted particles will have enough energy to cause ionization in atoms. Because of the high energy, nuclear particles or nuclear radiation is able to ionize atoms, and therefore it is called ionizing radiation. This ionization of atoms can be observed and the extent of the ionization can be related to the energy of the ionizing radiation and therefore provide a basis for the observation and identification of nuclear processes. Radiations that interact with

matter via electromagnetic forces (charged particles and photons), can cause direct ionization or excitation of the atoms. These types of radiation can be detected readily (Turner, 2007b).

2.4.2 Photon detection

The generation of a signal in radiation detection materials is a complex process in which energy is transferred from a radiation particle or quantum of radiation to electrons and atomic nuclei through a series of interactions. The energy is rarely transferred just in one interaction but through a number of interactions. These interactions cause ionization of atoms, thereby leading to the formation of positive and negative charges in the attenuating material. In radiation detection, these charges are called information carriers (Shahar et al., 2001). A radiation detection system is setup to collect these information carriers and create a pulse or signal. The pulses have different heights and can be collected, quantified and sorted by an electronic readout. An energy cascade is the process by which an incoming radiation loses and redistributes its energy to the detector material atoms via different interactions. The cascade starts when non-ionizing photons are converted into ionizing matter upon initial interaction with the detection material being used. Gamma radiation has low ionization ability and therefore it can be measured from a distance without having to worry about attenuation in air. Conversion of a gamma ray and its energy into one or more energetic electrons takes place primarily through the processes of photoelectric, Compton, and pair-production interactions which have already been discussed in preceding sections (Debertin and Helmer, 1988).

The energy cascade proceeds via a wide range of quantum energy transfer processes to electrons, plasmons, photons, phonons (heat), and atomic nuclei (Cobut et al., 2004). At the end of the energy cascade, all that remains are thermalized electrons and holes, phonons, and atoms displaced by energetic elastic scattering events. The energies involved in the cascade, range from several MeV in the incoming gamma photon to thermal energies in the electrons and nuclei that remain after the cascade. This sequential transfer of radiation energy is not well understood yet. Understanding it is crucial in determining the quality and therefore the effectiveness of a radiation detection material. At higher energies the energy transfer processes and the different interactions are well studied and there is a lot of information on reaction cross-sections that has been published from studies. Therefore at these energies the physics is well

understood and can be applied in radiation detection materials (Barrett et al., 1995). Monte Carlo simulation methods which simulate the stochastic nature of the interactions, have been widely used to describe gamma-ray and electron transport in materials. However, at the critical energies, below 1 eV, where the electron-hole pairs are formed, the physics that governs the interactions is poorly understood, and there is no cross-section data. Due to the lack of data, especially cross-section data, it is impossible to follow the cascade accurately and the number and distribution of electron-hole pairs that will be formed (Martinez et al., 1990, Fraser et al., 1994).

2.4.3 Semi-conductors as detection materials

Semiconductors are most useful in situations where high energy resolving power is needed because of their superior energy resolution for gamma spectroscopy. The major problems associated with semiconductors include, but not limited to; high costs in operation and procurement, low detection efficiency due to small size, the need for high purity, and the crystals must be free of defects, otherwise charge transfer over longer distances will be inhibited.

Semiconductors in general have way better energy resolution than scintillators because the information carriers that comprise the signal for semiconductors are the electron-hole pairs produced directly by the energy cascade produced by the incoming radiation, unlike in scintillation materials where the information carriers are produced by secondary photons. This leads to an improved energy resolution in two primary ways. Firstly, the efficiency with which information carriers can be collected and recorded is almost 100%. For a radiation interaction of a fixed energy, essentially all the electrons and holes serve as information carriers and yield maximum signal intensity, which supports improved statistical accuracy and lower energy resolution. The energy required to create an electron-hole pair through the energy cascade is proportional to the band gap, which is the difference in energy between the conduction band and the valence band, which is a couple of eV for semiconductors (Devanathan et al., 2006). On the contrary, to produce a single scintillation photon, several tens of electron volts are required. Due to the larger energy required to produce information carriers (electron-hole pair) in scintillation detection materials, its energy resolution is quite poor compared to semiconductor detectors in which the band gap is small.

The second reason why semiconductors typically offer better energy resolution involves the statistical character of the signal itself. The stochastic nature of the energy cascade determines the intrinsic variance of the semiconductor signal, whereas with scintillation material, the scintillation and light collection processes are not proportional to the energy that was deposited to the detection material. This non-proportionality contributes the most to the signal variance observed with scintillators. The variance of semiconductors is described by a measure called the Fano factor (Fano, 1946, Fano, 1947). The Fano factor is basically a ratio of the observed signal variance, *V*, divided by the variance that would be expected for a signal that adheres to the Poisson distribution, $F = V/\bar{N}$, where $\bar{N}$ is the average number of information carriers in the signal. For semiconductors, the Fano factors are typically of the order of 0.1 (Devanathan et al., 2006).

The band gap is a key feature of a semiconductor material that will be used for gamma detection. The smaller the band gap, the better is the semiconductor for detection applications. Semiconductors with large band gaps will require higher energies to create electron-hole pairs. If the energy needed to create electron-hole pair is high, it introduces a higher variance within the signal. Most semiconductors of interest in radiation detection have band gaps ranging from 0.7 to about 3 eV (Milbrath et al., 2008).

Electron-hole mobility as well as charge trapping and/or recombination are some of the other parameters that are important when considering a material for radiation detection. During counting of a sample, there are many interactions taking place within the detection material, very close to one another in terms of time. It is therefore of paramount important that electron-hole pairs that are produced within the bulk of the detection material are swept away as soon and as fast as possible to avoid over-lapping of signals and therefore signal variance. The same applies for the propensity of the detection material to trap charges that have been produced by a gamma within the bulk of the material. Charge trapping slows down the rate of mobility of the charges and will lead to a variance in the signal due to the delayed charge collecting with a charge that was formed after the initial deposition of energy from the previous interaction. Recombination also leads to signal variance because it removes charges which should have been contributing to the signal, causing a variation from the original signal of the specific gamma energy (Scholze et al., 2000).

2.4.4 Germanium as a semiconductor detection material

Germanium semiconductor detectors were first described and introduced in 1962 by Tavendale and Ewan (Tavendale and Ewan, 1963). In this type of detection material, charges, electron-hole pairs, are created on interaction of crystal with gamma rays and ionizing radiation in general. A signal is generated by the direct collection of these charges. The gap between the valence band and the conducting band for germanium crystal is about 3 eV. This means that about 3 eV of energy is needed to create one electron-hole pair. The charges are collected by applying an external reverse bias, to generate a signal (Khandaker, 2011). The small energy required to create an electron-hole pair means that when a gamma photon deposits its energy in the crystal, a large number of electron-hole pairs will be produced. The large number of charges leads to less fluctuations in the signal produced by the same gamma at different interactions. This is the basis for the high energy resolution of the germanium semiconductor detectors (Haller, 2006). Semiconductors have inherent impurities within their structures. Germanium has a valence of 4, and when impurities with valence of 3 or 5 are present in the crystal, they tend to lower the band gap energy, leading to the creation of noise in the spectrum produced.

Impurities with valence of 3 are called donor impurities and germanium crystals with this type of impurity are called p-type germanium crystals. Impurities with a valence of 5 are called acceptor impurities and crystals with this type of impurity are called n-type germanium crystals (Khandaker, 2011). This problem can be resolved to some extent by the creation of a p-n junction within the crystal structure as shown in figure 3. N-type crystal material has more electrons than holes, while p-type crystal material has more holes than it has electrons. When an n-type material and a p-type material are joined together, the point where they meet becomes a depletion zone. A depletion zone is a region where there are no free carriers, due to the combination of the excess electrons from the n-type material with the extra holes from the p-type material.

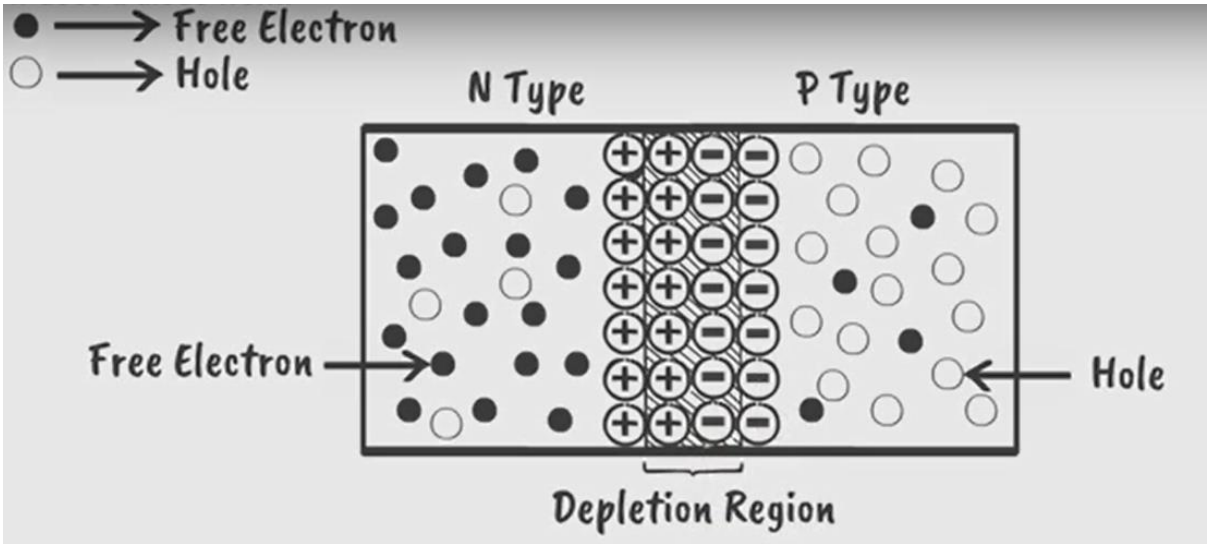

Figure 3: Creation of a p-n junction in a germanium crystal (Electrical4u, 2017).

After the absorption of free electrons from the n-side of the junction, positive donor ions will remain and on the p-side of the junction negative ions will remain due to the absorption of the holes in the depletion zone as seen on Figure 3. Due to the separation of charges in the region, an electrostatic field is created which forms a barrier potential. This potential limits the flow of free charges across the depletion region. If a forward bias voltage is applied to the crystal, charges will start to flow across the depletion region and its size will decrease. However, if a reverse bias is applied to the p-n junction, the size of the depletion region will increase and no charge will be able to flow across the junction (Electrical4u, 2017, Khandaker, 2011). The current can only flow across the depletion zone when the created current is greater than the barrier potential, as is the case when radiations deposit their energy and cause the generation of electron-hole pairs exceeding the saturation current of the diode. Therefore, the depletion region of the crystal is sensitive to ionizing radiation, and therefore the usefulness of germanium semiconductor material depends on the volume of this region. The depletion volume is also inversely related to the net impurity concentration of the crystal (Khandaker, 2011).

2.5 Radioactivity measurement

There are various types of instruments used to detect radiation and all of them depend on the ionizing nature of 'ionizing radiation' (Povinec et al., 2001). Even though these detectors differ in their fundamental functioning, several common criteria are used to evaluate and compare them. These are as follows;

- Energy Resolution

  The most important demand for gamma spectroscopy is the identification of the specific radionuclide emitting that specific gamma ray. If any real analytical work is to be achieved, then the analyst should be able to assign specific peaks to specific gamma energies. Each radionuclide emits a unique distribution of gamma energies. If a sample then contains multiple radionuclides, all emitting gamma rays of different energies, the spectrum of that sample will have a number of gamma rays with energies close to each other. The ability of a detector to present two peaks from gammas with close energies as separate peaks is critical in gamma spectroscopic measurements. If the energy resolution of a detector is good, then that detector will be able not only to identify specific radionuclides but to also quantify them. The full width at half maximum (FWHM) is usually used to describe the resolving power of a detector. The FWHM is energy dependant, describing the resolution at a specific photo-peak. In gamma spectroscopy, the gamma ray of ^{137}Cs at 662 keV is used as a benchmark. The energy resolution achievable by a particular detector is depends on a number of factors (Milbrath et al., 2008).

- Detection efficiency

  The detection efficiency for a detector is a measure of the fraction of incident radiation photons which are able to reach the sensitive volume of the detector that are detected. The full-energy peak efficiency describes a quantity which is specific to that particular peak; specifically, the fraction of detection events in which the full energy of the incident radiation has been deposited in the active volume of the detector crystal. Full-energy peak efficiency and detection efficiency are determined by the properties of the detector material in three different ways. Both efficiencies increase with the active volume of the detection material, secondly, both efficiencies increase as the mass density of the active medium increases and finally, both efficiencies depend on the composition of the active medium and generally increase as the atomic number, Z, of the constituents increase (McDonald et al., 2007).

- Geometric efficiency

  The geometric efficiency describes the fraction of gamma rays which are emitted by a radiation source that strike the active volume of the detector. This

efficiency will therefore depend on the cross-sectional area that the active medium presents to the source. It also depends on the geometry of the sample container. Different sample containers present different surface areas of the sample to the detector. A Marinelli beaker is one sample container in HPGe detector gamma spectroscopy that present maximum surface of the sample to the detector and therefore leads to higher geometric efficiencies. High efficiency reduces uncertainty and allows for shorter counting times (McDonald et al., 2007, Siciliano et al., 2005).

2.5.1 High Purity Germanium Detectors

In gamma spectroscopy the main aim is to detect photon energies with different energies and be able to distinguish between the different energies. Gamma photons have high energies, in the order of hundreds of keV to a couple of MeV (Boukhenfouf and Boucenna, 2011). To be able to detect a photon and its approximate energy, that particular photon must first enter the germanium crystal and then interact with the atoms of the crystal material to depletion, leading to the deposition of all of its energy within the crystal. Photons of high energy don't interact easily, they therefore have a high mean free path. This therefore means that they will need a greater length of crystal material to deposit their energy (higher depletion depth) than lower energy photons. Germanium crystals of normal purity can only achieve a few mm in terms of depletion depth (Povinec et al., 2001).

2.6 Chemistry and speciation of Radionuclides

2.6.1 Uranium

The predominant isotopes of uranium in natural waters are ^{234}U and ^{238}U. As a result of its low abundance in the earth's crust and long half-life, ^{235}U typically occurs in low concentrations in natural waters. An excess of ^{234}U occurs in natural waters (higher levels than produced by the decay of ^{238}U). The high ^{234}U-to-^{238}U ratio is believed to be due to β recoil propelling the ^{234}U progeny into solution after decay from the rock source. Under oxidizing conditions, uranium is in the +6 state and forms highly soluble uranyl carbonate complexes. In a reducing environment, uranium (in the +4 state) is relatively immobile (Aieta, et al., 1987).

Uranium compounds that occur in the solid state have been studied extensively because of their magnetic properties and their inertness. Industrially they are usually

made by a direct interaction with metallic uranium. The main oxides are UO_2, U_3O_8 and UO_3. UO_2 is brown-black, highly unreactive and is the most abundant form of uranium oxide. U_3O_8 is the second most abundant uranium oxide and is greenish-black in colour while the other oxide is UO_3 which is orange yellow in colour. The oxides are readily soluble in nitric acid to give the uranyl (UO_2^{2+}) ion (Gómez et al., 2006). Addition of H_2O_2 to solutions of UO_2^{2+} gives a pale yellow peroxide which can be best represented as $(UO_2^{2-})(O_2^{2-})(H_2O)_2$, while a reaction with hydrogen peroxide and sodium hydroxide forms a stable salt $Na_4[UO_2(O_2)_3]$. When uranium oxides are mixed with alkali and alkali earth carbonates, or thermal decomposition of uranyl acetate anion, produce yellow or orange materials known as uranates. Uranates do not contain discrete ions such as UO_4^{2-} (Kopylova et al., 2015).

The speciation and therefore solubility and concentration of uranium in natural waters depends on the pH, pe, concentration of organic and inorganic ligands as well as phosphates, carbonates and sulphates. At pH levels below 5 in oxidizing natural waters that have very few organic ligands (organic matter), the uranyl ion dominates. Hydroxy complexes are dominant in waters with pH less than 6.5 (Kopylova et al., 2015). In a system where there is carbonate, an increase in pH above neutral will lead to the formation of di- and tri-carbonate complexes due to the anions, CO_3^{2-} and HCO_3^-. High concentrations of phosphate in the water system will lead to the sorption of uranium (Wu et al., 2014, Wang et al., 2014).

The most common and thermodynamically stable form is the hexavalent dioxo-complex UO_2^{2+}.This ion forms stable negative complexes in the presence of carbonates , the most common being $UO_2(CO_3)_3^{4-}$and $UO_2(CO_3)_2^{2-}$, although some reactions of uranium are explained by the formation of the positive ion $(UO_2)_3(OH)^{5+}$. The fact that more than 99 percent removal is accomplished by the use of anion exchange resins strongly supports the former two species as those that predominate. It is, of course, possible that waters with low alkalinity could contain $(UO_2)_3(OH)^{5+}$ because then the UO_2^{2+} ion has strong complexation tendencies (Hussain and Krishnaswami, 1980).

Under oxidizing conditions the uranyl ion (uranium (VI)) is the predominant uranium oxidation state. This species binds strongly to iron hydroxides, while under alkaline conditions in the same waters; the formation of highly mobile carbonate complexes

will be favoured. The +4 oxidation state is observed under reducing conditions and it is highly susceptible to precipitation on forming humic complexes. Therefore under reducing conditions the mobility and solubility of uranium in underground waters is lower than it is under oxidizing conditions (Wang et al., 2014).

Uranium sulphate complexes are more likely to be dominant in acidic waters or in mine waters with high concentrations of sulphate ions. Phosphate complexes are also important in waters, but their concentration is dependent on both the phosphate concentration in the system and also the solubility of these phosphate complexes (Gómez et al., 2006). Figure 4 shows the speciation of uranium (VI) in the UO_2^{2+}/H_20 system (Krestou and Panias, 2004).

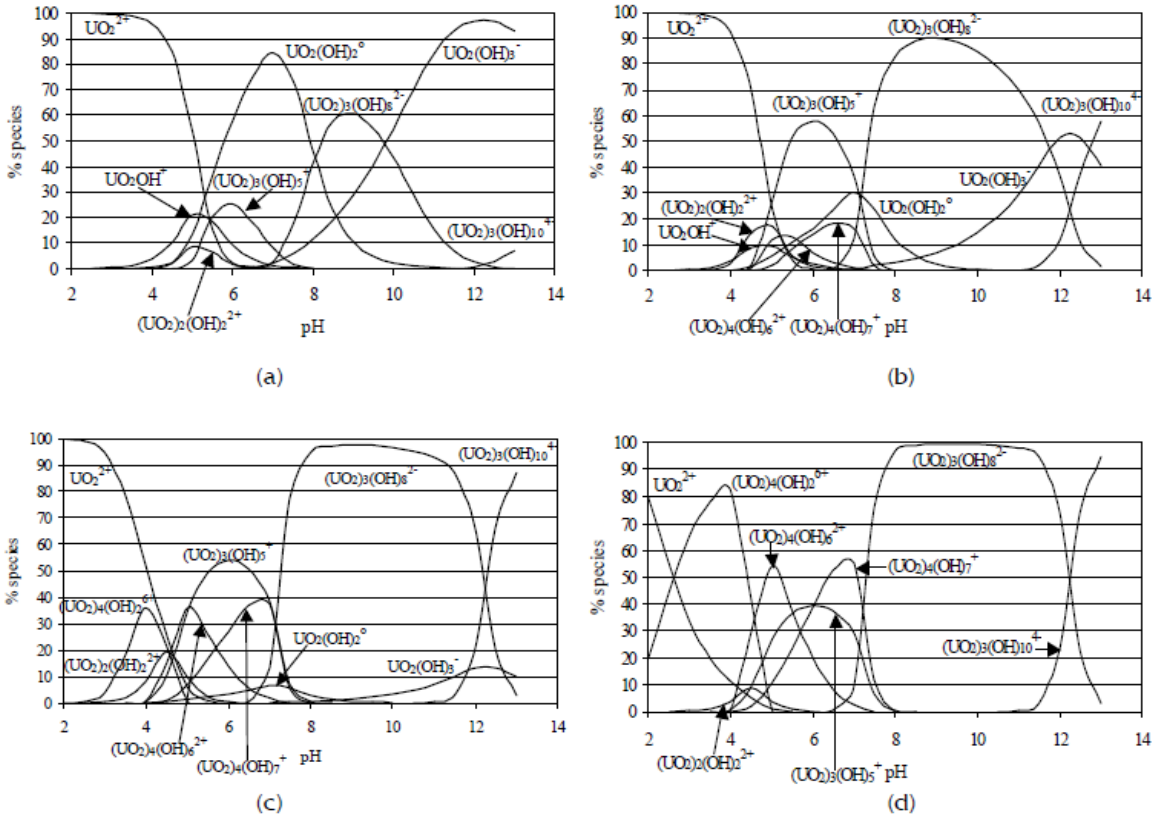

Figure 4: Uranium (VI) speciation at ionic strength 0.1 M and concentration: (a) 1×10^{-5} M (b) 1×10^{-4} M (c) 1×10^{-3} M (d) 1×10^{-2} M (Krestou and Panias, 2004).

2.6.2 Radium

Radium is an alkaline earth metal, belonging to group 2 in the periodic table. Therefore it shares a lot of chemical characteristics with the group metals. Within the group, the

atomic radius has a big influence on the reactivity and chemistry of the metal. Radium has a similar atomic radius to barium, which belongs to the same group of elements. Therefore in some cases where radium data is not available, the chemistry of barium can be used to predict how radium would behave in that particular chemical system. Radium occurs in nature in the +2 oxidation state (Carvalho et al., 2014). Radium enters groundwater by the dissolution of solids, by direct recoil across the liquid-solid boundary during its formation, by radioactive decay of its parent in the solid, and by desorption. Redox potential has a huge influence on the solubility of radium in underground waters. A low redox potential ensures a low to none concentration of sulphates and therefore leads to the dissolution of higher concentrations of radium. Therefore, it is expected that in low pe waters with very low sulphate concentrations, higher concentrations of radium can be observed (Dickson, 1990). Iron and manganese oxy-hydroxides are also important in controlling the sequestration of radium in ground water (Moore and Reid, 1973). Oxidation of underground water, like AMD, when it decants to the surface may lead to the removal of radium from solution if the oxidation leads to the precipitation of iron and manganese oxides (Felmlee and Cadigan, 1979). Table 1 shows the different radioactive isotopes of radium found in nature. The predominant Ra isotopes in water are ^{226}Ra and ^{228}Ra. ^{228}Ra is usually assumed to be less abundant than the ^{238}U progeny, ^{226}Ra, but ^{226}Ra-to-^{228}Ra ratios range from 14 to 0.07. Radium generally occurs in low levels in surface waters (Aieta et al., 1987).

Table 1: Radioactive isotopes of radium

Isotope	**half-life**	**series**
^{223}Ra	11.43 d	Actinium series
^{224}Ra	3.632 d	^{232}Th series
^{226}Ra	1600 a	^{238}U series
^{228}Ra	5.75 a	^{232}Th series

Electrophoretic methods were applied in studying the mobility of radium in chloride solutions of 0.01 M. The results suggested that only Ra^{2+} cations were present in the solution in the pH range 2-7. Solutions containing ligands such as phosphate, sulphates and carbonates were also studied and a number of radium complexes with

these ligands were detected. Complexes such as $RaSO_4$, $RaCO_3$ and $RaHCO_3\_(RaHCO_3)_2$ were detected when ligand concentrations between 0.001 and 0.1 M were used (Dickson, 1990). In solutions with high concentrations of sulphate, above 20 mg/L, at least 10% of the radium will exist as $RaSO_4$ complexes. $RaCO_3$ complexes will only be significant at pH levels above 10.25 in solutions with high carbonate concentrations (above 60 mg/L) (Benes, 1982). The species $RaCl^+$ will only become significant in solutions with high salinity and chloride concentrations above 5 g/L (Dickson, 1990).

Table 2: Ra^{2+} reactions

Complex	***logK(association)***	
	(Langmuir and Riese, 1985)	(Benes, 1982)
$Ra^{2+} + OH^- = RaOH^+$	0.5	
$Ra^{2+} + CI\_ = RaCl^+$	-0.10	
$Ra^{2+} + CO_3^{2-} = RaCO_3$	2.5	2.48
$Ra^{2+} + SO_4^{2-} = RaSO_4$	2.75	2.43
$Ra^{2+} + HCO^{3-} = RaHCO_3^+$		2.89

2.6.3 Thorium

Thorium metal is a highly electropositive element. Concentrated nitric acid renders thorium passive but the addition of fluoride ion causes the dissolution to continue. Due to its small size and large charge, thorium is highly reactive in water, interacting with both the water molecules and most anions present in the water. Thorium has only one oxidation state in water and therefore there are no complex redox reactions associated with it. Thorium forms water soluble salts with the nitrate, sulphate, chloride and the perchlorate anions. Th^{4+} has a high tendency of forming complex ions with anions that are usually found in solutions. The tetra positive thorium ion is more readily adsorbed and adsorbs more strongly onto cation exchange resins than most ions. Because of this, cation exchange resins are very good at removing thorium from a solution containing a mixture of cations (Hyde, 1960).

Table 3: Thorium isotopes (Santschi et al., 2006)

Isotope	Half-life	Method of production
^{234}Th	24.1 d	Natural radioactivity; daughter of ^{238}U
^{233}Th	22.1 m	^{232}Th + neutrons
^{232}Th	1.39×10^{10} a	Natural thorium is 100% ^{232}Th
^{231}Th	25.64 h	Natural radioactivity; daughter of ^{235}U
^{230}Th	7.5×10^{4} a	Natural radioactivity; daughter of ^{234}U
^{229}Th	7340 a	Daughter of ^{233}U
^{228}Th	1.9 a	Natural radioactivity; daughter of ^{228}Ac
^{227}Th	18.17 d	Natural radioactivity; daughter of ^{227}Ac
^{226}Th	30.9 m	Daughter of ^{230}U
^{225}Th	8 m	Daughter of ^{229}U
^{224}Th	~ 1 s	Daughter of ^{228}U
^{223}Th	~ 0.7 s	Daughter of ^{227}U

Thorium which exists only in the tetravalent oxidation state can form both mono and poly-nuclear hydrolysis products. At concentrations below 10^{-4} M, the species $ThOH^{3+}$ and $Th(OH)_3^+$are dominant as the pH increases above 2. At higher pH levels, the species $Th(OH)_4$ is the major species in natural waters (Choppin, 2006). Tetravalent actinide cations like thorium (IV) do not form carbonate complexes in significant amounts in natural waters because the formation of the $Th(OH)_4$ species, which is insoluble, is more favourable (Grenthe and Lagerman, 1991). The pH (acid-alkaline) conditions have a major effect on the behaviour and speciation of thorium in water. In carbonate rich waters, the species $ThCO_3(OH)_3^-$ dominates in slightly acidic conditions. It makes up more than 95% of all thorium in the system. Its proportion increases to 100% under neutral pH conditions. $Th(OH)_3^+$ and $Th(OH)_3^+$ are observed at pH 5.9-6.2 (Kopylova et al., 2015). Figure 5 shows the speciation of thorium in a system rich in dissolved carbon dioxide.

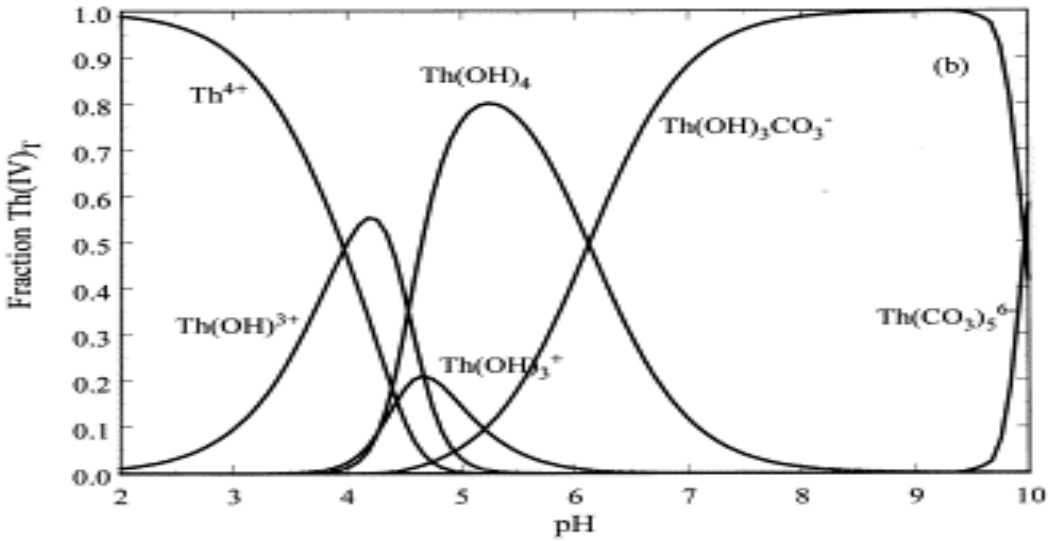

Figure 5: Thorium species modelled with a concentration of 8.3×10^{-14} M (Murphy et al., 1999).

2.7 Modelling of Radionuclides speciation

The modelling of the behaviour of materials which pose serious hazards under environmental conditions is one of the most important applications of natural and technical sciences in environmental protection (Tipping et al., 1998). Radionuclides are some of the harmful contaminants in the environment and understanding their behaviour in specific natural systems of importance is critical. Certain chemical conditions are either expensive or difficult to study in the laboratory. In a chemical system of AMD for example, the chemistry is complex and difficult to study and understand well. There are too many reactions going on and those reactions vary with the slightest changes in chemical and physical parameters. Computer codes have been written to model or simulate the equilibrium chemistry of a chemical system. Within the written codes are databases of the thermodynamics of the different possible chemical species that can exist in chemical systems (Periáñez, 2004). Using data from experiments that were performed, extrapolation can be made to give an idea of the chemistry under different chemical and physical conditions. Modelling is a powerful tool when it is used correctly because it can give scientists an idea of how a chemical system will behave even before actual experiments.

In environmental radioactivity studies, understanding the behaviour and chemistry of radionuclides in the natural environment such as water (ground and surface), and in soil can be useful in predicting the mobility within that particular environment and

therefore predict the extent of the potential impact. Though modelling can be a powerful tool, it can also be harmful if not used carefully and with understanding. Most of the modelling packages that exist today have flaws inherent within them (Markich, 2002). They all use data that is sourced from studies done by scientists all over the world. There is always a possibility that the data that is being used as a basis for modelling is wrong. If that data is wrong, then the model will predict wrongly and wrong predictions can be made. Therefore, modelling should be used as a tool to understand experimental data and should be tested for its validity under lab friendly experimental conditions.

Most water treatment plants use precipitation processes for the effective removal of uranium. Predominant uranium species influence the sorption and precipitation behaviour due to their varying charge states. Therefore, the speciation has great impact on the procedure and effectiveness of water treatment processes (Markich, 2002).

2.7.1 JESS

Important inputs to this code are pH and pe in order to set the redox conditions. All the elements which will be present in the system are also an input, from which JESS automatically generates what are called the "basis species". The basis species is the smallest group of species which can be used to express all other species in the system in terms of reactions. The rest of the species that are involved in the system which are not basis species are called the "non-basis species" (Murray and May, 2000).

In JESS modelling and equilibrium calculations there are three basis sets that are used. The first basis set is made up of those species that will be used to evaluate the stability of all the species in the system with respect to one another. These species are called the "thermodynamic basis species". The second basis set is made up of those species which will be used as unknowns in solving the thermodynamic equations. These set of species are called the "variable basis species". The third basis set is made up of the species in the thermodynamic problem that will be used to define the total concentrations of components. These are the masses which are added up to check for mass balance. These last set of species are called the "mass balance units" (or MBU). MBU species should be selected based on the analytical information reflecting the model being developed. The “variable” and “MBU” basis species sets,

usually have the same number of species but the identity of the species may differ. The thermodynamic basis species will be equal or less in number compared to the MBUs and the variable basis species (May and Murray, 2001).

In JESS, all reactions in the database are based on experimental data and the experimental conditions under which these data are obtained varies. This therefore brings in some level of variability, in that the reactions being used to accurately define a reaction might differ depending on some experimental parameters such as the ionic strength, pressure and temperature which are being used for the equilibrium model. In the “LGK” stage of equilibrium modelling, JESS selects the necessary reactions based on these experimental parameters. These reactions are combined linearly and their equilibrium constants are calculated. The suitability of a reaction is determined using the number of constants in the JESS database, NCST (May and Murray, 2001). This database is a measure of how reliable constants are based on their weights and the suitability of the specific experimental conditions under which they should apply, and the “intrinsic reliability” of the reaction. The selection of the best reactions cannot be done reliably and consistently when the experimental conditions are not specified in the LGK stage. Therefore specifications like calculating the ionic strength of the system at equilibrium leads to inconsistencies. This therefore means that different answers will be obtained from different models under the same conditions due to selection of different reactions. Therefore for consistent and reliable results, it is important to select and specify the correct set of experimental conditions during the LGK stage of the equilibrium calculations (May and Murray, 1991).

2.7.2 Procedure in Modelling

A JESS equilibrium calculation comprises of five sequential steps, called ‘the GEM stages’. GEM stands for “Generalized Equilibrium Modelling”. These stages are the heart of JESS modelling. Everything that is required, in terms of input and output is covered under these GEM stages (May and Muray, 1991).

2.7.2.1 SUB stage

This is a stage where chemical elements (symbols) and/or JTH species symbols occurring in the chemical system being modelled are specified. The choice of entering either a JTH species or chemical symbol is dependent on whether or not the expected dominant species in the system is known. If it is known, then the species symbol is

entered, but if it is unknown, then the chemical symbol is entered and JESS determines the dominant species in the specific chemical environment. JESS then collects species information only relevant to the species that are part of the system from the main JESS database and creates a sub-database relevant to the chemical system specified. All the data entered and generated at this stage is stored within the working directory in the computer for use in the next GEM stage (May and Murray, 1991).

2.7.2.2 LGK stage

The LGK stage is where the specific experimental conditions of the system being modelled are entered. This has a huge influence in selection of reactions used by JESS, as well as the consistency of the equilibrium calculation. This stage has an influence on the reactions that JESS prioritises and also the thermodynamic data that will be used in the model (May and Murray, 2001). This stage uses stored data and in some cases some of the data may be incorrect and therefore need some editing. The Jess database can be edited to reflect better thermodynamic data as understood by the modeller. In most cases these inconsistencies don't affect the model. This is due to the fact that the inconsistencies involve minor species which have no influence in the overall chemistry at equilibrium (Murray and May, 2000).

2.7.2.3 BAS stage

The two preceding stages establish first a stable set of reactions and then determine and select the relevant thermodynamic data for the equilibrium calculation model. This information is then used by JESS to determine the "basis set of species". The basis species set is basically a small set of species from which all the complexes that can be formed in the chemical system being modelled can be formed through a linear combination. They are basically the basic building blocks in the system which can be combined to form all allowable chemical states at equilibrium. There are cases when the basis species for a certain element might need to be changed to allow equations to solve at equilibrium (Murray and May, 2000).

Some kinetic inputs can be introduced at this stage, which will impose some constraints on the equilibrium calculations. "This is done by re-assigning appropriate sets of species from a specified thermodynamic basis species to a species which you want to become a basis species in your modelling calculations"(Rowland and May,

2010). Reactions for all the species specified are then expressed in terms of the species specified at the BAS stage instead of the ones determined in the LGK stage.

2.7.2.4 QED stage

The QED stage is the step where the actual equilibrium calculation is done. The equations that will have to be solved are constructed at this step in the modelling. Mass balance equations, which are equations that are used to calculate the total concentration of the chemical system by taking the sum of all the species. Equations which govern the solubility products of precipitates which are in chemical equilibrium with solution. Equations that describe the adsorption isotherms of species are also introduced at this stage where necessary (May and Murray, 1993).

The analytical concentrations of the chemical inputs into the system are entered at this stage in the equilibrium calculation. Any precipitates which are allowed to form are also specified at this stage for inclusion in the equilibrium calculation. A precipitate may be present at equilibrium or it may be allowed to dissolve or precipitate freely. The influence of certain factors, such as pH or ionic strength can be evaluated by doing equilibrium calculation at different points of the concerned factor. This is referred to as scanning (Murray and May, 2000).

2.8 Water treatment

2.8.1 Coagulation filtration

Conventional treatment follows these particular processes: coagulation, flocculation, clarification, and filtration. The feed water goes through a process of sedimentation as a precursor to the coagulation-filtration process. Coagulation-filtration is almost always accompanied by the addition of powdered activated, and the utilization of granular activated carbon as a filtration or adsorption media (Bratby, 1980).

In coagulation, a positively charged coagulant (usually an aluminium or iron salt) is added to the feed water. This is then followed by a fast mixing step. The coagulant changes the macro-structure of or destabilizes negatively charged particles, colloidal and dissolved contaminants leading to the formation of micro-flocs. Turbidity and total organic carbon are two factors that have a considerable effect on coagulation process (Bratby, 1980).

After the fast mixing, a gentle mixing step follows and the role of this step is to increase the rate at which particulate collide. The collisions cause destabilization and the destabilized particles form aggregates, leading to the formation of macro-flocs. Factors including but not limited to speed of mixing, intensity of mixing and the mixing time have an influence on flocculation.

Charge neutralization and sweep flocculation are the two main de-stabilization mechanisms in coagulation-filtration. The choice of destabilization mechanism is dependent on the dose of coagulant to be used. Sweep flocculation is the de-stabilizing mechanism that is used in most water treatment plants. This mechanism utilizes a large dose of coagulant. With charge neutralization, the metallic coagulant, which is positively charged, is electrostatically attracted to the colloids which are negatively charged. As the colloids and coagulant particles continue to collide, aggregates begin to form. To form precipitates, more metal coagulant dose is added to the water beyond the neutralization point. These metal hydroxide compounds are heavy, attract each other and are larger. In sweep flocculation the colloidal contaminants move together with the metal hydroxide precipitates as they move from the surface of the feed water to settle at the bottom (Crittenden et al., 2012).

If aluminium sulphate is being used as a coagulant, the optimal pH ranges between 6-7 and 5.5-6.5 when using iron based coagulants. Feed waters with high pH (highly alkaline) may need an adjustment of the pH to the optimum range for the particular coagulant being used (Hassan et al., 2009). This is one way of lowering the operation costs, mainly by saving on the amount of coagulant to be used. Colour causing compounds, inorganic molecules, particulate matter and disinfection by-product precursors are being removed using the process of enhanced coagulation. The coagulant dose is extremely important in all coagulation & filtration. Application of the optimal dose is paramount, as a low dose might not cause enough particle destabilization while a high dose might cause restabilization and the production of excessive amounts of sludge as well as corrosion of the treatment plant (Shammas, 2005).

Temperature, pH, and alkalinity have a huge influence on how effective the coagulation-filtration treatment is. The pH of the feed water has a profound effect on the destabilization stage, and therefore influences the effectiveness of the method

directly. The pH determines the speciation of all the chemical constituents in the feed water as well as the coagulant. The chemical form (speciation) of the coagulant has a large influence on its solubility in the water and thus also influences the amount of coagulant dose needed. Viscosity of the water being treated is influenced a lot by the temperature, and it affects the process of coagulation. Low temperatures slow down reactions in most cases, and in coagulation, it affects the rate hydrolysis and the kinetics of precipitate formation. Parameters such as iron, manganese or sulphate concentration can affect this method of water treatment, with the extent of the impact highly dependent on the chemistry of the coagulant being used. Alternative coagulants such as poly-aluminium chloride, can be more effective in terms of performance and cost compared to the normally used coagulants in feed waters with low temperature. The alternative coagulants are already hydrolysed cancelling the effect of temperature on the coagulation process in which the process is slowed down due to slow hydrolysis rate.

After flocculation, the aggregates go into the clarification unit. In the clarification unit, the aggregates can be removed by skimming them from the surface or via gravity sedimentation. In the sedimentation stage, most of the aggregates are heavy and therefore settle at the bottom and therefore are practically removed from the water. Certain particles will not settle and these are removed from the water during the filtration stage. In most plants sedimentation is done in circular or rectangular basins, often improved by the adding inclined plates or tubes. The inclined plates or tubes increase the surface area of the sedimentation basin and thereby improving the process of sedimentation. Dissolved air flotation (DAF) is another clarification process whereby air is diffused as fine bubbles into the water. These fine air bubbles float suspended particles to the surface where they are removed by skimming (Shammas, 2005).

The filtration stage in most cases is achieved with the use of what is referred to as a dual-media filter. This filter is made up of a combination of sand and anthracite coal, and is the most commonly used filter in water treatment. It is not uncommon though to find treatment plants using different filter configurations. These might be mono-media filters, which use just one medium such as sand filtration, multi-media filtration, which uses a composite of filtration media (anthracite coal, sand and garnet) and other configurations. Granular activated carbon may also be used for polishing of the treated

water. Most of the suspended particles are removed in the top layer of the filtration medium being used. Media are usually backwashed from time to time to avoid loss of pressure in the process and to generally keep the plant clean (Bratby, 1980).

Waste that is generated by this treatment method consists mainly of coagulation solids (referred to as sludge) and spent backwash solution. In most treatment plants, it is common to return backwash into the treatment process to reduce losses. Waste solids from the process contain enhanced concentrations of contaminants. Depending on the concentration of specific contaminants in the feed water, it might be necessary to have a special disposal plan for the sludge that is generated. The constraints and requirements for disposal will always depend on the local and state regulations. Coagulation/filtration processes are commonly used for uranium removal. The mechanism involves adsorption and co-precipitation of U(VI) to a coagulant precipitate. Both aluminium sulphate (alum) and iron based coagulants have been shown to successfully remove uranium to concentrations below the maximum contaminant level (MCL) with the coagulation & filtration water treatment method. The optimal pH of 6.0 was shown to be ideal for uranium removal using either of these coagulants (Stechemesser and Dobiáš, 2005).

2.8.2 Ion Exchange

Ion exchange is a treatment method, whereby ions that are in aqueous solution are removed from solution by replacing them with ions that are in a stationary column having a similar charge. Ion exchange is primarily used for softening purposes, which is a process in which magnesium and calcium ions are removed from water. But with improved ion exchange technologies being developed, it is increasingly being used to remove other ionic soluble contaminants from water (Crittenden et al., 2012).

Cation exchange is a process where positively charged ions in the water are being exchanged with positively charged ions on the surface of the cationic exchange resin. Cationic exchange resins are mainly used for water softening by removing sodium. Anion exchange process involves the exchange of negatively charged ionic species in the water with negatively charged species on the surface of the anionic exchange resin. Fluoride, sulphate, nitrate, arsenic and many others can all be removed using anionic exchange process. The removal of chloride is the most commonly used application of anionic exchange resins.

The ion exchange medium is usually made up of a solid phase of either a synthetic resin or a naturally occurring material. The medium has two parts; one is a mobile ion which is bonded to a fixed functional group. Depending on whether an anionic or a cationic exchange medium, the functional group can be acidic or basic. Cationic and anionic exchange media are both made from the same type of polymer in terms of bulk structure, the only difference comes from the functional group that is attached on the surface for the exchange reactions. The exchange of the mobile ions and the exchange medium ions occurs because the mobile ions in solution have a higher affinity for the functional group in the exchange medium (Crittenden et al., 2012).

After being used for a while, the ion exchange medium will be saturated in a way, whereby more than 99% of the functional groups on the surface of the exchange medium have undergone a reaction and there are no more sites available for exchange. When that happens ionic species in the solution goes right through the ion exchange medium without being removed. The ion exchange resin at that point will need to be regenerated. Regeneration is achieved by using a saturated solution containing the original ion that was in the exchange medium. The ion displaces the contaminant ion on the functional group, thereby returning the ion exchange resin to its original state and capacity. In most cases a saturated solution of sodium chloride is used. Strong acids such as hydrochloric acid and sulphuric acid or strong bases such as sodium hydroxide are also used in treatment plants.

There are two operational modes in the ion exchange process and these are, batch mode or the continuous mode. The continuous operational mode is the most commonly used mode in most ion exchange water treatment processes. This operational mode is mainly used with packed-bed or down-flow column type.

The most important factor affecting the effectiveness of ion exchange treatment process is the competition for exchange sites on the resin between ions of the same charge. A contaminant might have a lower affinity for the functional group than other ions present in the feed water. This does not only reduce the exchange of the contaminant on the resin, it also causes the capacity of the exchange resin to be exhausted faster than usual. This slows down the process and increases operational cost as more regenerant solution will be needed and other costs associated with

reduced productivity. Hard atoms (high valence and smaller radii) with high Z usually have higher affinities for ion exchange sites. Relative affinities of common ions are:

$$Ag^{+} > Cs^{+} > K^{+} > Na^{+} > Li^{+}$$

$$Ba^{+2} > Sr^{+2} > Ca^{+2} > Mg^{+2}$$

$$I^{-} > NO^{3-} > CN^{-} > HSO_4^{-} > NO^{2-} > Cl^{-} > HCO^{3-}$$

This therefore means that in the presence of ions with higher affinities for the ion exchange sites, contaminant ions will start getting displaced as the ion exchanged resin gets to higher levels of loading. This will lead to higher concentrations of the contaminant in the treated water than in the feed water. The process whereby ions with higher affinities replace other exchanged ions on the resin, with those with lower affinities displacing those with even lower affinities is referred to as chromatographic peaking.

Resin fouling is one other process that has a huge influence on the effectiveness of an ion exchange treatment process. Resin fouling is caused by chemical precipitants, chemical clogging and scaling of minerals. To reduce the effect of resin fouling, pre-treatment processes such as filtration of suspended solids and addition of chemicals which can reduce scaling may be necessary.

The major waste or residual that is generated in an ion exchange treatment plant is spent regenerant solution. The spent regenerant solution will have all the ions that have been removed from solution as well as the original regenerant ions. This makes the spent regenerant solution to have high total dissolved solids (TDS) concentrations. The spent regenerant solution might require special discharge or disposal due to the potential high concentration of heavy toxic contaminants. Usually this is discharged into a waste water disposal or waste treatment plant. The TDS of the waste water as well as the concentration of other contaminants will play a big role in the decision making on how the waste water is treated. The decision making will have to depend on the local government policy as well as international standards that govern waste water discharge from treatment plants.

2.8.3 Reverse Osmosis

Nano filtration and reverse osmosis are two treatment methodologies that use the concept of reverse osmosis (Mondal and Wickramasinghe, 2008). Osmosis is a process in which water flows from a solution with high water concentration to a solution with low water concentration through a semi-permeable membrane. It can also be defined as the movement of water molecules from a dilute solution to a concentrated solution through a semi-permeable membrane. A semi-permeable membrane is a membrane which allows water molecules to pass through it but does not allow contaminant molecules to pass through. This process is also called passive osmosis and the flow of the water following the osmotic potential will continue until the osmotic pressure on both sides of the membrane is balanced (equal concentration on either side of the membrane). The osmotic pressure is the pressure that is equal but opposite the osmotic potential. It is the amount of pressure that needs to be applied to stop the process of passive osmosis. Reverse osmosis is the opposite of the normal osmotic process. Natural osmosis is of no use in water treatment because it does not lead to treated water with lower concentrations of contaminants (Mondal and Wickramasinghe, 2008). In reverse osmosis, pressure that overcomes the osmotic pressure is applied to the feed water which has a higher concentration of the contaminants. The pressure pushes the water across the osmosis membrane against the normal concentration gradient. This leads to a higher concentration of the contaminants on the feed water side of the membrane and a low contaminant concentration on the treated water side of the membrane. To obtain high levels of removal high pressures are required. Nano filtration membranes require more pressure (125 to 1200 psi) than reverse osmosis membranes (50 to 150 psi) (Ning, 2002).

There are three major streams associated with reverse osmosis: the feed water stream, permeate or treated water stream and the waste water stream which is the rejection stream. Depending on the chemistry and physical characteristics of the feed water there might be a need for pre-treatment. There are three main pre-treatment process in membrane systems and these are: (1) condition the water to maximize membrane performance, (2) modification of the feed water to minimize membrane fouling and clogging and (3) reduce the amount of time spent cleaning the membrane in order to maximize membrane life and productivity (Mondal and Wickramasinghe,

2008). For reverse osmosis the feed water must be completely devoid of suspended particles and solids. Surface waters usually have more suspended solids than underground waters and therefore in reverse osmosis processes they might require more pre-treatment. The extent of suspended solids in the feed water is usually measured using two parameters; turbidity and the silt density index. An antiscalant or an acid are usually used if scaling is the major culprit in membrane fouling (Greenlee et al., 2009).

Scaling occurs in the membrane occurs as a result of high concentrations of contaminants in the rejection or waste stream. The concentration of the dissolved contaminants exceeds the solubility product associated with them. Calcium carbonate, calcium sulphate, barium sulphate, and silica are normally the compounds that control the rate of membrane fouling. System recovery is the measure of the effectiveness of the reverse osmosis system (Crittenden et al., 2012). It is the percentage of feed water that comes out in the permeate stream. The higher the ratio, the better the system is running. The concentration of the limiting compounds in the permeate stream greatly affects system recovery. During the reverse osmosis process, the concentration of contaminants in the waste stream can increase to more than ten times the concentration in feed water stream depending on the system recovery. Normal reverse osmosis and Nano-filtration membrane elements have system recoveries of around 80-85% (Malaeb and Ayoub, 2011).

Temperature is one feed water parameter that can have a large impact on membrane performance. Water temperature affects the density of the water as well as its viscosity. These two parameters affect the membrane flux, which is the rate of permeate flow through the membrane. An increase in viscosity and density leads to an increase in the transmembrane pressure necessary to force the water across the membrane. This results in an increased specific flux, which is the ratio of the flux and the transmembrane pressure. Solubility of chemical constituents in the water is also a function of temperature. At lower temperatures the solubility of most contaminants is reduced. If a high system recovery is maintained at low temperatures, there might be increased scaling on the membrane. Therefore at lower temperatures, low recoveries may have to be maintained to reduce membrane scaling. High temperatures may cause degradation of reverse osmosis membranes as well as membrane compaction. Reverse osmosis removes bicarbonate and alkalinity from the water leading to

permeate with lower pH than the feed water. This calls for the need to adjust the pH to limit corrosion in the system (Malaeb and Ayoub, 2011, Mondal and Wickramasinghe, 2008).

All water treatment methods will ultimately generate waste. Waste that is generated from reverse osmosis treatment systems is mainly the rejected stream and the spent chemicals that are used to treat membrane fouling and scaling. The waste water from the rejection is stream present the biggest disposal problem due to its bulk, high TDS and high concentration of contaminants. Disposal into any water body will require that the water body be large enough to allow for adequate dilution, otherwise it must be disposed into a waste water treatment plant which will lead to higher production costs (Crittenden et al., 2012).

2.9 Liquid Scintillation Counting

Liquid Scintillation Counting (LSC) is the best method for detecting and counting low energy β emitters (Peng, 1970). Liquid scintillation is similar in many ways to solid scintillation in terms of the physics employed, with both methods taking advantage of a fluorescent material that release light after interaction with radiation. The main difference is that the scintillation takes place in a solution of scintillation material, instead of a solid crystal for LSC. Since the emitters are in close proximity with the phosphor molecules, low energy beta particles can also be detected because they don't have to travel longer distances to reach a phosphor molecule (Horrocks, 2012a).

Liquid scintillation cocktails absorb the energy emitted by radionuclide and re-emit it as visible light. There are two different components of a cocktail that helps with the absorption and re-emission, solvent molecules absorb the energy of the incoming radiation. This energy is then transferred to phosphor molecules which then re-emit the energy as visible light of a specific wavelength (Broda et al., 2007).

2.9.1 The Role of the Solvent

The solvent portion of an LSC cocktail makes up about 60% – 99% of the total analysis solution (Gibson and Lally, 1971). When a radionuclide dissolved in the cocktail's solvent decays, it is likely that the emission will encounter only solvent molecules before it is totally absorbed. For this reason, the solvent must act as an efficient collector of energy, and it must conduct that energy to the phosphor molecules instead

of dissipating the energy by some other mechanism. The solvent must not quench the scintillation of the phosphor, and, finally, the phosphor must be totally soluble in the solvent to produce a stable solution that can be counted easily (Horrocks, 2012b).

Aromatic compounds are the best solvents for LSC. The most commonly used LSC solvent is toluene. The π-cloud of the toluene ring (or any aromatic ring) provides a target for β-interaction, which captures the energy of the incident particle. Toluene then loses the captured energy through a transfer to another solvent molecule. Thus, a β-particle will excite a number of solvent molecules as it interacts with them via the aromatic ring. This energy is transferred between solvent molecules and will eventually be absorbed by phosphor molecules (Birks, 2013).

2.9.2 The Role of Phosphors

Scintillators are classified into two categories: primary and secondary scintillators. Primary scintillators absorb the energy from the solvent molecules and re-emit it as visible light. They usually make up between 0.3 and 1% of the cocktail volume (Peng, 1970). The molecules of scintillator appear to induce a dipole moment in their solvation shell, allowing direct transfer of energy between the scintillator and excited solvent molecules separated by up to 10 other solvent molecules. Primary scintillators must be excitable to a light emitting state by excited solvent molecules, and they must be soluble in the solvent at a sufficient concentration to give efficient energy capture (Horrocks, 2012b).

Secondary scintillators, also called wavelength shifters, were originally included in scintillation cocktails to compensate for the narrow spectral response of early photomultiplier tubes (PMTs). Most primary scintillators emit light below wavelengths of 408 nm. Earlier PMTs were not very responsive at this wavelength. A secondary scintillator captures the fluorescence energy of the excited primary scintillator, and re-emits it as a longer wave length signal. Even though modern PMTs don't have the same problem, secondary scintillators have been found to increase the efficiency of LSC process and are therefore still included in LSC cocktails (Birks, 2013).

2.9.3 Quenching in LSC

In LSC quenching is any phenomenon that has an effect on the production or detection of light produced by phosphor material. Quenching can be caused by physical processes (excited molecules recombine, absorption of phosphor light) or chemical

processes, when a chemical interaction of the excited molecules leads to thermal emission instead of light emission (Birks, 2013). The level of quenching in LSC determines the detection efficiency of the counting system. A higher rate of quenching will lead to low levels of detection efficiency. There are basically four different types of quenching in LSC: absorption, chemical quenching, solvent dilution quenching and colour quenching. Chemical quench occurs during the transfer of energy from the solvent molecules to the phosphor. Any chemical species that is electronegative will influence the energy transfer process by sharing the π-electrons associated with the aromatic solvent in a chemical reaction and thus reduce the availability of π electrons necessary for efficient energy transfer, leading to poor transfer and therefore lower detection efficiencies (Horrocks, 2012a). Colour quenching is caused by the attenuation of the photons that are produced by the scintillator before they reach the Photo Multiplier Tubes (PMTs). The photons produced are absorbed or scattered by the colour in the sample mixture resulting in pulse loses. Quenching therefore results in a reduced number of counts per minute (CPMs) and a correction factor has to be applied to re-adjust to the correct decays per minute (DPMs) of the sample (Peng, 1970).

The level of quenching is defined in terms of the quenching index. The quenching index is then used to determine the quenching curves, which are representations of the relationships between the quenching level and the detection efficiency of a specific radionuclide being measured. Chemical quenching is always expected in LSC samples, and therefore if the counting of samples is to be meaningful, it is one of the measure problems that need dealing with. It is possible to compensate for quenching in LSC if the counting efficiency of the specific radionuclide being measured is known (Jia and Jia, 2012).

Chapter 3: Materials and Methods

3.1 Study Area

The Central Rand Basin geography is made up of diverse topographical features. Mountainous ranges on the northern and western sides surround Johannesburg, located in the Gauteng province of South Africa. The eastern sides of the city are flatter in comparison. The latitude of Johannesburg is -26.195246 and the longitude is 28.034088. Johannesburg is located 1765 meters above sea level. Many towns and cities encompass Johannesburg. Hillbrow and Yeoville lie towards the western region of the city, Orange Grove is in the north; Kenilworth, Turffontein and Rosettenville, borders the southern region of the city; Kensington, Malvern and Alberton are towards the east (Tutu, et al., 2008). Johannesburg has a population of over 4.4 million as of 2016, with a mostly dry and sunny climate (Beavon, 2017). There are occasional rains during the summer, which is between October and April. Johannesburg witnesses moderate weather because of its extremely high altitude. The average temperature recorded during the day, in the month of January is 26°C. The temperature falls to 16°C, during the month of June.

3.2 Sampling

Samples were collected from mining shafts and decant sites within the central basin of the Witwatersrand area. Forty samples were collected from the central basin ensuring that the sampling is as representative as possible. Samples were collected into 3 L containers to ensure there is enough sample for all analytical procedures. The water samples were acidified with concentrated HNO_3 (1.25 mL L^{-1}) for preservation.

3.3 Field measurements

A multimeter was used to take field measurements of different relevant parameters. For this study temperature, pH, conductivity and total dissolved salts were measured at the sampling sites and recorded for each sample collected.

3.4 ICP-MS for Elemental analysis and ion chromatography

For ion chromatography, the sample's electrical conductivity was determined and dilutions were done accordingly. The diluted sample was then pushed through a 0.45 µm filter and analyzed using a 761 Compact IC (ion chromatography) from Metrohm.

For ICP-MS, sample collection and sample preparation was done according to specifications and procedures described in the method, 200.8 (Creed, et al., 1994).

For the elemental analysis of the water samples the Perkin Elmer NexION 350 ICP-MS instrument was used. The detection limits for the instrument for different elements are shown in Table 4. The method 200.8 developed by the US Environmental Protection Agency was adopted for the elemental analysis in this study. Method 200.8 is a general analytical method which recommends procedures for selecting masses of analytes, calibration and tuning of the instrument, interference corrections, and sample collection instructions for optimum results, sample preservation and treatment. In addition, Method 200.8 also includes a specific set of quality assurance/control protocols to be run along with samples to ensure that data of high quality is obtained. Method 200.8 is an excellent and trusted analytical procedure which has been successfully used for the determination of trace elements in environmental samples for the past 17 years. The method includes the following steps but is not limited to them (Creed, et al., 1994):

- Ignite plasma, allow 30 minutes to warm up,
- Optimize instrument, as per instrument manufacturer's instructions,
- Perform mass calibration check – adjust if change is > 0.1 amu,
- Perform resolution check – adjust if > 0.75 amu at 5% peak height,
- Calibrate using blank and standards,
- Monitor all masses necessary for interference correction,
- Screen new samples for relative levels and presence of internal standards,
- Run instrument performance evaluation tests,
- Run quality control samples (QCSs) or standard reference materials (SRMs) such as: High-Purity Standards Trace Metals in Drinking Water (TMDW), both neat and diluted,
- Run unknown samples.

Table 4: Detection limits for different metals for ICP-MS

Step	Mass (amu)	Element	DL (ppm)
1	9	Be	1.67E-06
2	11	B	1.32E-03
1	23	Na	1.43E-02
1	24	Mg	1.48E-03
2	27	Al	3.45E-04
1	28	Si	1.20E-02
1	31	P	1.16E-03
1	34	S	1.19E-01
2	39	K	2.73E-03
1	43	Ca	5.21E-03
1	47	Ti	1.11E-05
2	51	V	3.00E-06
1	53	Cr	4.68E-05
2	55	Mn	1.92E-05
2	57	Fe	1.19E-03
1	59	Co	1.57E-06
2	60	Ni	1.36E-05
1	63	Cu	2.85E-05
2	66	Zn	2.25E-04
2	75	As	6.26E-06
1	82	Se	2.26E-04
1	85	Rb	1.97E-06
1	88	Sr	2.30E-05
1	95	Mo	2.06E-05
1	105	Pd	1.34E-06
1	107	Ag	2.23E-05
1	111	Cd	1.20E-04
1	121	Sb	3.04E-06
1	127	I	6.09E-03
1	137	Ba	1.77E-05

Step	Mass (amu)	Element	DL (ppm)
1	195	Pt	3.12E-06
1	197	Au	6.92E-06
1	202	Hg	1.29E-05
1	205	Tl	5.28E-06
1	208	Pb	5.83E-06
1	209	Bi	3.32E-06
1	232	Th	1.04E-06
1	238	U	4.33E-06

3.5 Gamma spectroscopy

The equipment used for gamma analysis consisted of; Canberra Model GCW 2021 HPGe Well detector, with relative efficiency of 20%. The resolution: FWHM @ 122 keV < 1.2 keV and FWHM @ 1332 keV < 2.1 keV and Well size: 10 mm diameter: 40 mm depth Aluminium end cap with a 2002 CSL preamplifier. It has an ultra-low background, top loading lead shield with a thickness of 100 mm. The inner dimensions are 279 mm diameter x 406 mm height, weighing 1100 kg. It has an inner lining of graded tin and copper to reduce X-rays background from lead shield interaction with gamma radiation from samples. For spectrum acquisition and analysis, Genie 2000 software was used, with a Canberra Model DSA 1000 Digital Spectrum Analyser, featuring: Integrated desktop Multi-channel Analyser, which includes DSP based pulse processing, 16 K Channel spectrum memory, multi range HVPS, digital stabilizer, USB & RS-232 serial interface.

3.5.1 Energy and Peak efficiency calibration

Energy calibration is basically matching a channel number or range of channels to a particular gamma ray energy. In this study this was achieved by measuring a combination of point sources covering the energy range 59.54 keV to 1332.5 keV (^{241}Am, ^{57}Co, ^{137}Cs, ^{54}Mn and ^{60}Co). The gain of the system was set to 0.5 keV per channel. Strong point sources were used which allowed for shorter counting times. The centroids of the peaks were then plotted against the channel numbers on the MCA.

For peak efficiency calibration two methods were used for quality assurance purposes. In the first method, LabSOCS sample and source geometry composer was used to do an efficiency calibration. This method is a simulation software from Genie 2000 which utilizes libraries and the given geometries as well as sample matrix to estimate the efficiencies at different energies using Monte Carlo methods. In the second method deionized water sample was prepared into a Marinelli beaker. The water was then spiked with measured standards of ^{238}U, ^{241}Am and ^{152}Eu. The efficiencies at given energies were calculated according to equation (5) and plotted as a function of energy (Murray et al., 1987).

$$\varepsilon(E) = \frac{N_c}{t \times Y \times m \times A}, \quad (5)$$

where:

N_c is the net peak area of the peak under consideration,
t live time of the measurement,
Y the gamma emission probability of the calibration nuclide at the energy,
m mass of standard spiked into sample,
A source activity at the time of measurement.

^{152}Eu decay with a cascade of gamma rays at different energies and due to the proximity of the sample to the detector, two different gamma rays from a cascade might reach the detector at the same time, resulting in coincidence summing. The detector adds energies of the two gamma rays and record the sum as a separate peak in the spectrum leading to loses at the original peaks. Corrections for the different gamma ray lines were effected using values obtained by Anas & Molham (2015), Schima & Hoppes (1983) and Dias et al. (2002) as well as simulation based corrections using Genie 2000 software.

Table 5: Efficiency calibration data and calculations

Energy (keV)	Intensity	Net peak area	Error	Activity (Bq)	Actual Activity (Bq)	Efficiency	error
59.540	0.359	9630.000	274.940	0.167	0.466	0.001	2.86%
92.600	0.056	1430.000	328.350	0.025	0.443	0.008	22.96%
121.782	0.286	340000.000	723.750	5.903	20.654	0.018	0.21%
244.698	0.079	94000.000	438.420	1.632	20.702	0.018	0.47%
344.278	0.265	279000.000	582.530	4.844	18.278	0.016	0.21%
411.116	0.022	20100.000	158.060	0.349	15.620	0.014	0.79%
443.965	0.028	27200.000	269.460	0.472	16.740	0.015	0.99%
778.904	0.129	80600.000	349.260	1.399	10.812	0.009	0.43%
867.378	0.042	24100.000	153.450	0.418	9.856	0.009	0.64%
964.079	0.146	83300.000	329.860	1.446	9.902	0.009	0.40%
1085.869	0.102	54200.000	206.600	0.941	9.219	0.008	0.38%
1089.737	0.017	9270.000	93.400	0.161	9.319	0.008	1.01%
1112.074	0.136	72200.000	303.940	1.253	9.187	0.008	0.42%
1212.948	0.014	6860.000	139.710	0.119	8.375	0.007	2.04%
1299.140	0.016	7350.000	76.600	0.128	7.862	0.007	1.04%
1408.006	0.215	94100.000	311.130	1.634	7.599	0.007	0.33%

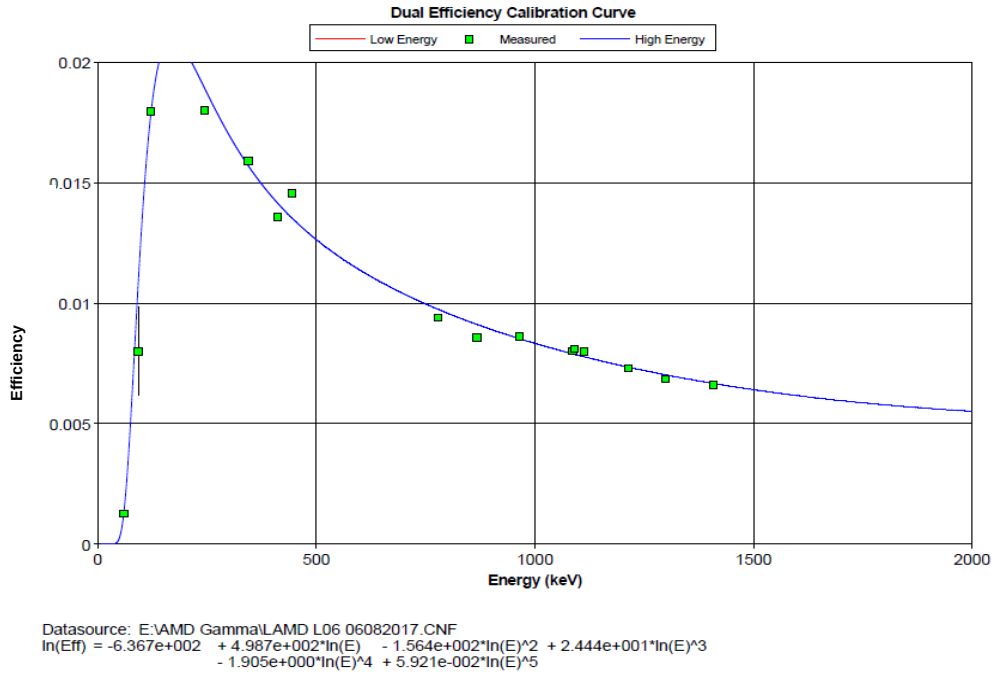

Figure 6: Efficiency calibration curve with fifth order polynomial fit on a linear scale.

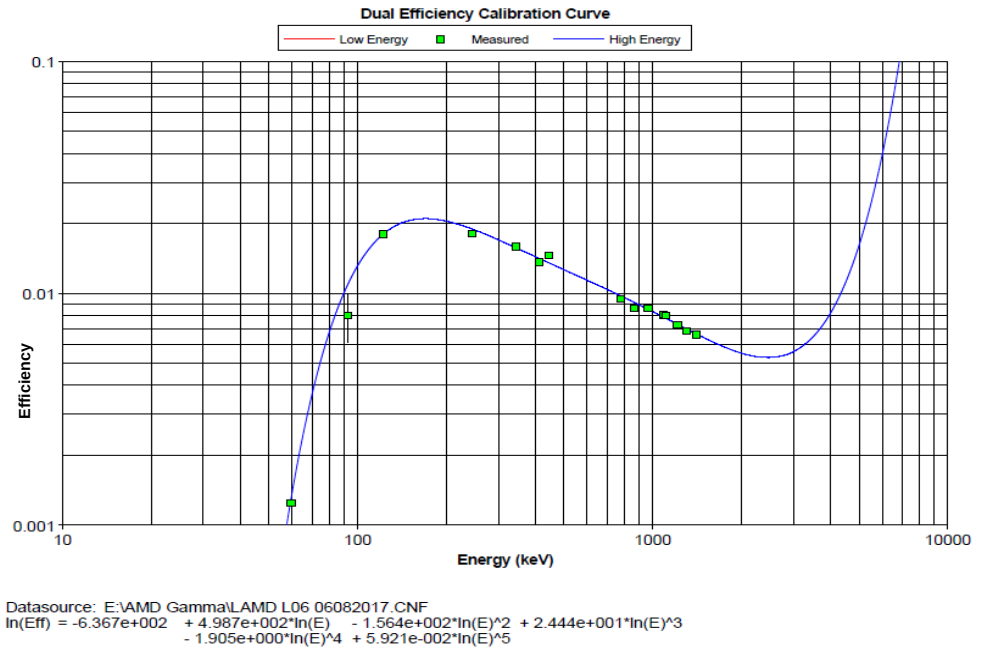

Figure 7: Efficiency calibration curve with fifth order polynomial fit on a logarithmic scale.

Figure 6 and Figure 7 show the efficiency calibration curve for the HPGe detector. The maximum efficiency attainable was 2.2% at an energy of 180 keV. The efficiency is very low at low energies, mainly due to the fact that low energy gammas are easily absorbed by the sample and therefore the high loses leads to lower efficiencies. The

efficiency then rises quickly to reach a maximum at around 180 keV, after which it exponentially decreases as the energy of the gamma decreases. The data shown in Table 5 was fitted into a fifth order polynomial using Genie 2000 software from Canberra. The relationship between the efficiency and the gamma energy is given in equation (6).

$$\ln(Eff) = -636.7 + 498.7\ln(E) - 156.4\ln(E)^2 + 24.44\ln(E)^3 - 1.905\ln(E)^4 + 0.0592\ln(E)^5 \quad (6)$$

Where Eff is the photo-peak efficiency and
E is the photo-peak energy.

3.5.2 Activity Analysis

To measure the activity of ^{238}U in the water samples, secular equilibrium with its immediate daughter nuclides, ^{234}Th was assumed because the AMD has been formed for a long enough period to have established equilibrium. ^{234}Pa gives off two reasonable gamma ray lines, with energies 766.36 keV and 1001.03 keV. Both gamma lines have very low intensities and are also in the low efficiency region of the detector. The positive part about them is that the level of background in that region is quite low and therefore the lines, especially the 1001.03 keV line can be identified with ease. ^{234}Th has a gamma line with energy of 63.29 keV which doesn't have major interferences from other NORM nuclides. The problem with the gamma line is its low intensity and the fact that it is found in a low efficiency, high background region in the gamma spectrum. It also has two gamma lines at 92.38 keV and 92.8 keV, with a combined intensity of 5.8%. This line is in a region where the background is not too high and the efficiency of the germanium detector is good. Lines from ^{231}Th, ^{234}U and ^{235}U present negligible interference to the combined gamma line, 92.6 keV. Therefore in the analysis of ^{238}U activity concentration, the 1001.03 keV gamma line from ^{234m}Pa and the 92.6 keV gamma line from ^{234}Th were used.

^{226}Ra has a half-life of 1600 years and is a long lived radionuclide in the uranium decay series. ^{214}Pb and ^{214}Bi are two daughter radionuclides of ^{226}Ra that can be used to measure its activity. For ^{226}Ra to be evaluated using these daughter nuclides, they have to be measured after the establishment of radioactive secular equilibrium between ^{226}Ra, ^{222}Rn, ^{214}Bi and ^{214}Pb by sealing of samples for about 30 days. Another

method is to measure the activity directly using the ^{226}Ra peak at 186.1 keV. The problem with that is the interference caused by the 185.7 keV ^{235}U peak, which will need corrections and lead to introduction of extra uncertainty. For this study the average activity concentration obtained from the ^{214}Pb line at 351.9 keV and the ^{214}Bi line at 609.31 keV was used in the determination of ^{226}Ra because these lines have no problems with summation of peaks from different but close energy emissions.

^{232}Th has a half-life of 1.41×10^{10} years and is the parent radionuclide of the thorium decay series. Thorium-232 has a gamma ray line at 63.81 keV which overlaps a line of ^{234}Th at 63.28 keV. Therefore it cannot be determined directly via gamma spectroscopy in samples. ^{228}Ac has a half-life of 6.15 h and will be in secular equilibrium with ^{232}Th within 5 days. The 911.2 keV gamma line of ^{228}Ac was used as the primary line for the determination of ^{232}Th activity. Other lines that were considered in the evaluation of the ^{232}Th activity were the 338 keV line from ^{228}Ac, 238.6 keV line from ^{212}Pb and the 583 keV line from ^{208}Tl. ^{40}K was determined directly from its 1461 keV gamma line.

3.6 Gross alpha & gross beta counts

Gross alpha and beta activity in drinking water samples will be determined according to a modified Standard Test Method for Alpha- and Beta-Activity in water by Liquid Scintillation Counting (ASTM D7283-06) (Todorović et al., 2012). The method describes the measurement of gross alpha & beta counts in environmental water samples. The counting efficiencies for alpha and beta components depend on the energy of the alpha or beta emitter used for calibration. This relationship therefore means that the radionuclides that were used as calibration standards resembled as close as possible the alpha or beta emitters expected to be in the sample being measured.

When counting gross alpha and beta activity with liquid scintillation counter using alpha/beta discrimination, some pulses resulting from alpha particles are detected as beta particles and some pulses resulting from beta particles are detected wrongly as alpha particles. The process is called spill-over, and occurs in both the alpha and beta channels. The percentage spill-over for alpha particles onto the beta channel and the percentage spill-over for beta particles onto the alpha channel was calculated during the calibration of the instrument.

Quenching of the photon output in the liquid scintillation cocktail reduces detection efficiency and introduces additional uncertainty in spill-over corrections. Quenching is caused by the absorption of emitted visible and UV photons by molecular species in the sample and cocktail mixture before detection. The effects of quenching were minimized by using an external standard source, ^{226}Ra. Samples were filtered prior to analysis since the presence of solid matrices in the sample would have caused interference and led to misleading results (Todorović et al., 2012).

3.6.1 Materials

For the measurement of gross alpha and beta counts, an ultra-low background level liquid scintillation counter, Wallac Quantalus 1220, was used. The Quantulus 1220 is fitted with an external capsule of 37 kBq of ^{152}Eu, which is used to measure the SPQ(E) of the samples/standards used. Twenty millilitre polyethylene liquid scintillation vials supplied by Perkin Elmer were used. Cocktail, Ultima Gold uLLT, optimised for measurement of environmental water samples was used for all measurements in the study. The following standard solutions were used: ^{241}Am with an activity of 375.6 kBq on the 1 November 2015, supplied as a 20 ml solution by Eckert & Ziegler Isotope products (source number: 1839-40-1) and ^{90}Sr with an activity of 392.9 kBq on the 1 November 2015, supplied as a 20 ml liquid solution by Eckert & Ziegler Isotope products (source number: 1839-40-2).

3.6.2 Methods

Acid mine drainage samples used in this study were collected from an AMD pumping station as well as an AMD seepage dam. Alpha standard was prepared from the ^{241}Am standard solution obtained from Eckert & Ziegler. 100 ml of AMD sample was transferred into a graduated beaker using a measuring cylinder. The AMD sample was filtered through a Whitman number 42 filter paper as is the practice in the analysis of water samples. A new standard alpha standard solution was prepared by pipetting 200 µL of the ^{241}Am Eckert & Ziegler liquid standard into the 100 ml AMD sample and the solution was stirred for 3 minutes to achieve homogeneity. The activity concentration of the created standard solution was then calculated as 18.7 kBqL^{-1}, with an activity of 1122 DPM per millilitre of standard solution, considering decay from reference date of the original standard. The reason for preparing the alpha standard in this way was to

have a common solution with a uniform activity concentration, from which different volumes can be taken to create increasing quench levels. It was observed under earlier attempts that preparing different standards separately by pipetting individual standard volumes leads to differences in the activities in the created standards, mainly due to inconsistencies in transferring the standard using the micro pipette. The beta standard, ^{90}Sr was prepared in a similar manner as the alpha standard using the same AMD sample to create an internal standard. The activity concentration of the created beta standard was 19.0 kBqL^{-1}, with an activity of 1140 DPM. The reference date of the original standard was 2015, therefore ^{90}Sr is expected to be in equilibrium with its daughter nuclide ^{90}Y. This means that the expected decay rate of the standard solution will be double that of the ^{90}Sr.

Standards, quenching at different levels were created by mixing different volumes of the created standard with Ultima Gold uLLT cocktail. The total volume of the solution to be counted was 20 ml, with minimum volume of 10 ml for the cocktail and a maximum of 10 ml for the aqueous standard solution. Two sets, one set comprising of the alpha standards and the other of the beta internal standard solutions were created by combining the spiked AMD samples and Ultima Gold uLLT cocktail in the following ml ratios; 1:19, 2:18, 3:17, 4:16, 5:15, 6:14, 7:13, 8:12 and 9:11.

3.6.3 PSA optimization

The Quantulus 1220 uses two Multi Chanel Analysers (MCA), one being used as an active shield while the other one is used for sample spectrum recording. Each of the two MCAs has two halves, each half having 1024 channels. Each half corresponds to either alpha or beta pulses. PSA is used to set a discriminator for alpha and beta pulses. There are 256 PSA discriminator settings in the Quantulus, and they can be pre-set by the user before counting of a sample. Discriminator uses the tail area of the pulses generated during counting, alpha events have longer tails compared to beta events (Stojković et al., 2016). PSA calibration/optimization in this study used percentage misclassification or spill-over of alpha and beta pulses into the wrong channel. Equations (7) and (8) were used to evaluate the percentage misclassification or spill-over for alphas and betas respectively (Perera, 2005).

$$\alpha_{mc}(\%) = \frac{\alpha_{\beta}}{\alpha_{\alpha+\beta}}.100\ , \qquad (7)$$

$$\beta_{mc}(\%) = \frac{\beta_{\alpha}}{\beta_{\alpha+\beta}}.100 \ , \qquad (8)$$

where $\alpha_{mc}(\%)\ and\ \beta_{mc}(\%)$ are the percentage alpha and percentage beta misclassifications respectively, $\alpha_{\beta}\ and\ \beta_{\alpha}$ are the alpha counts in beta channel and beta counts in alpha channel respectively and $\alpha_{\alpha+\beta}\ and\ \beta_{\alpha+\beta}$ are the total alpha counts and total beta counts in the spectrum. The optimum PSA value is the one where there is equal and minimum alpha and beta misclassification, marked with an X in Figure 8. In this study, 9 alpha and 9 beta internal standards were counted with PSA setting from 30 to 150, increasing by steps of 10. Each of the 9 internal standards for either alpha or beta had increasing quenching levels. So the PSA optimization involves the optimization of PSA at different sample quenching levels, since the level of quenching also has an effect on the percentage misclassification. Each standard was counted for 10 minutes because the activity of each standard was high enough to attain negligible counting errors. The samples were also counted with the same PSA settings, but without spiking with internal standards in order to subtract their activity from that of the spiked samples.

Pulse discrimination is important in the seperation of alpha and beta pulses. Poor discrimination results in the misclassiffication of either alpha pulses as beta pulses and beta pulses as alpha pulses. Therefore at an optimized PSA setting, the pulse discrimination is such that there is the lowest level of misclassification of either alpha or beta pulses. In this study at low PSA values, PSA< 100, the misclassification of alpha pulses as beta pulses is minimal, with a maximum misclassification observed of 0.58% with the highest quenching level used in this study. The misclassification of alpha pulses then increase exponentially at PSA setting values above 100. Therefore if a study is optimizing the measurement of an alpha emmiter, PSA 100 or lower is recommended. Higher PSA settings will result in higher misclassification and loss of alpha counts into the beta channel. Higher PSA settings lead to low misclassification of beta pulses. The highest misclassification at PSA settings above 100 was 1.67%, observed in the lowest quenching level in the study. Therefore to optimize for the counting of a beta emmiter, especially in the absence of an alpha emmiter, higher PSA settings are recommended. But in the presence of an alpha emmitter, it is not recommended to use higher PSA settings, even when optimizing for the counting of a beta emmiter. This is due to the fact that at higher PSA settings, misclassification of

alpha pulses increases, and therefore it would lead to an over estimation of the actual beta activity. This results in the need for a good tradeoff setting where there is minimum alpha and beta pulse misclassification. In this study pure alpha and pure beta emmiters were counted over a range of PSA settings, and the percentage misclassification was evaluated. Figure 8 demonstrates the variation of both alpha and beta misclassification over a range of PSA settings. The crossover point of the graphs for alpha and beta misclassification represents the optimum PSA setting for that specific quench level. Small errors in the optimum PSA settings of less than 6 do no lead to huge errors in the misclassificiation. The impact of an error in PSA setting is much more pronouced if the error is towards a higher PSA setting than the optimum. At SPQ(E) 757, an error of +10 in the optimum PSA setting leads to a 6% alpha misclassification and less than 1.5% beta misclassification, while an error of -10 leads to less than 0.5% alpha misclassification and 2% beta misclassification. This gives an allowance to optimise more for alpha counting by using a PSA value that is less than the experimentally determined optimum PSA because as much as it reduces the alpha misclassification it doesn't increase the beta misclassification by much. This suggests therefore that the best PSA for counting a sample might actually be 15-25 PSA values below the experimentally determined PSA setting. As an example, the samples shown in Figure 8 with an SPQ(E) value of 757 can be counted at PSA 80, with 0.05% alpha misclassification and 4% beta misclassification. This approach must be avoided though in a case where the beta activity of the sample being counted is expected to be very high compared to the alpha activity, as this might lead to significant increase in the alpha activity.

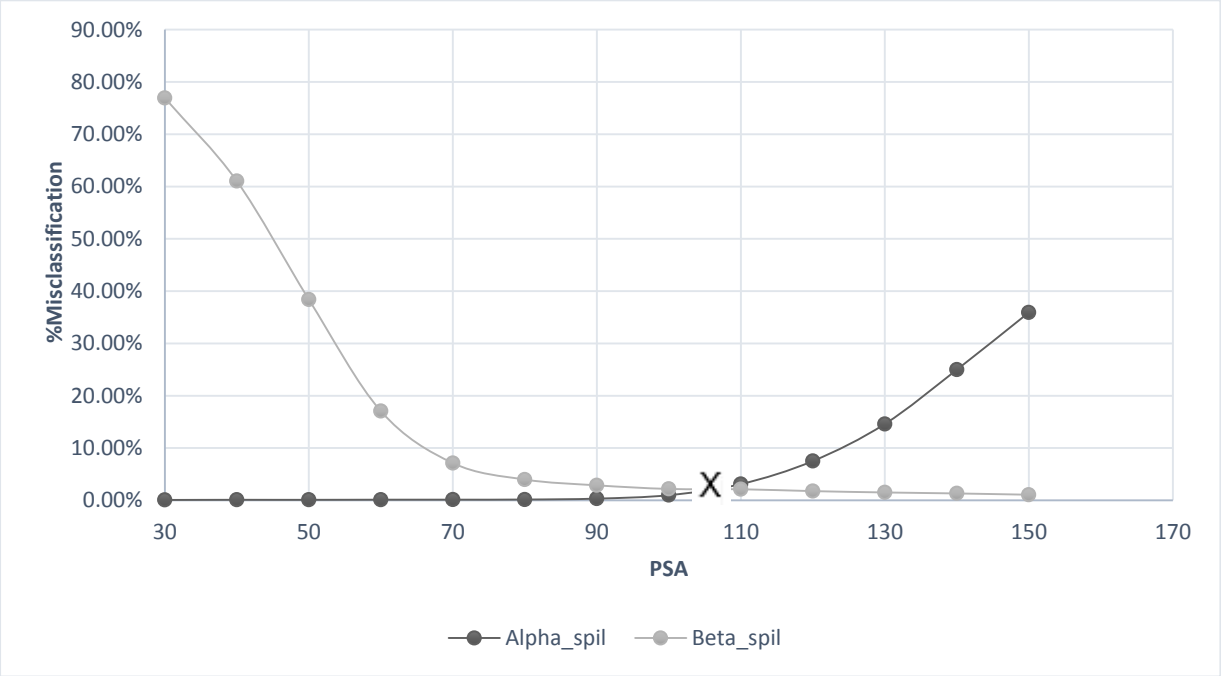

Figure 8: The effect of PSA on the percentage misclassification of alpha and beta pulses.

Figure 9 demonstrates the relationship between the optimum PSA setting and the level of quenching of the sample being counted. Generally, the optimum PSA value increases as the level of quenching decreases. The highest quenching sample in this study had an SPQ(E) value of 715 and the optimum PSA value for counting that sample was 94, while the least quenched sample counted in this study had an SPQ(E) value of 788 and an optimum PSA value of 117. A linear curve was fitted into the data to enable the determination of the optimum PSA value for samples that are quenching at least within the SPQ(E) range 700-800. The regression fit is presented in equation (9). The regression coefficient (R^2) of the fit is 0.94.

$$Opt.PSA = 0.2768 * SPQ(E) - 103.51 \quad (9)$$

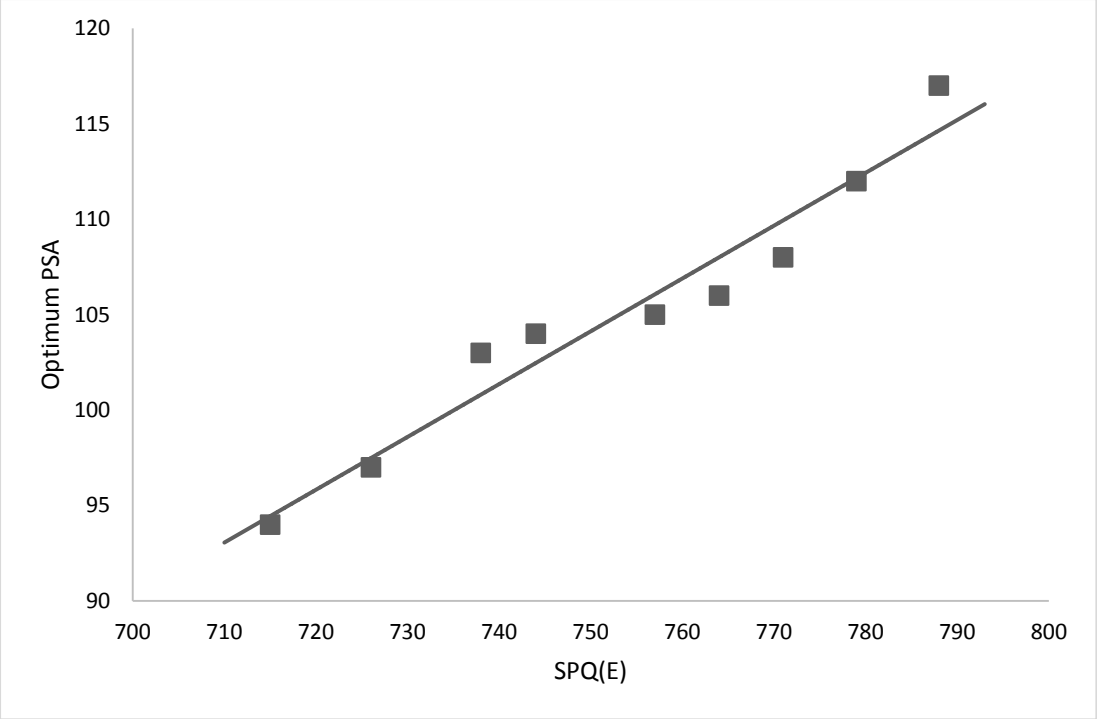

Figure 9: Optimum PSA settings for different levels of quenching.

3.6.4 Efficiency calibration

The efficiency of a liquid scintillation system is dependant of factors that cause the loss of pulses generated by incoming radiation. In liquid scintillation counting those factors are quenching and pulse discrimination settings. The energy of the incoming alpha or beta radiation also has an effect on the counting efficiency of the system (Salonen, 2005). For that reason, when performing an efficiency calibration the energy of the standard radionuclides must resemble the intended analytical targets as far as possible. The counting efficiency for alpha radiation is different from that of beta radiation and therefore in a calibration a beta standard as well as an alpha standard has to be used, as was in this study. The counting efficiency can be defined as the percentage of radiation particles detected and recorded by the detector as compared to the number produced from the decay radioactive source. The counting efficiency can be calculated using equations (10) and (11).

$$\varepsilon_{\alpha}(\%) = \frac{\alpha_{CR}}{\alpha_{DR}}.100, \quad (10)$$

$$\varepsilon_{\beta}(\%) = \frac{\beta_{CR}}{\beta_{DR}}.100, \quad (11)$$

where $\varepsilon_\alpha \; and \; \varepsilon_\beta$ are the alpha and beta efficiencies, $\alpha_{CR} \; and \; \beta_{CR}$ are the count rates of the standards and $\alpha_{DR} \; and \; \beta_{DR}$ are the alpha and beta source disintegration rate.

Sample quenching in LSC leads to a reduction in the number of both alpha and beta counts and therefore a reduction in the counting efficiency of the detection system. The effect of quenching differs for alpha and beta radiation. Alpha counting efficiency is more resistant to quenching than beta counting efficiency. The beta counting efficiency decreases with increasing quench to a minimum at SPQ(E) 740 and then it starts to increase with increasing quench. The beta efficiency varies as a second polynomial, according to equation (12).

$$\varepsilon_\beta = 2 \times 10^{-5}(SPQ(E))^2 - 0.0225\big(SPQ(E)\big) + 9.2983 \qquad (12)$$

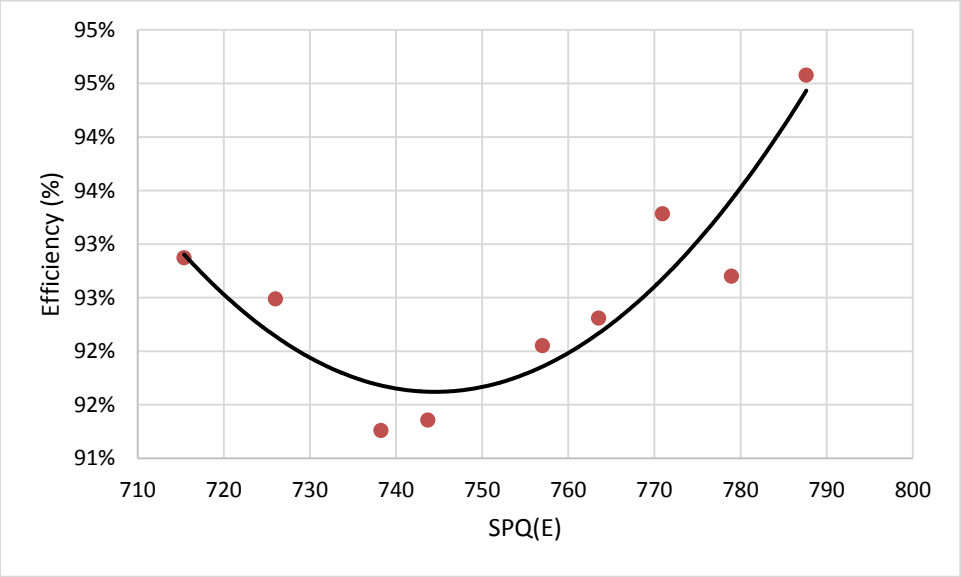

Figure 10: Beta counting efficiency dependence on the quenching level of a sample.

The alpha counting efficiency generally decreases as the quenching of the sample increases as seen in Figure 11. It varies as a second order polynomial and the relationship is described by equation (13).

$$\varepsilon_\alpha = 1 \times 10^{-5}(SPQ(E))^2 - 0.0145\big(SPQ(E)\big) + 6.1963 \qquad (13)$$

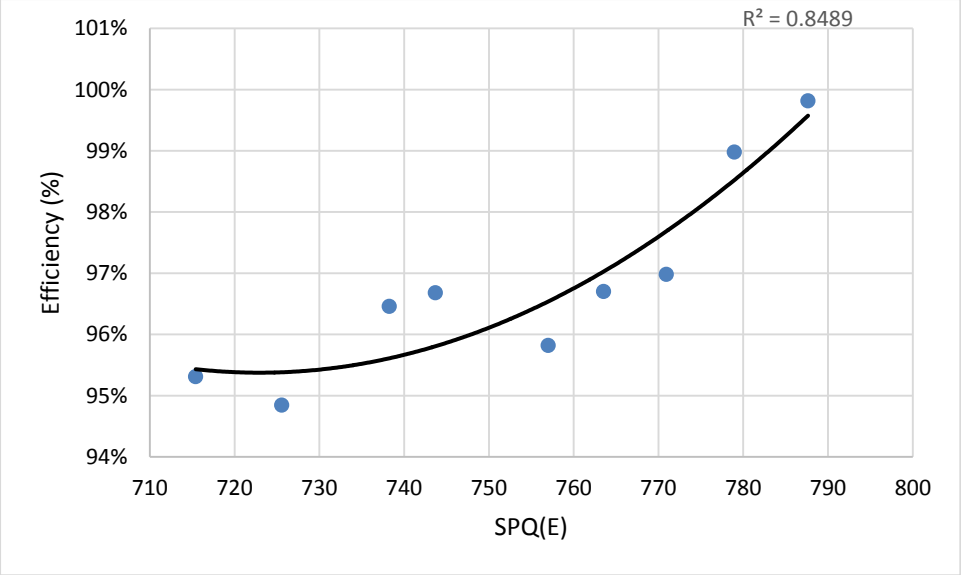

Figure 11: Dependence of alpha counting efficiency on the quenching level of a sample.

3.6.5 Effect of Quench on spill-over

Quenching has an effect on the misclassification of both alpha and beta pulses in liquid scintillation counting. There is a general increase in the misclassification of alpha pulses as the quenching of the sample increases (decreasing SPQ(E) value). Figure 12 demonstrates the variation of misclassification of both alpha and beta pulses as the level of sample quenching changes. The effect of quenching on misclassification is not the same for betas as it is for alpha pulses. Beta misclassification is low, 1% at quenching levels of around SPQ(E) 715, increasing slightly to a maximum of 2.3% at SPQ(E) 744 and then drops to 1.41% at SPQ(E) 788. The variation of the misclassification with quenching follows a similar trend at the different PSA settings, though the misclassification values will vary from one PSA value to the next.

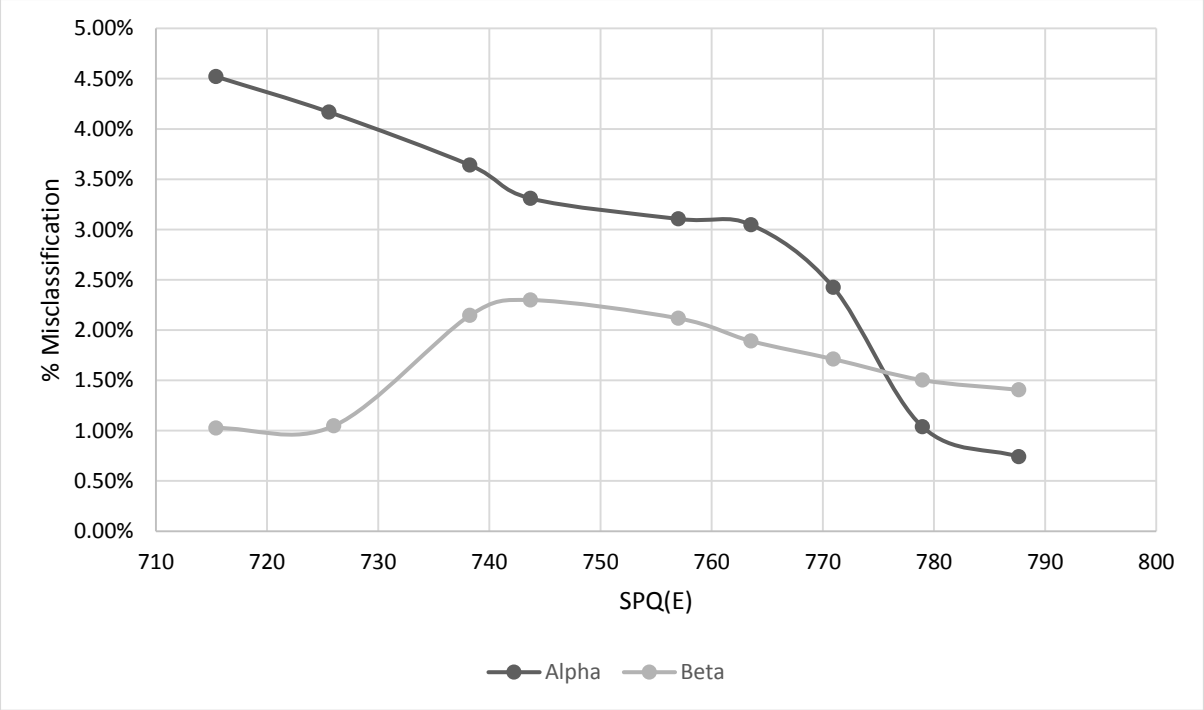

Figure 12: The effect of quenching on alpha and beta misclassification/ spill-over.

3.7 Treatment methods

3.7.1 Coagulation & Filtration

A common purification method for water is a combination of chemical coagulation–flocculation and filtration. In this study the coagulant that was used was Aluminium sulphate hydrate. The reason for the choice was that all other major inorganic coagulants lower the pH of the water, which was not desirable when the pH was already very low, as it was in AMD. Samples were adjusted for pH using a 2.5 M solution of sodium hydroxide. They were then filtered to remove any precipitates that were formed. The samples were then poured into 600 mL measuring cylinders and dosed with aluminium sulphate hydrate. A stuart® flocculator, model SW5, shown in Figure 13, was used for precise mixing speeds. A flash mixing step at 150 rpm for 60 s was then followed by a slow mixing step at 40 rpm for 30 minutes. The treated samples were then allowed to settle for 24 hours.

Figure 13: SW5 flocculator with variable mixing speeds.

Figure 14: Macro-flocs forming during the slow mixing stage of coagulation/flocculation.

3.7.2 Ion Exchange

To carry out the procedure, a 25 mm diameter borosilicate glass column with a sintered glass bottom was used. Two columns were connected one to the other. In the first column there was the anion exchange resin and in the second column there was the anionic exchange resin. The outlet at the bottom of the second glass column was fitted with a pipe connected to a flow controller, to control the flow rate through the columns. The second column was airtight and therefore the rate of flow through the first column was easily controlled by controlling the flow rate through the second column, keeping the flow arte through both columns constant and equal. A nylon cloth was placed at the bottom of each column to retain the resin in the bed. The design of the column was such that the holder of the nylon screen was not at the very bottom of the column, leaving about 10-15 cm in height of free space. This was important because it kept the resin above the treated water outlet, preventing it from blocking the outlet. Additional equipment used included a funnel, tubing, cotton or glass wool, and a graduated cylinder. The experimental setup is shown in Figure 15.

Figure 15: Experimental setup for ion exchange treatment.

Figure 16 to Figure 19 present data for four types of ion exchange resins from purolite. These are the raisins which were available for experimentation. MTA8000PPSO4 was used for the removal of anionic species in the treatment. The resin was chosen because from initial analysis, it was shown that the major contribution to the radioactivity in the AMD comes from uranium. The resin is designed specifically for the removal of uranium from any solution, including waste water. Purolite® C100H was used for the removal of cationic species from the AMD. The samples were adjusted to pH 8 using 2.5 M NaOH solution. This pH was predicted by the chemical speciation models and confirmed with satellite experiments.

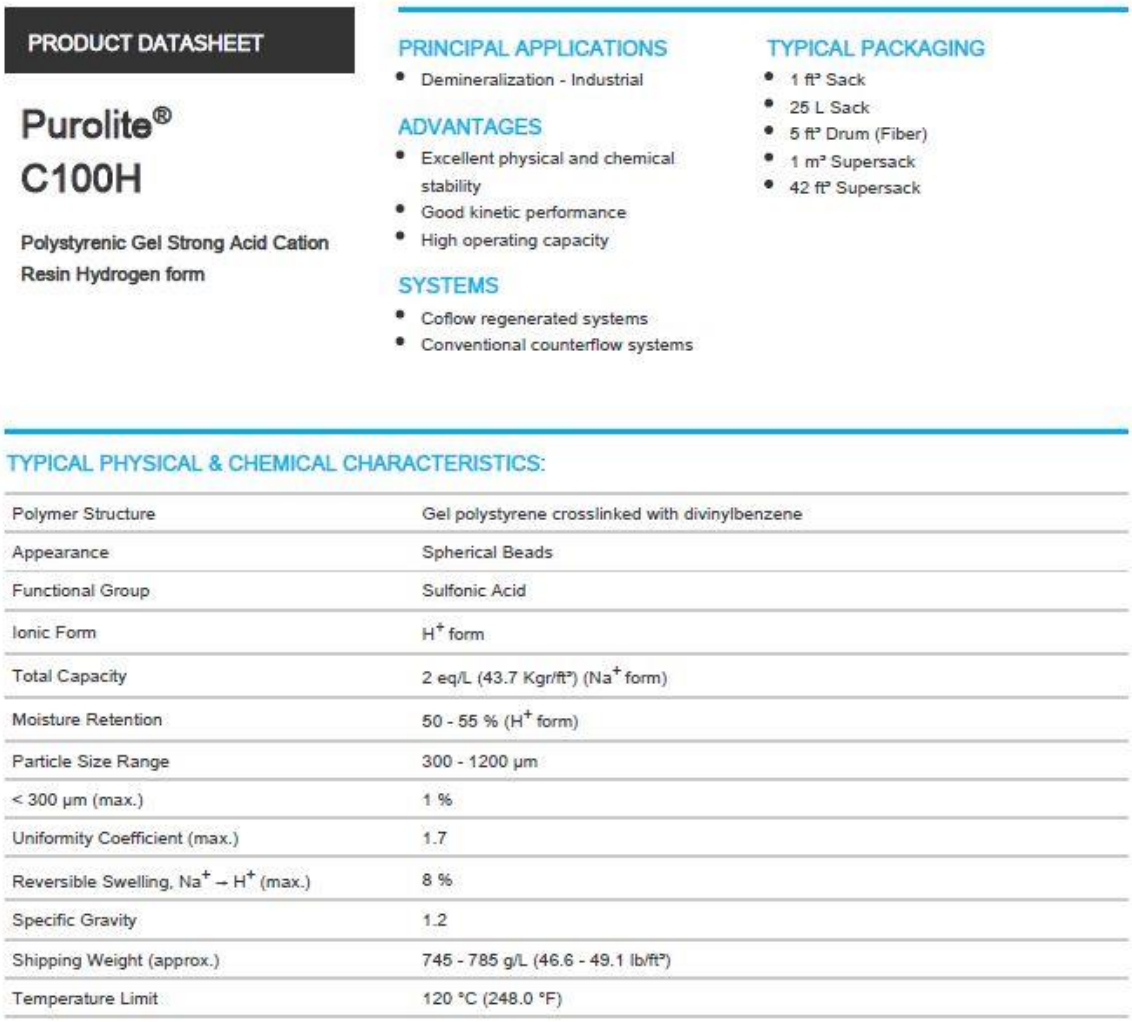

PRODUCT DATASHEET

Purolite®
C100H

Polystyrenic Gel Strong Acid Cation Resin Hydrogen form

PRINCIPAL APPLICATIONS
- Demineralization - Industrial

ADVANTAGES
- Excellent physical and chemical stability
- Good kinetic performance
- High operating capacity

SYSTEMS
- Coflow regenerated systems
- Conventional counterflow systems

TYPICAL PACKAGING
- 1 ft³ Sack
- 25 L Sack
- 5 ft³ Drum (Fiber)
- 1 m³ Supersack
- 42 ft³ Supersack

TYPICAL PHYSICAL & CHEMICAL CHARACTERISTICS:

Polymer Structure	Gel polystyrene crosslinked with divinylbenzene
Appearance	Spherical Beads
Functional Group	Sulfonic Acid
Ionic Form	H^+ form
Total Capacity	2 eq/L (43.7 Kgr/ft³) (Na^+ form)
Moisture Retention	50 - 55 % (H^+ form)
Particle Size Range	300 - 1200 µm
< 300 µm (max.)	1 %
Uniformity Coefficient (max.)	1.7
Reversible Swelling, $Na^+ \rightarrow H^+$ (max.)	8 %
Specific Gravity	1.2
Shipping Weight (approx.)	745 - 785 g/L (46.6 - 49.1 lb/ft³)
Temperature Limit	120 °C (248.0 °F)

Figure 16: Purolite C100H Cation exchange resin datasheet.

PRODUCT DATASHEET

Shallow Shell™ SSTC60

Polystyrenic Gel Strong Acid Cation Resin Sodium form, Shallow Shell™ Technology*

PRINCIPAL APPLICATIONS

- Softening - Industrial
- Demineralization when regenerated with acids

ADVANTAGES

- Highest regeneration efficiency
- Highly effective iron removal
- Highest salt efficiency
- Lower rinse volumes
- Excellent physical and chemical stability

SYSTEMS

- Coflow regenerated systems
- Counterflow regenerated systems
- Potable water treatment

REGULATORY APPROVALS

- Certified by the WQA to NSF/ANSI-61 Standard

TYPICAL PACKAGING

- 1 ft³ Sack
- 25 L Sack
- 5 ft³ Drum (Fiber)
- 1 m³ Supersack
- 42 ft³ Supersack

** SST® is a registered trademark of Purolite Corporation.*

TYPICAL PHYSICAL & CHEMICAL CHARACTERISTICS:

Polymer Structure	Gel polystyrene crosslinked with divinylbenzene
Appearance	Spherical Beads
Functional Group	Sulfonic Acid
Ionic Form	Na^+ form
Dry Weight Capacity (min.)	3.8 eq/kg (Na^+ form)
Moisture Retention	36 - 46 % (Na^+ form)
Particle Size Range	300 - 1200 µm
< 300 µm (max.)	1 %
Uniformity Coefficient (max.)	1.7
Reversible Swelling, $Na^+ \rightarrow H^+$ (max.)	6 %
Shipping Weight (approx.)	775 - 825 g/L (48.4 - 51.6 lb/ft³)
Temperature Limit	60 °C (140.0 °F)

Figure 17: Purolite Shallow shell technology cation exchange resin datasheet.

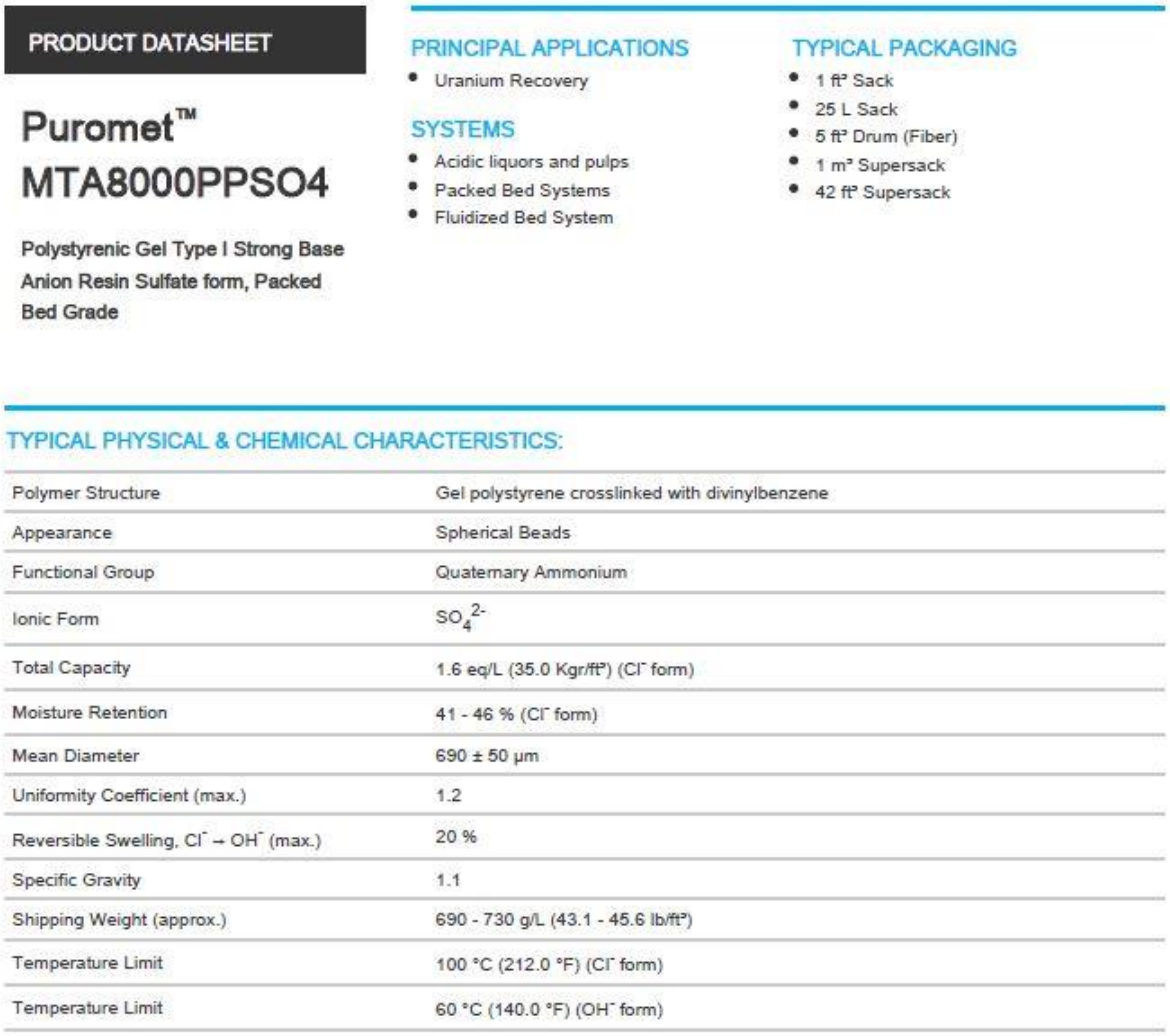

PRODUCT DATASHEET

Puromet™ MTA8000PPSO4

Polystyrenic Gel Type I Strong Base Anion Resin Sulfate form, Packed Bed Grade

PRINCIPAL APPLICATIONS

- Uranium Recovery

SYSTEMS

- Acidic liquors and pulps
- Packed Bed Systems
- Fluidized Bed System

TYPICAL PACKAGING

- 1 ft³ Sack
- 25 L Sack
- 5 ft³ Drum (Fiber)
- 1 m³ Supersack
- 42 ft³ Supersack

TYPICAL PHYSICAL & CHEMICAL CHARACTERISTICS:

Polymer Structure	Gel polystyrene crosslinked with divinylbenzene
Appearance	Spherical Beads
Functional Group	Quaternary Ammonium
Ionic Form	SO_4^{2-}
Total Capacity	1.6 eq/L (35.0 Kgr/ft³) (Cl^- form)
Moisture Retention	41 - 46 % (Cl^- form)
Mean Diameter	690 ± 50 µm
Uniformity Coefficient (max.)	1.2
Reversible Swelling, $Cl^- \rightarrow OH^-$ (max.)	20 %
Specific Gravity	1.1
Shipping Weight (approx.)	690 - 730 g/L (43.1 - 45.6 lb/ft³)
Temperature Limit	100 °C (212.0 °F) (Cl^- form)
Temperature Limit	60 °C (140.0 °F) (OH^- form)

Figure 18: Purolite packed bed grade anion exchange resin datasheet.

PRODUCT DATASHEET

Shallow Shell™ SSTPPA64

Polystyrenic Gel Type I Strong Base Anion Resin Chloride form, Shallow Shell™ Technology*, Puropack Grade

PRINCIPAL APPLICATIONS
- Demineralization
- Silica Removal

REGULATORY APPROVALS
- Certified by the WQA to NSF/ANSI-61 Standard

ADVANTAGES
- Highest regeneration efficiency
- Very low silica leakage

TYPICAL PACKAGING
- 1 ft³ Sack
- 25 L Sack
- 5 ft³ Drum (Fiber)
- 1 m³ Supersack
- 42 ft³ Supersack

SYSTEMS
- Packed Bed Systems
- Coflow regenerated systems
- Potable water treatment

** SST® is a registered trademark of Purolite Corporation.*

TYPICAL PHYSICAL & CHEMICAL CHARACTERISTICS:

Polymer Structure	Gel polystyrene crosslinked with divinylbenzene
Appearance	Spherical Beads
Functional Group	Type I Quaternary Ammonium
Ionic Form	Cl^- form
Dry Weight Capacity (min.)	2.7 eq/kg (Cl^- form)
Moisture Retention	43 - 51 % (Cl^- form)
Mean Diameter	650 ± 50 µm
Uniformity Coefficient (max.)	1.3
Reversible Swelling, $Cl^- \rightarrow OH^-$ (max.)	20 %
Specific Gravity	1.08
Shipping Weight (approx.)	670 - 710 g/L (41.9 - 44.4 lb/ft³)
Temperature Limit	60 °C (140.0 °F)

Figure 19: Purolite shallow shell technology anion exchange resin datasheet.

3.7.3 Reverse Osmosis

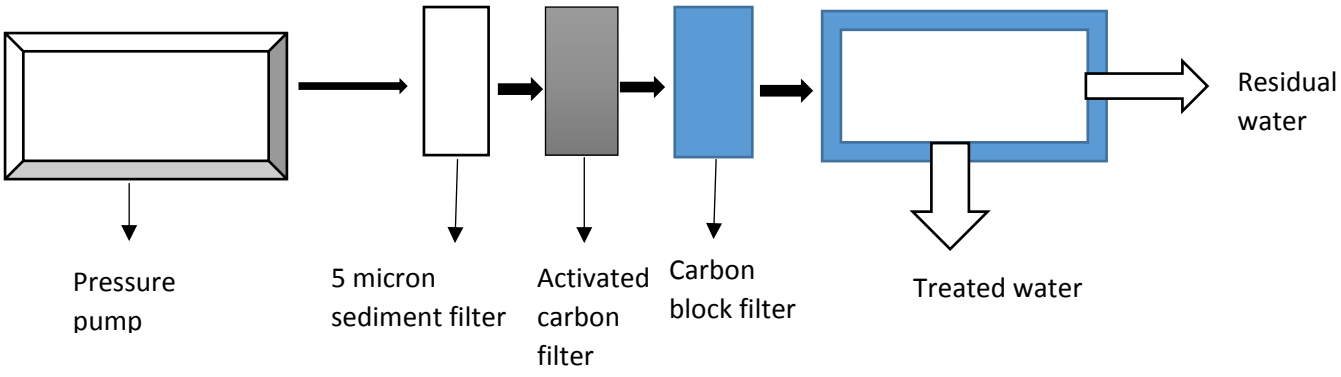

Figure 20: Schematic diagram of reverse osmosis experimental setup.

Figure 21: Reverse osmosis water purification system.

Figure 20 shows the schematic setup which was employed in the study, with Figure 21 showing the commercial system that was used. Samples collected were used as feed-water into a reverse osmosis water treatment equipment with components as shown in Figure 20. Depending on the pH and membrane requirements, pH adjustment was performed using 2.5 M sodium hydroxide solution. The first part of the setup was a pressure pump to provide pressure to force the water through the membrane against gradient. The water was pre-processed via three steps, the first of which was sediment filtration using a 5 micron sediment filter to remove any dirt, sand or any other solids. The second stage was filtration using an activated carbon filter to remove odor in the water. The final pre-treatment step was a Carbon Block filter which removed chlorine and organic chemicals from the water. After the three pre-treatment steps, the water went into a TFC reverse osmosis membrane for rejection of most inorganic species in the water including heavy metals and radionuclides. Treated

water was collected and stored in sample containers and the residual water was collected and disposed into storage tanks within the CARST facilities.

3.7.4 pH adjustment

The pH of the AMD water samples was very low, in some samples it was below 2. Reverse osmosis is most effective when the pH of the feed water is around pH 8 or 8.5. Therefore the pH of the AMD samples had to be raised to that level. Two stock solutions of NaOH were used in the adjustment of the pH. The primary stock solution was a 2.5 M solution which was used for coarse adjustment and a 1.25 M solution which was used for finer pH adjustment. Lower concentration solutions were initially tested but they led to a significant increase in the volume of the samples, which was not desired. Figure 22 shows the evaluation of the stock solution for suitability as a pH adjustment solution. From the figure, the solution starts off being clear, and then with the addition of the stock solution in increments of 1 mL, the color of the solution changes from clear to golden, then to golden brown and as the pH is increased further the higher concentration of the precipitate leads to a darker shade of golden brown in the solution. The experiment was done by adding 1 mL of the 2.5 M NaOH solution to 200 mL of a sample that was chosen at random. After each addition, the pH was then monitored using a digital pH meter as shown in the Figure 22. There are two different types of AMD samples that were collected, one set was collected through a pump from the underground mining shafts and the other set was collected from the surface. The two samples have different chemistry and therefore the adjustment of the pH would vary for each in terms of the amount of NaOH needed to increase the pH by a specific amount. After the addition of the NaOH solution, a plot of volume of pH vs NaOH volume, was created. Figure 23 shows the adjustment curve obtained for the AMD samples that were collected on the surface.

Figure 22: Picture collage showing steps in the evaluation of the 2.5 M NaOH solution for pH adjustment purposes.

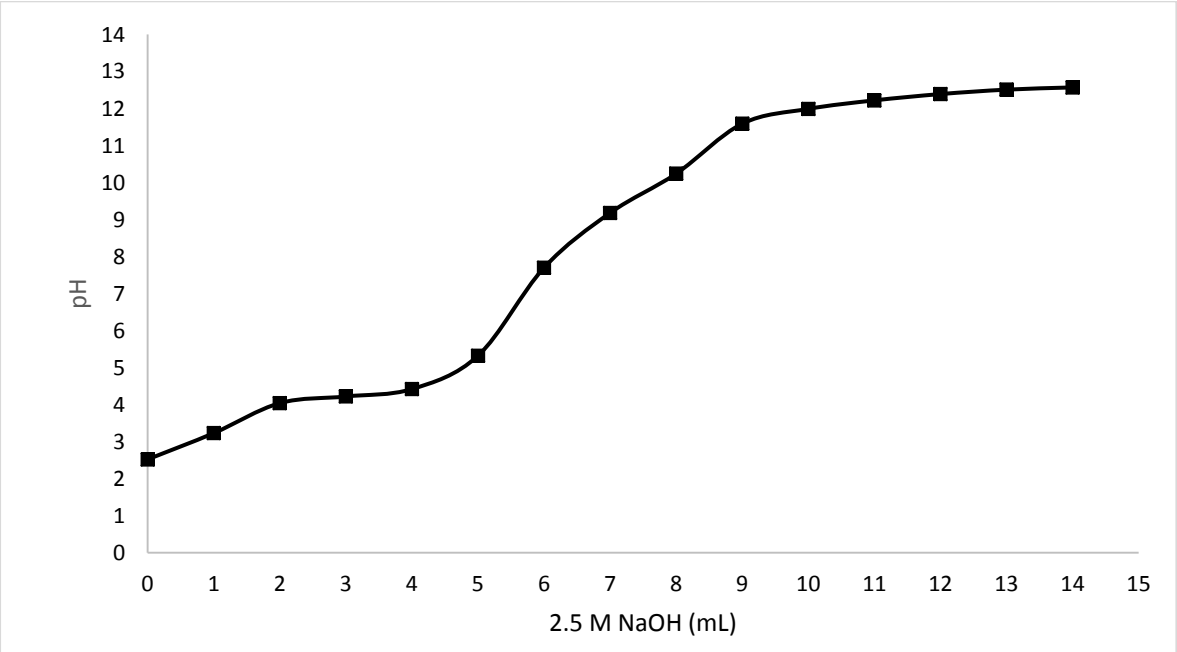

Figure 23: The pH adjustment of surface AMD with 2.5M NaOH solution to calibrate for pH adjustment of samples.

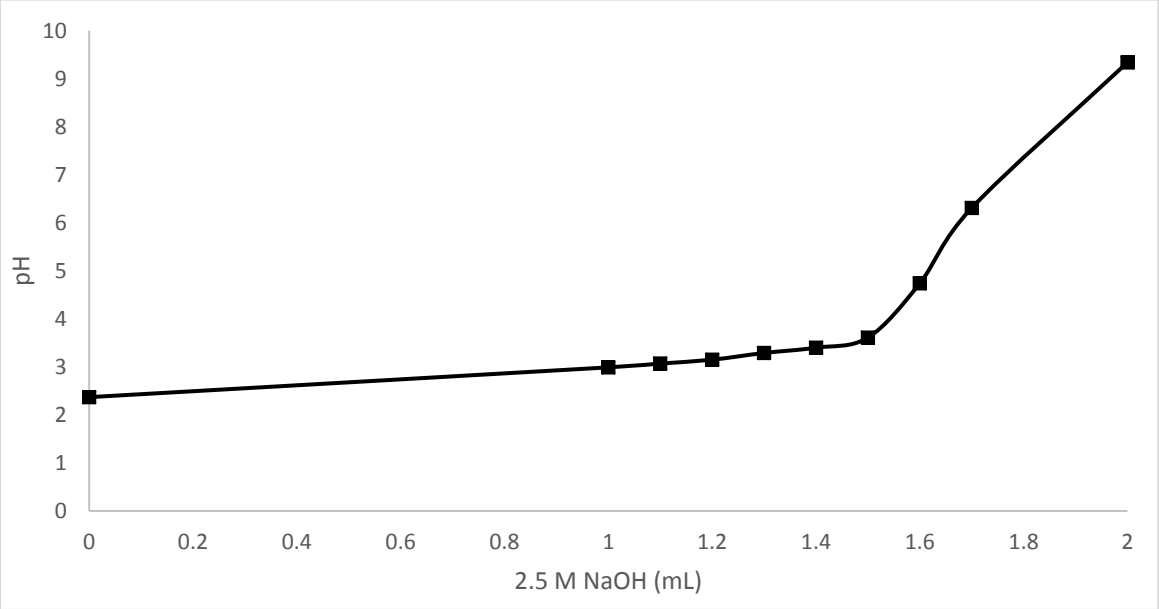

Figure 24: Titration of Mine Shaft AMD with 2.5M NaOH solution for pH adjustment.

For the AMD collected from the mine shaft, the pH increased modestly with the first addition of 1 mL, but then it shoots to pH 9 from pH 3 after the addition of the second milliliter. Therefore after the initial addition of 1 mL, there was a subsequent addition of 0.1 mL of the NaOH solution to avoid the sudden jump in pH level. The plot of the pH adjustment for mine shaft AMD is presented in Figure 24. After the adjustment of the pH, the precipitates in the samples were allowed to settle and then the samples were filtered using vacuum filtration. .

Chapter 4: Results and Discussions

4.1 Field parameters for AMD samples

Table 6 shows the field parameters for both mine shaft and surface AMD. The data shows extremely elevated levels of conductivity and Total Dissolved Solids (TDS). Normal water has TDS levels below 1000 ppm and a (Mateo and Bosch-Reig, 1998). This shows that AMD is able to dissolve large quantities of solids.

Table 6: Field parameters for AMD samples

Mine shaft AMD				**Surface AMD**			
Sample ID	**pH**	**EC(µS/cm)**	**TDS(ppm)**	**Sample ID**	**pH**	**EC(µS/cm)**	**TDS(ppm)**
G1	4.41	4639	2475	L1	1.49	5995	3292
G2	4.37	4606	2457	L2	1.53	6008	3286
G3	4.41	4629	2469	L3	1.54	5969	3256
G4	4.44	4577	2439	L4	1.53	6002	3280
G5	4.31	4601	2451	L5	1.32	6007	3305
G6	4.41	4580	2439	L6	1.87	6047	3220
G7	4.42	4606	2451	L7	1.54	6087	3251
G8	4.43	4619	2463	L8	1.41	6009	3298
G9	4.43	4613	2460	L9	1.33	6034	3302
G10	4.43	4580	2439	L10	1.47	5899	3294
G11	4.42	4587	2445	L11	1.74	6102	3233
G12	4.42	4587	2445	L12	1.66	6057	3247
G13	4.44	4613	2457	L13	1.29	5991	3311
G14	4.42	4600	2451	L14	1.38	5978	3299
G15	4.43	4632	2469	L15	1.27	5951	3308
G16	4.42	4587	2445	L16	1.37	5932	3300
G17	4.42	4600	2451	L17	1.44	5998	3296
G18	4.41	4603	2451	L18	1.30	6001	3310
G19	4.42	4603	2448	L19	1.29	6008	3312
G20	4.41	4616	2457	L20	1.40	6013	3299

This is mainly due to its acidity which increases as the AMD is exposed to oxidizing conditions as can be seen in Table 6, where surface AMD show lower pH values than mine shaft AMD. The dissolved solids in the AMD also lead to an increase in the electrical conductivity of the AMD water. Surface AMD, which is oxidized shows higher concentrations of dissolved solids as well as higher levels of electrical conductivity

4.2 Gross Alpha/Beta activities of untreated AMD samples

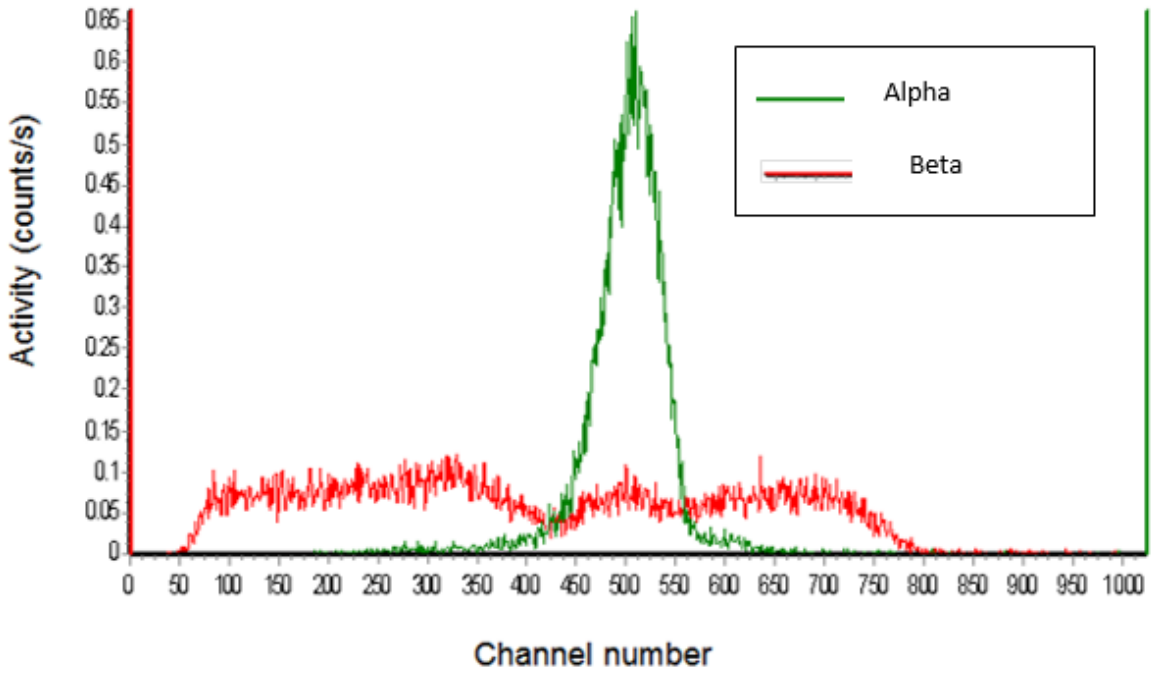

Figure 25: Gross alpha/beta spectrum of surface AMD.

Figure 25 shows the spectrum obtained from the liquid scintillation counting of a surface AMD sample. The spectrum show that there was very little misclassification, especially of alpha particles into the beta window. This is shown by the presence of a small peak beneath the main alpha peak shown in Figure 25 in the color green. The position of the peak also suggests that the main alpha emitter in the sample is uranium. This was determined via semi-qualitative calibration of the detector using alpha emitters. There is also minimal spill-over of beta particles into the alpha window.

Table 7: Gross alpha/Beta activities in surface AMD

Sample ID	Beta Activity (cpm)	Uncertainty (cpm)	Alpha Activity (cpm)	Uncertainty (cpm)
L01	41.577	0.342	42.172	0.322
L02	42.317	0.344	45.161	0.333
L03	39.674	0.335	40.660	0.317
L04	40.570	0.338	41.933	0.322
L05	34.557	0.482	37.935	0.467
L06	34.420	0.481	36.652	0.460
L07	34.210	0.480	36.282	0.457
L08	35.556	0.488	37.907	0.467
L09	34.949	0.484	36.998	0.462
L10	34.914	0.484	37.327	0.464
L11	34.937	0.484	36.800	0.460
L12	34.931	0.484	36.804	0.460
L13	33.989	0.479	37.583	0.465
L14	35.818	0.489	37.344	0.464
L15	34.732	0.483	38.145	0.469
L16	35.903	0.490	37.305	0.464
L17	36.863	0.496	37.878	0.467
L18	36.221	0.492	37.765	0.466
L19	33.591	0.476	38.253	0.469
L20	35.284	0.486	37.867	0.467

Table 7 presents raw gross alpha and gross beta counts in counts per minute and Table 8 presents the gross alpha and gross beta activities in Bq/L, of all surface AMD samples collected. The activity concentrations are quite elevated as expected, showing gross alpha values which are more than 140 times above the World Health Organization (WHO) guidance level of 0.5 Bq/L (WHO, 2006). The gross beta activity concentrations are also largely elevated, showing values over 60 times above the WHO guidance level of 1 Bq/L (WHO, 2006). The elevated gross alpha and gross beta activity concentrations observed in the AMD is testament to the potential pollution that

a free decant of such water into the natural environment can cause. A release of this AMD into a river system will cause a sudden and sharp increase in the radioactivity of the river and if such a river is being utilized by humans for any purpose, it would expose them to serious health hazards.

Table 8: Gross Alpha/Beta activities in surface AMD in Bq/L

Sample ID	Beta Activity (Bq/L)	uncertainty (Bq/L)	Alpha activity (Bq/L)	uncertainty (Bq/L)
L01	69.30	0.57	70.29	0.54
L02	70.53	0.57	75.27	0.56
L03	66.12	0.56	67.77	0.53
L04	67.62	0.56	69.89	0.54
L05	57.59	0.80	63.23	0.78
L06	57.37	0.80	62.09	0.77
L07	57.02	0.80	60.47	0.76
L08	59.26	0.81	63.18	0.78
L09	58.25	0.81	61.66	0.77
L10	58.19	0.81	62.21	0.77
L11	58.23	0.81	62.33	0.77
L12	58.22	0.81	61.34	0.77
L13	56.65	0.80	62.64	0.78
L14	59.70	0.82	62.24	0.77
L15	57.89	0.81	63.58	0.78
L16	59.84	0.82	62.17	0.77
L17	61.44	0.83	63.13	0.78
L18	60.37	0.82	62.94	0.78
L19	55.99	0.79	63.76	0.78
L20	58.81	0.81	63.11	0.78

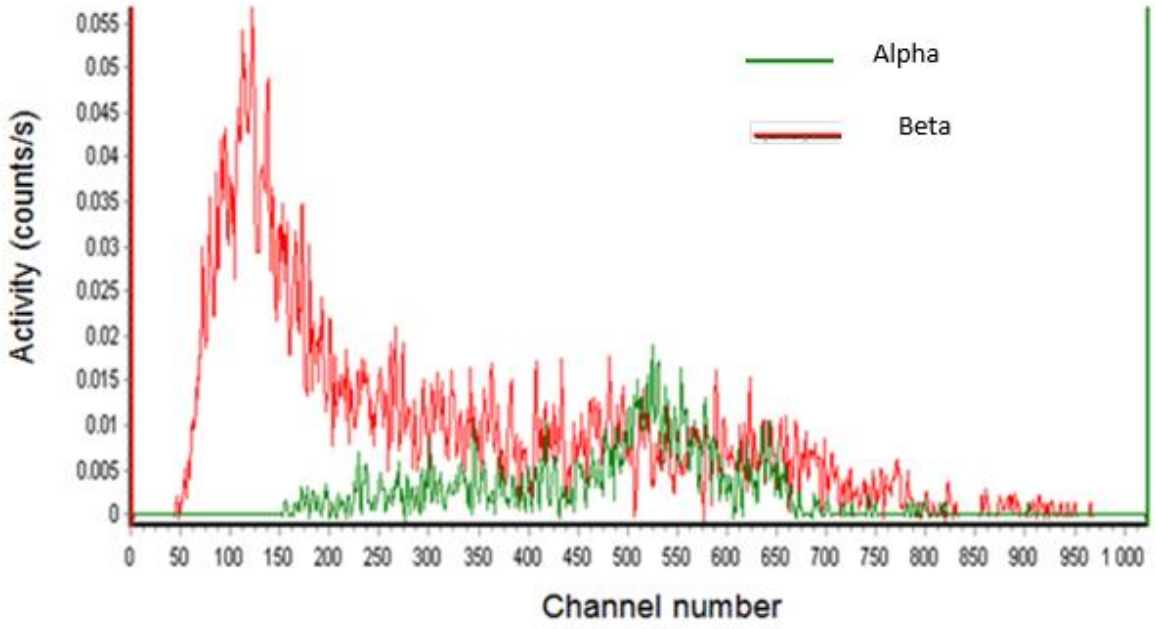

Figure 26: Gross alpha/beta spectrum of mine shaft AMD.

Figure 26 shows the gross alpha and gross beta spectrum of mine shaft AMD. The spectrum shows low gross alpha and gross beta activity compared to surface AMD. The main alpha contaminant still has its peak around channel 500. Since the samples had the same quench level, it can be concluded that the main alpha contaminant is still uranium. The lower activity concentration of both, total alpha and total beta reflects the chemistry of the two types of AMD. This is also reflected in Table 9 and Table 10. The mine shaft AMD is less oxidized compared to the surface AMD which has been exposed to atmospheric oxygen. Oxidation of AMD possibly leads to an increased ability of the AMD to dissolve metals, which includes radionuclides. Therefore the oxidized surface AMD has a higher concentration of radionuclides than the un-oxidized mine shaft AMD. This can also be observed in the difference in TDS of the two different types of AMD. This leads to the conclusion that AMD is less harmful when it is still in the mine shaft, away from the oxidizing conditions of the atmosphere. This is because the concentration of contaminants is lower in this type of AMD than in oxidized AMD.

Table 9: Gross Alpha/Beta activities of underground mining shaft AMD in cpm

Sample ID	Beta Activity (cpm)	Uncertainty (cpm)	Alpha Activity (cpm)	Uncertainty (cpm)
G1	0.730	0.131	1.288	0.066
G2	0.742	0.132	1.327	0.067
G3	1.837	0.141	1.251	0.066
G4	0.435	0.129	1.339	0.067
G5	0.812	0.132	1.181	0.064
G6	0.871	0.133	1.341	0.067
G7	0.581	0.130	1.456	0.069
G8	0.681	0.131	1.246	0.066
G9	0.856	0.133	1.395	0.068
G10	1.097	0.135	1.650	0.073
G11	1.662	0.140	1.614	0.072
G12	1.808	0.141	1.587	0.072
G13	1.852	0.141	1.558	0.071
G14	2.224	0.145	1.740	0.074
G15	1.918	0.142	1.655	0.073
G16	2.095	0.144	1.629	0.072
G17	2.212	0.145	1.748	0.074
G18	2.521	0.147	1.831	0.076
G19	2.429	0.146	1.833	0.076
G20	2.538	0.147	1.745	0.074

Table 10: Gross Alpha/Beta activities of underground mining shaft AMD in Bq/L

Sample ID	Beta Activity (Bq/L)	Uncertainty (Bq/L)	Alpha Activity (Bq/L)	Uncertainty (Bq/L)
G1	1.216	0.219	2.146	0.111
G2	1.236	0.219	2.211	0.112
G3	3.062	0.236	2.085	0.110
G4	0.725	0.214	2.231	0.112
G5	1.354	0.220	1.968	0.107
G6	1.452	0.221	2.235	0.112
G7	0.969	0.217	2.426	0.116
G8	1.135	0.218	2.077	0.110
G9	1.427	0.221	2.325	0.114
G10	1.829	0.225	2.751	0.121
G11	2.770	0.233	2.690	0.120
G12	3.014	0.235	2.645	0.120
G13	3.087	0.236	2.597	0.119
G14	3.707	0.241	2.901	0.124
G15	3.196	0.237	2.759	0.122
G16	3.492	0.239	2.714	0.121
G17	3.687	0.241	2.913	0.124
G18	4.202	0.245	3.051	0.126
G19	4.048	0.244	3.055	0.126
G20	4.231	0.245	2.909	0.124

4.3 Concentration of major anions in selected AMD samples

Data in Table 11 and Table 12 presents the concentration of major anions in AMD samples. Most water samples contain quantifiable amounts of carbonate. This is not the case with AMD samples from the Witwatersrand region. The main anions are the sulphate, nitrate, phosphate and chloride.

Table 11: Concentration of 3 major anions in selected AMD samples

Sample no.	Anion concentration in mg/L		
	PO_4^{3-}	SO_4^{2-}	NO_3^-
G2	1.58	4461.69	23.79
G3	1.55	4592.37	19.99
G5	0.71	4728.72	21.52
G11	0.43	4751.24	22.73
G12	1.86	4739.39	23.18
L5	1.55	8896.46	27.96
L8	2.74	8941.36	35.23
L11	2.59	9033.42	35.47
L15	1.26	9005.84	23.19
L19	1.59	9173.32	23.08

The concentration of the sulphate anion is very high for both types of AMD samples collected. But the AMD samples that were collected at the surface show higher sulphate concentrations than the AMD collected via the pumping station from the underground mining shafts. The surface AMD contains almost twice as much sulphate as the mine shaft AMD. However, there is no statistically significant difference in the concentration of the other anions between the two types of AMD collected.

Table 12: Concentration of 5 major anions in selected AMD samples

Sample no.	Anion concentration in mmol/L				
	PO_4^{3-}	SO_4^{2-}	NO_3^-	Cl^-	HCO_3^-
G9	0.15	45.76	0.22	3.62	0.00
G13	0.05	46.57	0.26	2.95	0.00
G17	0.03	47.95	0.36	2.86	0.00
G19	0.07	46.57	0.27	2.82	0.00
G20	0.00	47.80	0.23	2.88	0.00
L6	0.02	92.97	0.38	2.87	0.00
L13	0.06	92.68	0.29	2.95	0.00
L16	0.03	91.09	0.23	2.88	0.00
L18	0.19	92.50	0.24	2.93	0.00
L20	0.01	93.03	0.61	2.97	0.00

4.4 Metal concentrations

4.4.1 Metal concentration

Table 13: Concentration of metals in mine shaft AMD

Sample ID	Elemental concentration in mg/L														
	Al ($\times10^{-2}$)	Be ($\times10^{-4}$)	Mn ($\times10^{1}$)	Fe ($\times10^{2}$)	Co ($\times10^{1}$)	Ni ($\times10^{1}$)	Cu ($\times10^{-2}$)	Zn ($\times10^{-2}$)	As ($\times10^{-3}$)	Sr ($\times10^{-1}$)	Cd ($\times10^{-5}$)	Th ($\times10^{-4}$)	U ($\times10^{-3}$)	Mg ($\times10^{2}$)	Se ($\times10^{-4}$)
G1	112.9	2.521	2.287	4.326	3.135	6.993	1.240	13.69	0.9969	4.173	7.475	23.37	10.24	2.027	9.358
G2	10.70	1.699	2.451	4.825	3.200	7.063	0.6767	9.725	0.9831	4.496	0.3813	1.548	4.971	2.186	8.024
G3	10.21	0.9712	2.412	4.811	3.090	7.021	1.857	10.10	1.265	4.368	ND	0.9523	4.923	2.086	7.490
G4	123.5	2.521	2.342	4.669	3.369	7.249	1.569	15.32	1.059	4.484	9.770	1.000	10.86	2.140	0.01907
G5	10.33	1.513	2.422	4.736	3.146	7.024	0.9642	9.701	1.148	4.449	ND	ND	5.072	2.115	4.822
G6	9.557	0.9151	2.306	4.792	3.133	6.677	1.285	9.658	1.093	4.400	ND	ND	4.721	2.117	4.022
G7	9.069	1.475	2.460	5.117	3.144	7.082	1.027	9.899	0.8525	4.486	ND	ND	4.811	2.142	4.556
G8	9.093	1.606	2.527	5.185	3.241	7.293	0.7088	10.02	1.141	4.581	ND	ND	4.828	2.189	8.024
G9	8.793	0.9152	2.373	4.646	3.200	6.853	1.108	9.640	1.011	4.441	ND	ND	4.648	2.159	13.63
G10	9.386	1.625	2.418	4.813	3.152	6.958	0.9672	10.65	0.914	4.423	ND	ND	4.668	2.160	5.622
G11	8.933	1.158	2.424	4.866	3.247	6.987	2.026	10.62	1.114	4.519	ND	ND	4.483	2.185	ND
G12	9.707	0.8591	2.443	4.920	3.253	7.015	0.6883	9.741	0.9763	4.575	ND	ND	4.564	2.199	3.221
G13	9.902	1.326	2.470	4.934	3.227	7.052	0.6323	9.857	1.045	4.533	ND	ND	4.602	2.183	ND
G14	8.867	1.270	2.483	5.043	3.276	7.175	0.5628	9.677	1.107	4.638	ND	ND	4.696	2.215	4.555
G15	9.296	1.363	2.401	4.967	3.228	6.833	0.7216	10.36	0.8250	4.556	ND	ND	4.658	2.177	7.223
Mean	24.02	1.449	2.415	4.843	3.203	7.018	1.069	10.58	1.035	4.475	5.875	6.717	5.516	2.152	6.197

Table 14: Concentration of metals in surface AMD

Sample ID	Elemental concentration in mg/L																	
	Al ($\times10^{2}$)	Be ($\times10^{-2}$)	Cr ($\times10^{-1}$)	Mn ($\times10^{1}$)	Mg ($\times10^{2}$)	Fe ($\times10^{2}$)	Co ($\times10^{0}$)	Ni ($\times10^{1}$)	Cu ($\times10^{0}$)	Zn ($\times10^{1}$)	As ($\times10^{-2}$)	Se ($\times10^{-2}$)	Sr ($\times10^{-1}$)	Ag ($\times10^{-5}$)	Cd ($\times10^{-2}$)	Pb ($\times10^{-3}$)	Th ($\times10^{-2}$)	U ($\times10^{0}$)
L1	5.023	3.430	8.078	6.182	1.694	2.682	9.573	1.868	2.611	2.191	6.552	4.563	8.391	46.32	5.793	3.725	7.478	2.257
L2	5.393	4.019	9.351	6.571	1.942	2.900	11.11	2.021	2.935	2.355	7.141	5.455	9.859	10.93	6.673	3.426	8.757	2.673
L3	5.154	3.935	9.319	6.306	1.897	2.921	10.87	1.925	2.887	2.254	6.904	5.471	9.790	6.550	6.476	3.778	8.849	2.628
L4	5.079	3.889	9.258	6.379	1.921	2.789	10.90	1.940	2.906	2.276	6.886	5.567	9.837	4.169	6.757	3.706	8.906	2.693
L5	4.763	3.606	8.200	5.935	1.737	2.629	10.00	1.799	2.642	2.093	6.148	4.982	9.526	11.89	6.075	6.276	7.492	2.403
L6	4.726	3.674	8.050	5.906	1.726	2.589	9.881	1.778	2.591	2.088	6.168	4.889	9.510	ND	6.080	5.841	7.564	2.460
L7	4.589	3.462	8.053	5.774	1.677	2.572	9.947	1.780	2.574	2.057	6.036	5.092	9.567	ND	6.023	6.011	7.559	2.433
L8	4.479	3.435	7.826	5.629	1.623	2.511	9.575	1.719	2.525	2.002	5.920	4.638	9.379	7.322	6.061	6.379	7.653	2.457
L9	4.461	3.370	7.737	5.696	1.590	2.505	9.461	1.702	2.508	2.009	5.866	4.835	9.234	4.104	5.906	6.154	7.054	2.410
L10	4.389	3.252	7.502	5.624	1.563	2.483	9.311	1.674	2.445	1.992	5.857	4.697	9.200	0.6294	5.904	6.432	7.085	2.431
L11	4.135	3.463	7.968	5.277	1.650	2.331	9.846	1.591	2.582	1.906	5.657	4.835	9.904	4.298	6.311	6.540	8.098	2.603
L12	4.196	3.194	7.302	5.340	1.493	2.373	8.994	1.622	2.363	1.921	5.592	4.361	8.980	66.85	5.822	5.692	7.569	2.448
L13	4.120	3.066	7.139	5.286	1.471	2.337	8.894	1.597	2.335	1.887	5.460	4.350	8.961	5.777	5.691	5.726	7.380	2.405
L14	4.220	3.089	7.324	5.444	1.457	2.398	9.082	1.662	2.384	1.966	5.627	4.374	9.162	6.035	5.967	6.215	7.549	2.453
L15	4.223	3.190	7.321	5.487	1.484	2.425	9.101	1.642	2.396	1.952	5.676	4.534	9.261	10.41	6.055	6.433	7.768	2.515
Mean	4.597	3.472	8.029	5.789	1.662	2.563	9.770	1.755	2.579	2.063	6.099	4.843	9.371	14.25	6.106	5.489	7.784	2.485

Table 15: Guidance levels and normal occurrences for selected metals and anions in surface water and ground water (WHO, 2006).

Element	Guidance level (mg/L)	Occurrence (mg/L)
Arsenic	0.01	0.001-0.002
Cadmium	0.003	<0.001
Chromium	0.05	<0.002
Iron		0.5-50
Lead	0.01	<0.005
Mercury	0.006	<0.0005
Nickel	0.07	<0.02
Nitrate	50	<10
Selenium	0.04	<0.01
Sulphate	500	
Uranium	0.03	<0.01
Zinc		0.01-0.05

Table 13 presents the concentration of metals in mine shaft AMD samples. The concentration of some metals fall within the normal occurrence in surface water. Some metals have concentrations that are multiple times higher than the normal occurrence in surface or ground water sources. Table 15 presents the normal occurrence of some important metals in surface and ground water as well as the WHO guidance limits. The concentration of arsenic is within the normal occurrence limits for surface and ground water and therefore the AMD would not present any contamination danger to the environment due to the metal. Concentrations of cadmium and chromium were below the detection limit of the ICP-MS. The concentration of iron in the AMD is very high, with an average of 480 mg/L. This concentration of iron is to be expected from gold mining operations and is what drives the generation of AMD. This high levels of iron though presents a significant contamination risk to the environment if uncontrolled decant occurs. Zinc and nickel show concentrations that are slightly elevated compared to normal surface water. Selenium and uranium show levels that are normal for surface waters.

Table 14 presents metal concentrations for surface AMD. The concentration of the metals once the AMD is on the surface is high compared to the AMD that is in the

mining shafts. The oxidation leads to lower pH and increases the ability of the AMD to dissolve the metals. Almost all the metals listed in Table 15 show elevated concentrations. In most of the metals the concentration is enhanced by a factor of over 100 compared to normal surface water as described by WHO. Concentrations of toxic heavy metals such as chromium, cadmium, uranium and arsenic are highly enhanced in the surface AMD. Since this type of AMD is already on the surface, either formed there or decanting from underground mining shafts, it presents a significant risk to the environment. The concentration of uranium, which is not just chemically toxic, but also radiotoxic is significantly enhanced. This is also due to the known elevated concentrations of the radioelement in gold mining environments in the Witwatersrand basin.

The elevated concentration of metals in the surface AMD compared to the mine shaft AMD clearly shows the dangers associated with freely decanting AMD or one that is formed at the surface. AMD that is in anoxic conditions, which is the case in the deeper mining shafts is less contaminated and therefore safer for the environment if treated before oxidation. Once the AMD is exposed to oxidising conditions, it becomes more contaminated and presents a greater threat to the environment.

Table 16 shows the activity concentration data for NORM parent nuclides calculated from elemental concentrations determined using ICP-MS. As noted already in the metal concentration data, the activity concentration of uranium isotopes is elevated. Uranium isotopes would contribute more than 60 Bq/L of gross alpha activity to the AMD. The concentration of thorium is not as elevated in the AMD samples, which is to be expected because unlike uranium, thorium concentration is not usually enhanced in gold mining. Potassium has very little contribution towards the radioactivity of AMD in this study.

4.4.2 NORM Activities calculated from ICP-MS concentrations

Table 16: Surface AMD samples Activities

Sample ID	Activity concentration in Bq/L				
	^{238}U	^{235}U	^{234}U	^{232}Th	^{40}K
L01	27.87±1.82	1.30±0.03	28.58±0.89	0.303±0.031	0.035±0.001
L02	33.01±0.41	1.54±0.02	33.85±0.42	0.355±0.003	0.034±0.002
L03	32.45±1.88	1.51±0.09	33.28±1.93	0.359±0.032	0.035±0.001
L04	33.25±1.90	1.55±0.09	34.10±1.95	0.361±0.032	0.032±0.001
L05	29.67±0.35	1.38±0.02	30.43±0.36	0.304±0.002	0.066±0.003
L06	30.38±0.18	1.42±0.01	31.15±0.19	0.307±0.002	0.062±0.002
L07	30.04±0.29	1.40±0.01	30.81±0.30	0.307±0.013	0.061±0.002
L08	30.34±0.29	1.41±0.01	31.11±0.30	0.311±0.014	0.060±0.002
L09	29.76±1.31	1.39±0.06	30.52±1.34	0.286±0.024	0.060±0.002
L10	30.02±1.17	1.40±0.05	30.79±1.20	0.287±0.021	0.061±0.002
L11	32.14±1.29	1.50±0.06	32.96±1.32	0.329±0.015	0.057±0.001
L12	30.23±0.33	1.41±0.02	31.00±0.33	0.307±0.004	0.057±0.001
L13	29.70±0.68	1.38±0.03	30.46±0.70	0.299±0.008	0.055±0.001
L14	30.29±0.54	1.41±0.03	31.06±0.56	0.306±0.006	0.055±0.001
L15	31.06±0.56	1.45±0.03	31.85±0.57	0.315±0.006	0.055±0.001

Table 17 shows the activity concentrations of NORM parent nuclides in mine shaft AMD. The activity concentration of the isotopes is low, reflecting the normal elemental concentrations of the metals. The contribution of potassium to the activity is higher than in surface AMD.

Table 17: Mine shaft AMD activities calculated from ICP-MS data in mBq/L

Sample ID	Activity concentration in mBq/L				
	^{238}U	^{235}U	^{234}U	^{232}Th	^{40}K
G1	126.45±7.74	5.90±0.76	129.68±3.70	9.48±3.18	470.21±20.23
G2	61.38±4.16	2.86±0.97	62.95±3.23	0.63±0.13	508.99±11.74
G3	60.79±1.81	2.83±0.95	62.34±2.87	0.39±0.23	499.59±9.63
G4	134.10±2.57	6.25±0.99	137.53±3.66	0.41±0.23	485.66±12.20
G5	62.63±2.25	2.92±0.10	64.23±2.31	ND	504.14±16.81
G6	58.30±0.71	2.72±0.03	59.78±0.73	ND	481.11±25.12
G7	59.41±1.23	2.77±0.06	60.92±1.26	ND	513.83±12.93
G8	59.62±1.22	2.78±0.06	61.14±1.25	ND	530.50±14.36
G9	57.40±1.25	2.68±0.06	58.86±1.29	ND	505.05±5.98
G10	57.64±1.15	2.69±0.05	59.11±1.17	ND	506.26±5.10
G11	55.36±0.75	2.58±0.03	56.77±0.77	ND	515.96±1.06
G12	56.36±0.84	2.63±0.04	57.80±0.86	ND	513.83±5.28
G13	56.83±0.58	2.65±0.03	58.28±0.60	ND	515.05±6.61
G14	57.99±0.33	2.70±0.02	59.47±0.34	ND	523.53±9.21
G15	57.52±0.72	2.68±0.03	58.99±0.74	ND	510.50±5.54

4.5 Gamma spectrometry activity concentrations

Table 18 presents nuclide specific analytical results for surface AMD. The activity concentrations for nuclides in mine shaft AMD could not be determined using gamma spectroscopy because they were below the detection limits. The activity concentration for uranium isotopes from gamma spectrometry agrees with results obtained using ICP-MS. The activity concentration of ^{238}U is high for all samples analyzed. The activity concentration of ^{226}Ra in the samples is very low when compared to the parent nuclide ^{238}U. This disequilibrium is explained via radionuclide speciation which is discussed in section 4.7 of this document. Due to the high concentration of sulphate in the AMD, the radium exists predominantly as $RaSO_4$ which is sparingly soluble in water. Therefore, even though radium is expected to be present in the parent matrix, very little dissolves into the AMD.

Table 18: Surface AMD nuclide specific gamma spectroscopy analysis results in

Sample ID	Activity concentration in Bq/L			
	^{238}U	^{235}U	^{226}Ra	^{232}Th
L1	29.209±2.686	1.387±0.072	<0.151	<0.003
L2	30.431±2.591	1.366±0.065	<0.151	0.056±0.002
L3	25.408±2.240	1.566±0.085	0.294±0.105	<0.003
L4	29.758±3.472	1.527±0.085	0.273±0.095	0.160±0.008
L5	28.148±3.267	1.487±0.083	<0.151	<0.003
L6	20.797±2.795	1.119±0.088	0.269±0.080	0.026±0.001
L7	25.665±2.730	1.566±0.091	<0.151	<0.003
L8	27.854±3.060	1.469±0.085	0.389±0.096	<0.003
L9	26.437±2.991	1.304±0.085	0.378±0.099	<0.003
L10	26.621±2.898	1.333±0.088	0.518±0.096	<0.003
L11	27.479±3.189	1.437±0.079	<0.15	<0.003
L12	26.803±2.855	1.274±0.089	0.390±0.084	0.031±0.002
L13	28.466±3.539	1.333±0.086	0.453±0.106	0.071±0.002
L14	24.938±3.109	1.245±0.085	0.473±0.106	<0.003
L15	24.668±1.546	1.206±0.089	0.411±0.116	<0.003
L16	26.366±3.571	1.187±0.086	<0.15	<0.003
L17	26.923±1.554	1.381±0.088	<0.15	<0.003
L18	26.319±3.046	1.216±0.085	<0.15	0.024±0.002
L19	26.301±2.972	1.284±0.088	0.188±0.085	<0.003
L20	29.180±3.350	1.294±0.090	0.367±0.103	0.179±0.003

4.6 The effect of sulphate concentration on level of AMD radioactivity

4.6.1 Effect of sulphate concentration on uranium concentration in AMD

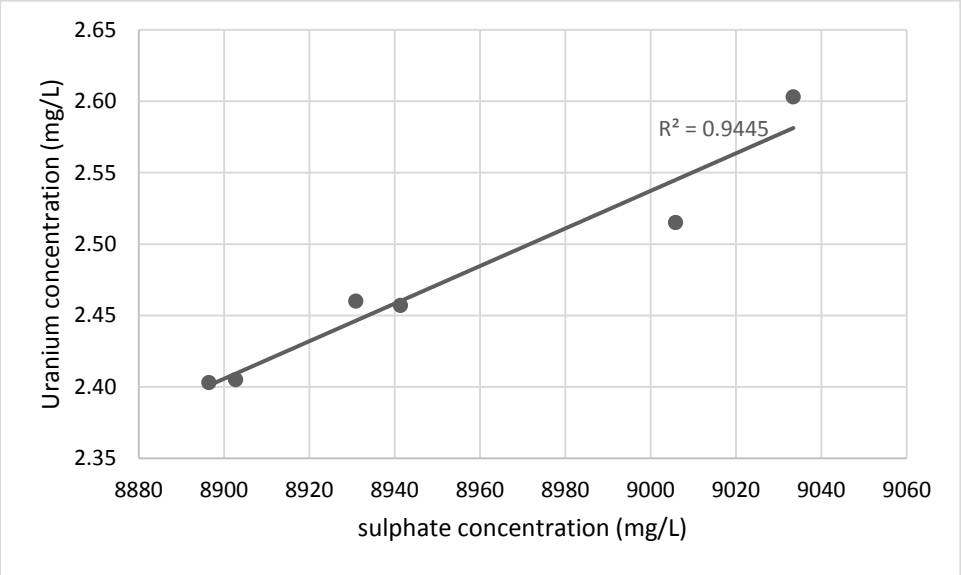

Figure 27: Effect of sulphate concentration on uranium concentration in surface AMD.

The concentration of sulphate in AMD is an important chemical parameter since it is the primary anion in the generation of AMD. Therefore, its concentration can be expected to play an important role in the concentration of nuclides. Uranium is the main radioactive contaminant in the AMD in this study and therefore contributes the most to the radioactivity. Figure 27 demonstrates the relationship between the concentration of sulphate and the elemental concentration of uranium in surface AMD. The graph shows a linear relationship, with a correlation coefficient (R^2) of 0.944. An increase in the concentration of sulphate in the AMD is associated with an increase in the concentration of uranium.

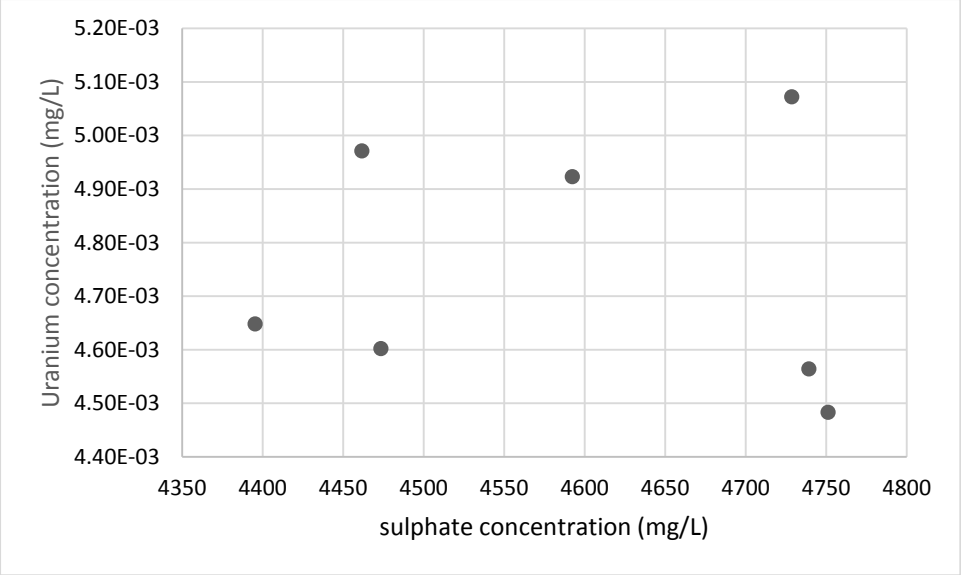

Figure 28: Effect of sulphate concentration on uranium concentration in mine shaft AMD.

Figure 28 shows the relationship between sulphate concentration and uranium concentration in mine shaft AMD. There is no significant correlation between the two parameters. The most likely reason for this lack of correlation is the stage of AMD generation. Mine shaft AMD is basically under reducing conditions because the concentration of oxygen in the deep shafts is very low. Under such conditions the generation of AMD is slow, and therefore the effect of the sulphate is not very pronounced.

4.6.2 Effect of sulphate concentration on gross alpha and gross beta activity concentration in AMD

Figure 29 and Figure 30 show the effect of sulphate concentration on gross alpha and gross beta activity concentration in surface AMD respectively. The gross alpha activity concentration in surface AMD increases with an increase in sulphate concentration. The relationship is linear, with a goodness of fit parameter (R^2) of 0.7533. Sulphate is the main component in the generation of AMD and therefore higher concentrations should lead to a quicker rate of AMD generation and greater ability to dissolve radionuclides from the surrounding matrix. The effect of sulphate on the gross beta activity concentration is different from that observed for gross alpha activity concentration. The effect for gross beta activity is such that there is an initial increase in the activity concentration in samples as the concentration of sulphate increases.

The relationship follows a second order polynomial, with a maximum at a sulphate concentration of 8600 mg/L. Beyond this concentration, any further increase in sulphate concentration leads to lower gross beta activity concentrations in the surface AMD.

There was no significant effect of sulphate concentration on both gross alpha and gross beta activity concentrations in mine shaft AMD samples as shown in Figure 31 and Figure 32. Oxidizing conditions are necessary for the generation of AMD, in which sulphate plays a major role. Therefore under the anoxic conditions that prevail in underground mine workings filled with water, the rate of AMD generation is very slow and therefore, the sulphate concentration is less important in the partitioning of radionuclides between the matrix and the AMD.

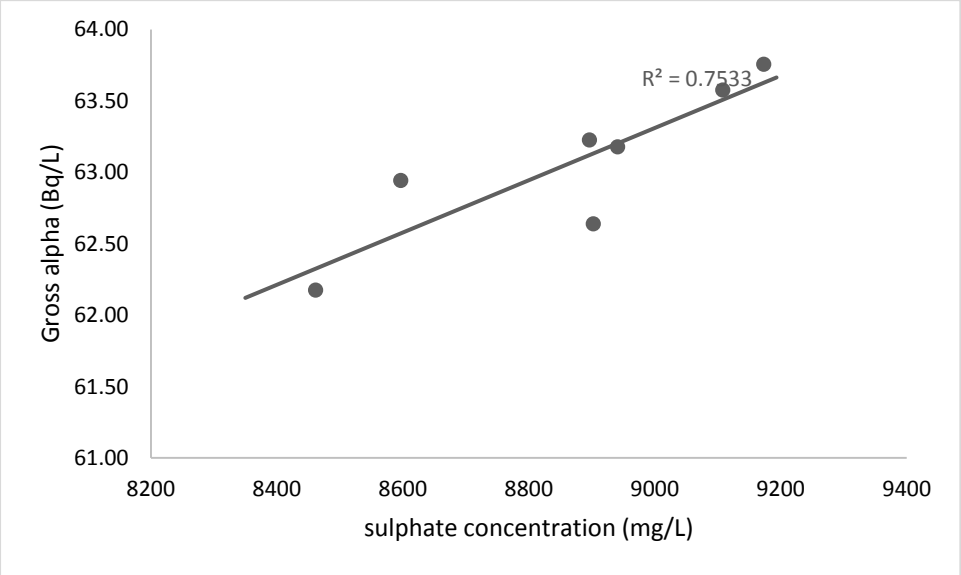

Figure 29: The effect of sulphate concentration on the gross alpha activity concentration in surface AMD.

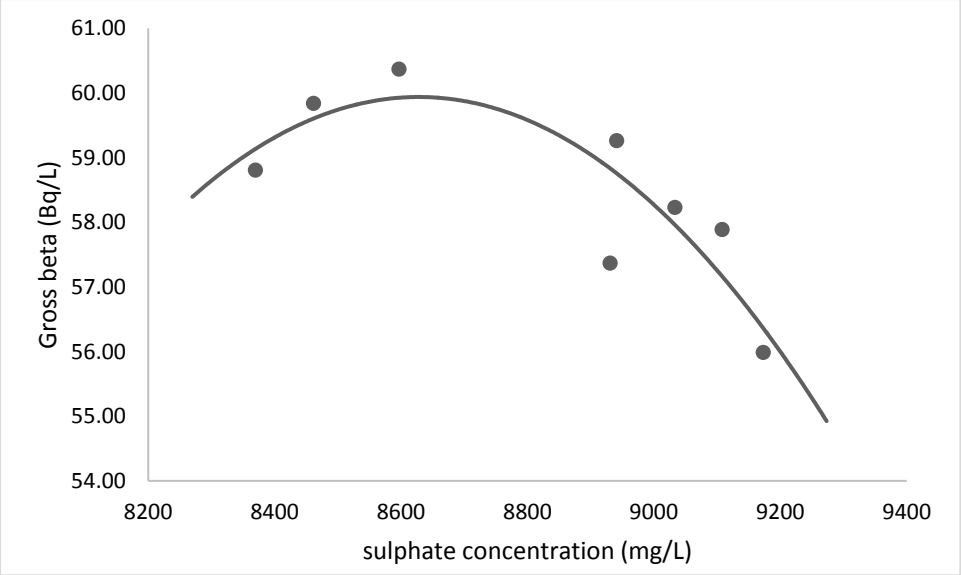

Figure 30: The effect of sulphate concentration on gross beta activity concentration of surface AMD.

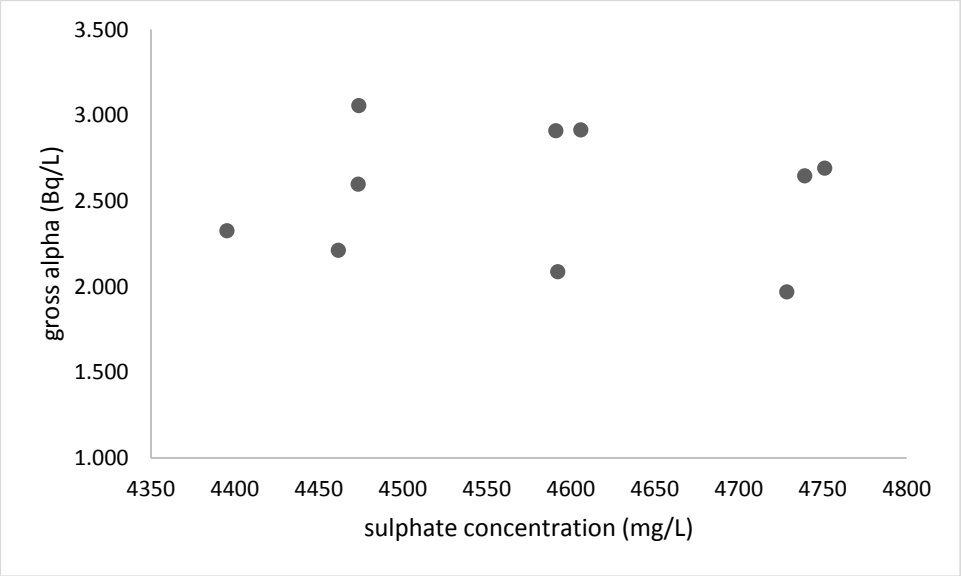

Figure 31: The effect of sulphate concentration on gross alpha activity concentration of mine shaft AMD.

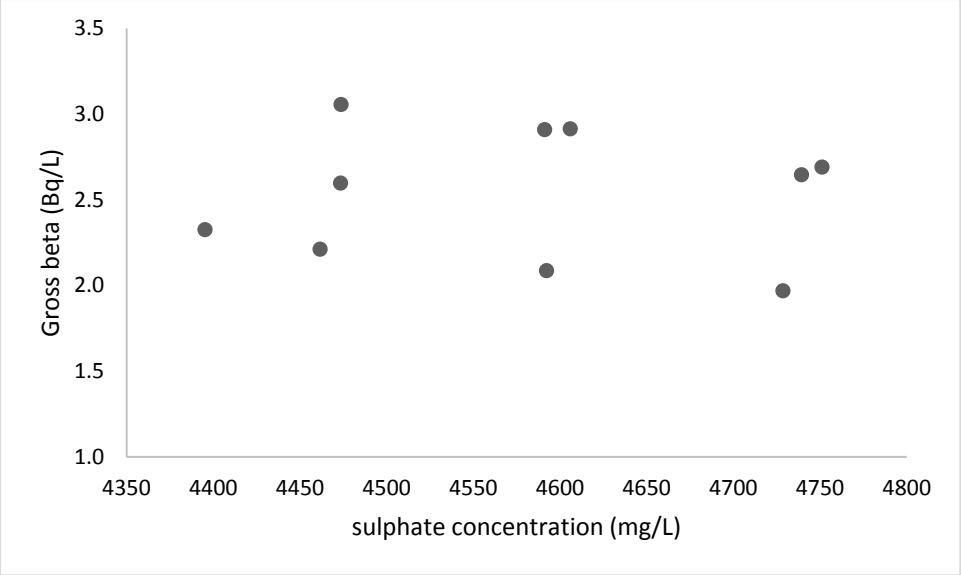

Figure 32: The effect of sulphate concentration on the gross beta activity concentration in mine shaft AMD.

4.7 Speciation modelling

4.7.1 Visual Minteq results

Table 19: Input data into the modelling facilities

Element	Concentration in mg/L	
	Oxidizing conditions	**Reducing conditions**
Al	459.7	0.2402
Be	0.03470	0.00015
Cr	0.8029	0.00005
Mn	57.89	24.15
Mg	166.2	215.2
Fe	256.3	484.3
Co	9.770	0.3203
Ni	17.55	0.7018
Cu	2.579	0.01073
Zn	20.63	0.1058
As	0.06104	0.00102
Se	0.04841	0.00067
Sr	0.9371	0.4475
Ag	0.00010	0.00002
Cd	0.0611	0.00017
Pb	0.00553	0.00001
Th	0.07787	0.00070
U	2.485	0.00552
SO_4^{2-}	6843	4655
PO_4^{3-}	1.590	1.230
NO_3^-	25.61	22.24
Cl^-	101.8	107.4
HCO_3^-	0.00000	0.00000

The ionic strength of the solution was calculated by the model from mass and charge balance at equilibrium.

4.7.1.1 Uranium speciation

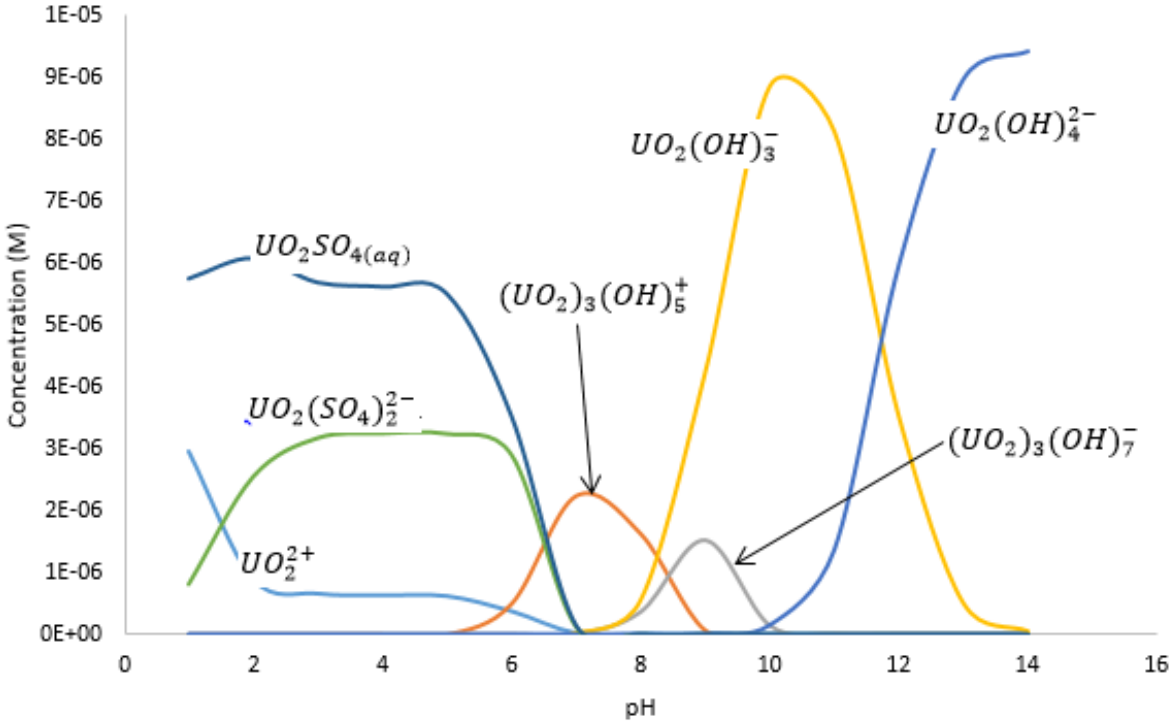

Figure 33: Uranium speciation diagram under oxidizing conditions.

Figure 33 shows the speciation of uranium in AMD as a function of pH. Visual Minteq model predicts that uranium exists mainly in +6 state, with the +4 state appearing at very low pH levels at extremely low concentrations. The uranyl cation, UO_2^{2+}, is dominant at low pH levels and it's concentration decreases sharply between pH 1 and 2. In general, under acidic conditions, the species, $UO_2SO_{4(aq)}$ dominates. Most of the uranium exists as a soluble neutral sulphate in solution. Over 60% of the uranium exists as this species between pH 1 and 5. The species disappears around neutral pH. Another major uranium species under acidic conditions is $UO_2(SO_4)_2^{2-}$. The concentration of this species increases between pH 1 and 3 and then it stays at a constant concentration until it starts to drop at pH 6. Under neutral conditions the hydroxo-uranyl species $(UO_2)_3(OH)_5^+$ is the dominant species.

The polynuclear species $(UO_2)_3(OH)_7^-$ starts to show up at pH 7 and increases in concentration, having a maximum concentration at pH 9 and making up 48.19% of the uranium (VI) in the system. The species disappears at pH 10. The mononuclear $UO_2(OH)_3^-$ is the major species in the pH range 8-11. The species starts growing at

pH 7, reaching its maximum concentration between pH 10 and 11. At its maximum, it makes up 93.18% of all the uranium (VI) in the system. It is the ideal species to target for removal of the radionuclide from the AMD using anion exchange resins. The species is present throughout the whole alkaline range of pH. $UO_2(OH)_4^{2-}$ is the most important species at pH levels above 12. Under extremely alkaline conditions the species makes up about 95% of the total uranium (VI) in the system. Negatively charged uranium species only begin to dominate above pH 8.

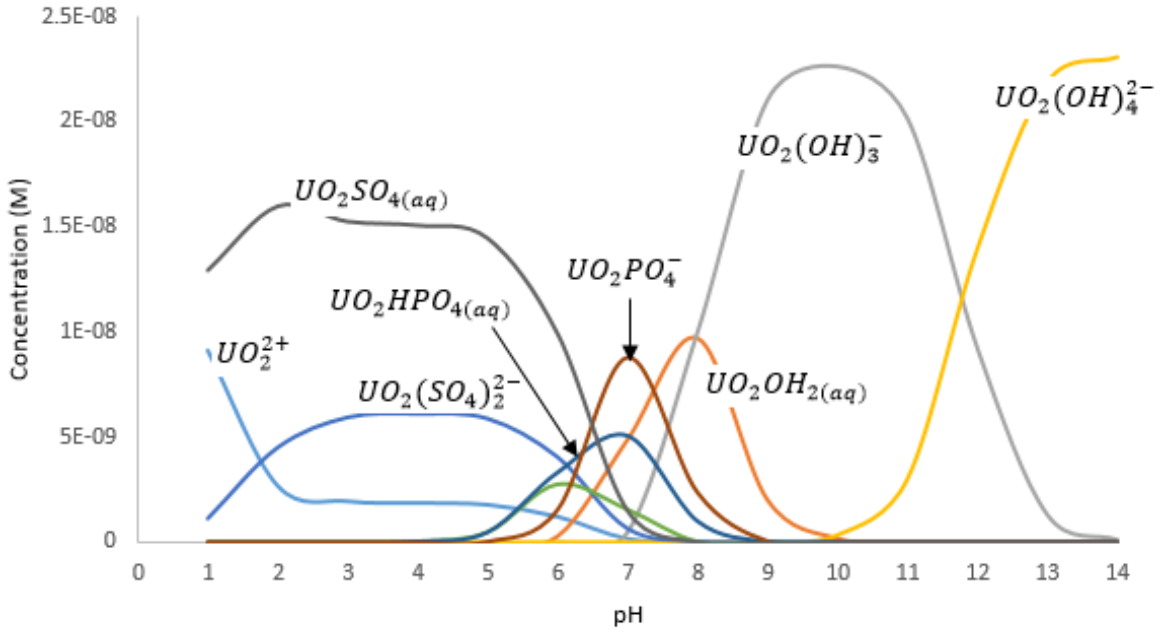

Figure 34: Uranium speciation diagram under reducing conditions.

Under reducing conditions, the proportion, distribution and identity of species at different pH regions change as seen in Figure 34. In the region pH 1-4 the same set of species dominate as under oxidizing conditions. $UO_2SO_{4(aq)}$ is the most dominant species within this pH region, making up more than 60% of the total uranium in the system. UO_2^{2+} is the second most abundant species at pH levels below 2, making up more than 30% of total uranium. Above pH 2 the species $UO_2(SO_4)_2^{2-}$ becomes more important than the uranyl ion, making up over 33% of the total uranium concentration. In the pH region 4-7 species not observed under oxidizing conditions are observed in the system. Phosphate species become important under oxidizing conditions in this pH range. They replace the polynuclear hydroxyl species observed under oxidizing conditions. Mononuclear hydroxyl species are also observed in this region. The major species is $UO_2PO_4^-$ which starts growing in at pH 5 and reaches a maximum

concentration at pH 7, making up 38% of the total uranium concentration. The species disappears at pH 9. The second most important species in this region is the mononuclear species UO_2OH^+, which reaches a maximum concentration at pH 7 as well, making up 22% of the uranium in the system. $UO_2HPO_{4(aq)}$ also exist in solution under these conditions, making up a maximum proportion of 12%. Under acidic conditions, the species are a mixture of neutral, positive and negative. Uranium in this study is removed using an anion exchange resin in one part, and therefore a negative speciation of the uranium is more favourable for removal from the AMD. At pH 6, negative species make up only 25% of uranium and at pH 7 they make up slightly over 40%. The neutral hydroxyl species $UO_2OH_{2(aq)}$ is another important species in the pH region 7-9, with a maximum concentration (42%) at pH 8. In the pH region 9-14, the same species as under oxidizing conditions dominate. In this pH region, the species are negative and more favourable for removal using an anion exchange resin. Stucker and others observed that even though positive species were dominant, anion exchange resin still managed to achieve 99.9% removal rate and they concluded that negative speciation was not necessary for anion exchange removal (Stucker et al., 2011). The dominance of neutral and positive species at low pH promotes the use of acid in regenerating the ion exchange resin and eluting the adsorbed uranium from the column.

4.7.1.2 Thorium speciation

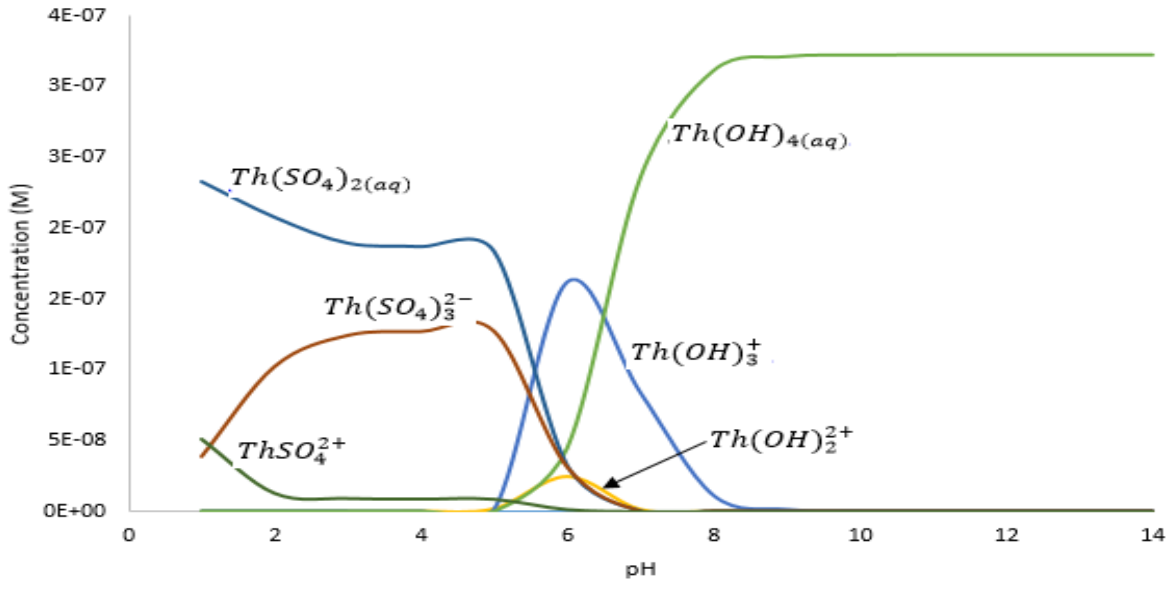

Figure 35: Thorium speciation diagram under oxidizing conditions.

Thorium exists only in the +4 oxidation state. Figure 35 shows the variation in speciation of thorium in acid mine drainage with pH under oxidizing conditions. There are three important species under acidic conditions, $Th(SO_4)_{2(aq)}$, $ThSO_4^{2+}$ and $Th(SO_4)_3^{2-}$. At low pH the dominant species of thorium is $Th(SO_4)_{2(aq)}$. The species makes up 72.17% of thorium in the system at pH 1. The concentration of the species drops slightly as the pH increases to 5. The concentration then drops sharply between pH 5 and 6, disappearing all together at neutral pH. $Th(SO_4)_3^{2-}$ is the second most important species in the pH range, 1-5. The concentration of the species increases slightly from pH 1 to 3 and then stabilizes until pH 5. The concentration then drops sharply in the pH range 5-7. The third species, $ThSO_4^{2+}$, makes up on average less than 3% of the total thorium in the system. In the pH region 5-7, two species, $Th(OH)_2^{2+}$ and $Th(OH)_3^{+}$ are important and they both start forming in appreciable concentration at pH 5. $Th(OH)_2^{2+}$ has its maximum concentration at pH 6, making up 8% of the total concentration. $Th(OH)_3^{+}$ is the major species in the system at pH 6, making up more than 50% of the total thorium concentration in the system. The species disappears from the system at a pH level slightly above 8. The species,$Th(OH)_{4(aq)}$, is the most important species under alkaline conditions in the system. The species starts to appear at pH 5 and increases reaching a maximum at pH 9, and then it maintains that maximum concentration level until pH 14. This neutral and species suggest that the solubility of thorium in alkaline water might be highly enhanced, and therefore there is a possibility that under alkaline conditions, the concentration of thorium in any environmental water interacting with a source might be enhanced. The speciation of thorium is not affected by oxidizing or reducing conditions appreciably in AMD. The speciation under oxidizing and reducing conditions is the same, showing no major change in both distribution and proportions of species involved as shown by Figure 36.

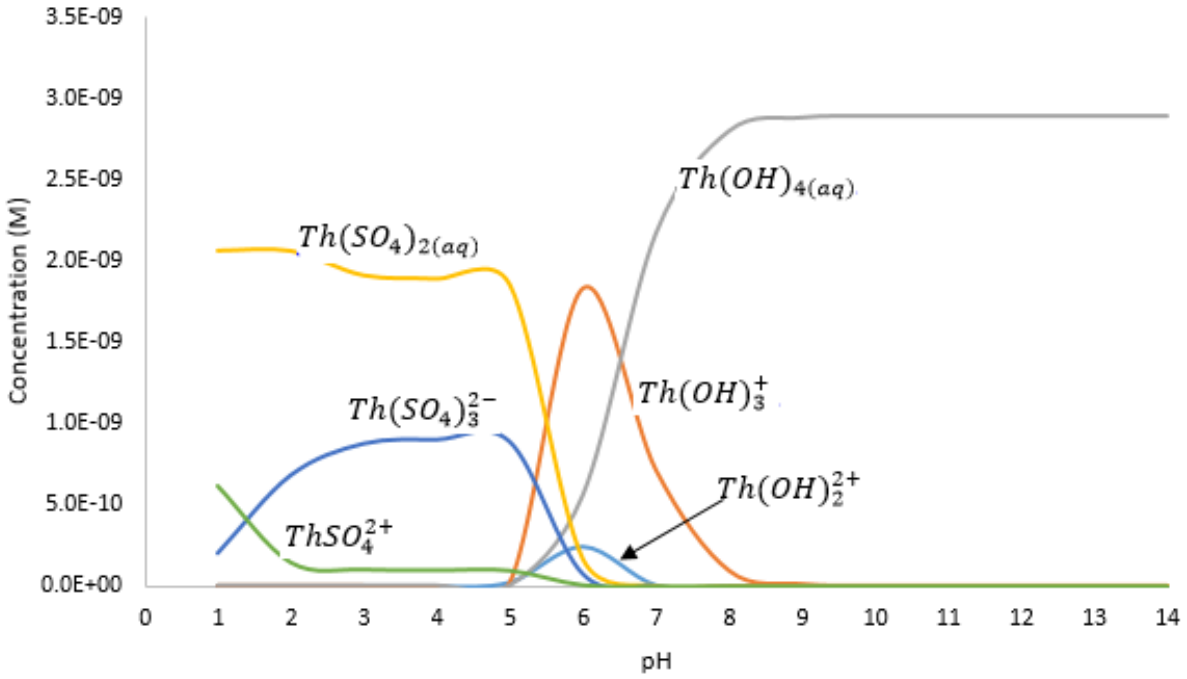

Figure 36: Thorium speciation under reducing conditions.

4.7.2 JESS speciation

4.7.2.1 Oxidizing conditions

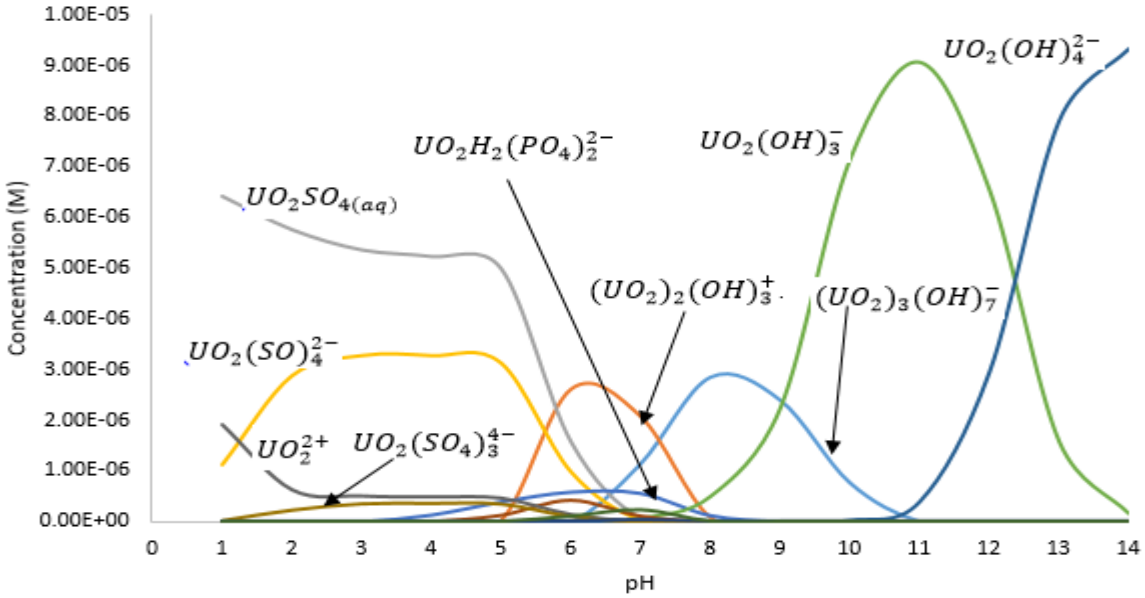

Figure 37: Uranium speciation under oxidizing conditions using JESS model

Using the JESS speciation model presented a number of problems at first, especially problems with overflow and underflow. The error of overflow arises when certain species in the equilibrium calculation has high stoichiometric coefficients. This problem

was resolved by reducing the initial estimates of the species concerned by a factor of -25. Some components; Se, As, Cr and Al were removed from the equilibrium calculation due to their difficult thermodynamics causing the failure in solving thermodynamic equations at most pH scan points. These were then introduced back into the problem, one by one to identify the elements that were causing problems in solving the equilibrium equations. In the final calculation, Se, As and Al were excluded from the equilibrium calculation. There was also a convergence problem arising due to an underflow. This was caused by PO_4^{3-} in the system. The concentration was too high, and therefore it was reduced to a tenth of the actual concentration. When that adjustment was done, all equations solved at all 14 pH scan points. In the pH region 1-5, there are three major species observed. The most dominant species throughout that pH region is $UO_2SO_{4(aq)}$. The species has a maximum contribution of 60% in that pH region (at pH 1). It only starts to disappear sharply at pH 5. The second most important species in this region is another sulphate species, $UO_2(SO)_4^{2-}$, which at its highest concentration makes up more than 30% of the total uranium in the system. This species also drops in concentration rapidly, between pH 5 and 6. The uranyl ion is another important species at low pH, making up about 25% at pH 1, and dropping in concentration between pH 1 and 2 and then disappearing at neutral pH. All of these species were also predicted by the modelling package, Visual Minteq, in almost the same proportions at the same pH range. The species $UO_2(SO_4)_3^{4-}$ is predicted by Visual Minteq as well but it is not a species that occurs in measurable amounts in the system. JESS predicts the species to be an important species in the pH region 1-5, making up about 7% of the total uranium.

In the pH region 5-8 there are four species that are important. The most dominant species in this region is the polynuclear species $(UO_2)_2(OH)_3^+$. Visual Minteq didn't predict this species as an important species in the system. But according to JESS the species is the most dominant in this pH region, having a maximum concentration at pH 6.5, making up 67% of the total uranium in the AMD. The next most available species in this region is the negatively charged poly-nuclear phosphate species $UO_2H_2(PO_4)_2^{2-}$. The species doesn't contribute that much, as at its maximum concentration it makes up about 5% of the uranium in the AMD under oxidizing conditions. The other species in this region are the hydroxy species, one mononuclear and one polynuclear species. The polynuclear species $(UO_2)_3(OH)_5^+$ is the one

predicted by Visual Minteq to be the most dominant in this region, but JESS predicts that it will only make up a maximum of 6% of uranium. The mononuclear species UO_2OH^+ is also not predicted as an important species by Visual Minteq, while JESS predicts it to be important in this region.

In the region, pH 8-14, there are three major species that are predicted by the modelling platform JESS. Around pH 8, the species $(UO_2)_3(OH)_7^-$ is the most dominant species, making up 91% of all the uranium in the AMD. This species disappears at pH 11. In the pH range 10-12, the negatively charged mono-nuclear species $UO_2(OH)_3^-$ dominate, having a maximum concentration at pH 11 (95%). Another negatively charged species, $UO_2(OH)_4^{2-}$ starts to grow in concentration in the system at pH 11 to become the major species above pH 12.

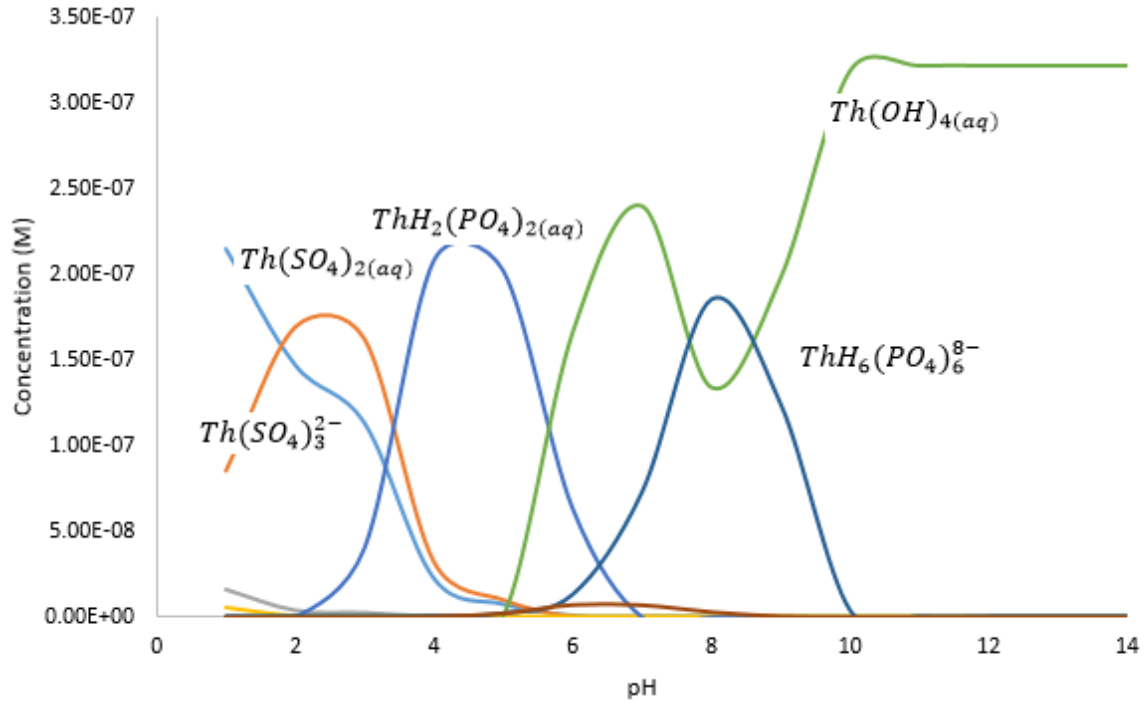

Figure 38: Thorium speciation under oxidizing conditions using JESS model.

Figure 38 shows the speciation of the natural radionuclide thorium in AMD under oxidizing conditions modelled using the JESS chemical speciation modelling system. In the pH region 1-4, the two major thorium species in AMD are $Th(SO_4)_{2(aq)}$ and $Th(SO_4)_3^{2-}$. The neutral sulphate species dominates below pH 2 (maximum 56%) while the negatively charged sulphate species dominates in the pH region 2-4 (maximum 50%). In the pH region 4-6 the neutral hydrogen phosphate species $ThH_2(PO_4)_{2(aq)}$ is

the dominant thorium species, making up a maximum of 61% at pH 5. From pH 6 to pH 14, two species dominate. The neutral hydroxy species, $Th(OH)_{4(aq)}$ initially dominates between pH 6 and 7, but then loses its dominance as the negatively charged hydrogen phosphate species, $ThH_6(PO_4)_6^{8-}$ comes in strongly at pH 8. This species has its maximum concentration at pH 8, making up 68% of the thorium, and then it disappears from solution at pH 10. Above pH 8, the neutral hydroxy species regains its dominance, making up 100% of the thorium in the AMD at pH levels above 10.

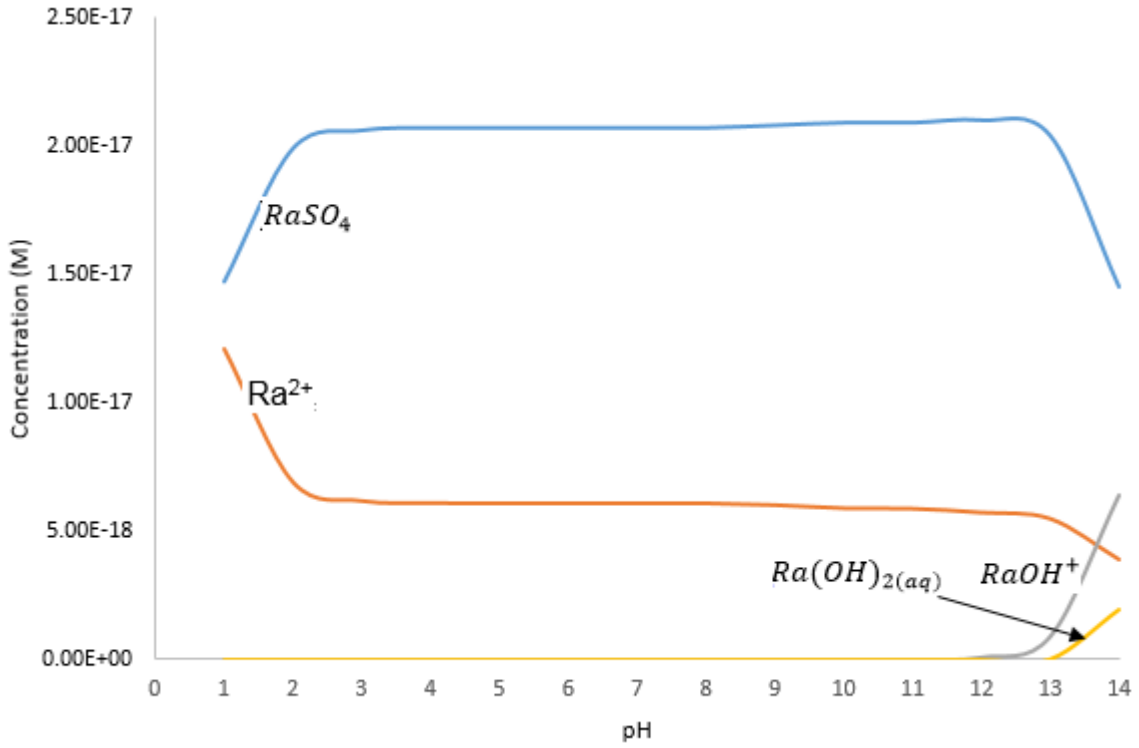

Figure 39: Radium speciation in AMD under oxidizing conditions.

Radium speciation could only be modelled using JESS since the Visual Minteq software doesn't have radium in its range of input parameters. Radium speciation is the simplest of the radionuclides being investigated. The speciation of radium was modelled using the detection limit for radium for the ICP-MS used as listed in Table 4.

Only four species of radium were predicted by JESS under oxidizing conditions over the pH range 1-14 as seen in Figure 39. The most dominant species of radium in the AMD is radium sulphate ($RaSO_4$). This species is sparingly soluble in water, and is even less soluble than barium sulphate. The low solubility of this dominant species explains why the concentration of radium in the sulphate rich acid mine water is so low. Under normal conditions of equilibrium, the activity concentration of radium should be similar to the activity concentration of ^{238}U in the walls of the mine shaft. Therefore if the solubility of the uranium and radium were the same, they should have similar activity concentrations in the acid mine water. But the activity of radium is below the lower limit of detection (LLD) for gamma spectrometry and the detection limit for ICP-MS, unlike the uranium. The dominance of the radium sulphate is a good explanation for why the activity is so low. The species make up 77% of all radium in the AMD between pH 2 and 12.5, its concentration dropping only slightly above pH 12.5 as some hydroxy species start to come into the system. The other species that exist throughout the pH range 1-14 is Ra^{2+}, which consistently makes up about 23% of radium in the AMD. The species also decreases in concentration slightly at pH 12.5. Under extreme alkaline conditions, pH≥12.5, two hydroxy species are predicted to be present in the AMD. These species are $RaOH^+$ and the neutral species $Ra(OH)_{2(aq)}$. $RaOH^+$ starts to appear in solution at pH 12.5 and increases in concentration, making up a maximum of 24% of radium at pH 14. The neutral hydroxy species only starts to appear in solution at pH 13 and increases slightly to make up 7% radium at pH 14.

4.7.2.2 Reducing conditions

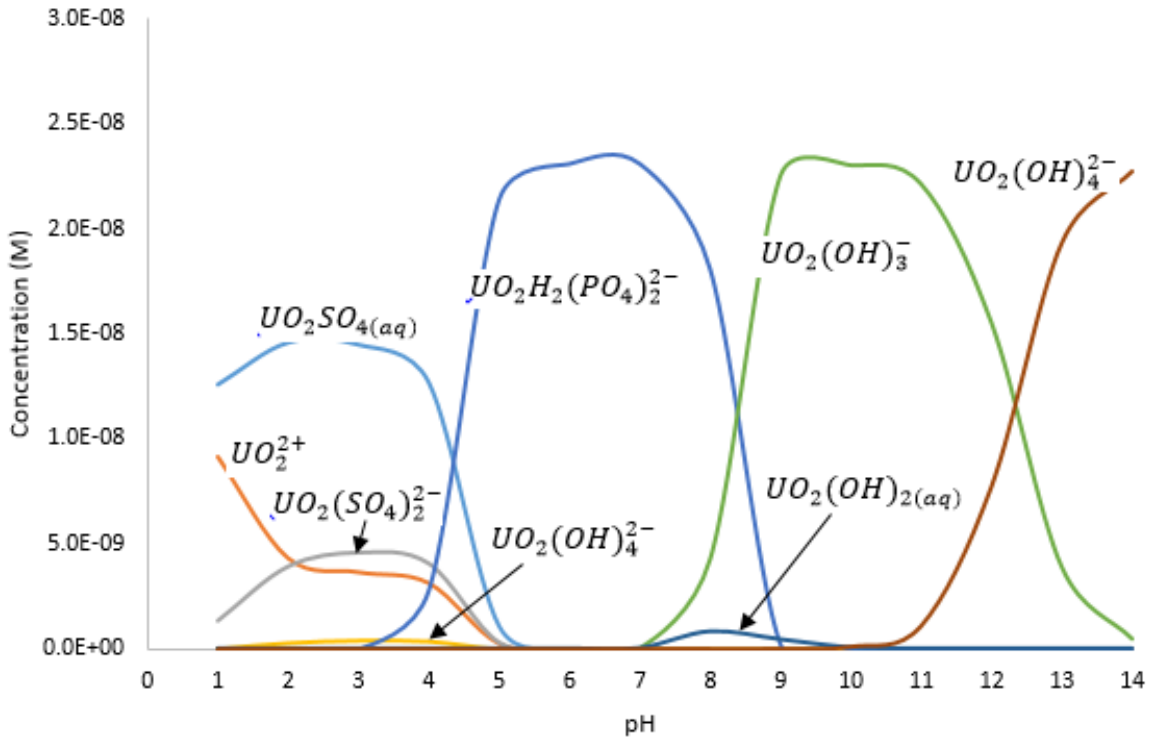

Figure 40: Uranium speciation under reducing conditions modelled using JESS.

Figure 40 shows the speciation of uranium under reducing conditions as predicted by JESS. Under acidic conditions JESS predicts the same species to exist in solution as Visual Minteq. But there is a difference in the pH range under which those species exist and also there is a difference in the proportions of the different species. Four species are predicted in the system in this pH range, three sulphate species and the uranyl species. The dominant species in this region is the neutral uranyl sulphate species $UO_2SO_{4(aq)}$. The species dominates between pH 1 and 4.5, having a maximum concentration at pH 2 (63%), and disappears from the system at pH 5.5. The uranyl species has its highest concentration at pH 1 which is the lowest pH scanned in this study, making up 40% of the uranium. The concentration of the species drops sharply between pH 1 and 2, and stays at an almost constant concentration until pH 4 after which it drops sharply again to become insignificant at pH 5. The next species in terms of importance in this pH region is the negative sulphate species $UO_2(SO_4)_2^{2-}$. The species increases in concentration between pH 1 and 2, then it stays almost constant until pH 4 and decreases to insignificance at pH 5. The last species in this region is

$UO_2(SO_4)_3^{4-}$, whose concentration is quite low even at its maximum it makes up about 1% of the uranium species.

In the pH region 5 to 8.5 the negatively charged mononuclear species $UO_2H_2(PO_4)_2^{2-}$. The species is predicted to appear at pH 3, increasing to a maximum concentration at pH 7, where all the uranium in the AMD exist at this species. It is the perfect species to target for ion exchange resin removal of uranium from the AMD. The species decrease in concentration sharply between pH 7 and 9, becoming insignificant at pH 9. The neutral species $UO_2(OH)_{2(aq)}$ is also predicted to exist between pH 7 and 9, but in low concentrations. In the pH region 9-14 only two species, $UO_2(OH)_3^-$ and $UO_2(OH)_4^{2-}$ exist in significant concentrations in the AMD. $UO_2(OH)_3^-$ is predicted to exist in the AMD in significant concentrations starting at pH 8, reaching a maximum concentration at pH 9 where all the uranium in the AMD exists as this species. The concentration of this species drops sharply between pH 11 and 13. $UO_2(OH)_4^{2-}$ is the dominant species under extremely alkaline conditions, appearing in the system at pH 11, making up almost all the uranium in the AMD at pH 14.

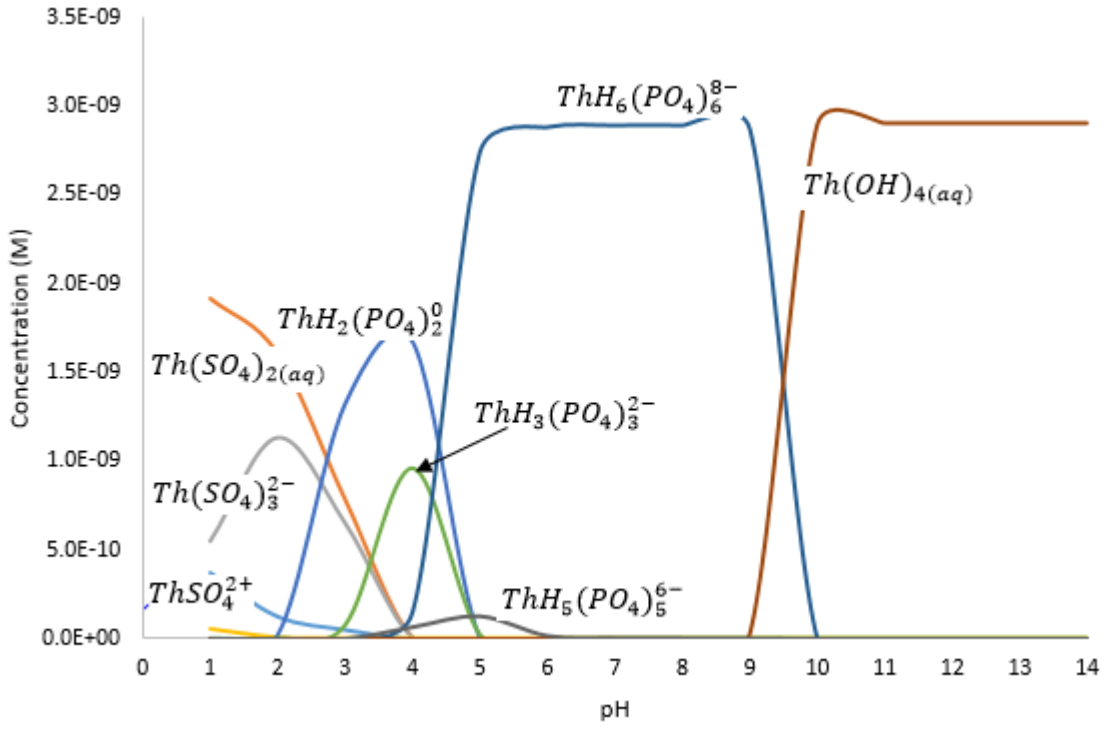

Figure 41: Thorium speciation in AMD under reducing conditions modelled using JESS.

Figure 41 shows the speciation of thorium under reducing conditions as a function of pH. There is a notable difference both in the number and identity of species predicted by JESS under these conditions than those predicted by Visual Minteq under the same set of conditions. In the pH region 1-3, there are three major thorium species. These three species; $ThSO_4^{2+}$, $Th(SO_4)_{2(aq)}$ and $Th(SO_4)_3^{2-}$, are also predicted by the Visual Minteq facility.In addition to these three JESS predicts that the species $ThH(SO_4)_2^{+}$ will exist within this region in significant concentrations. The most dominant species is the neutral sulphate species, $Th(SO_4)_{2(aq)}$, which makes up more than 65% of all the thorium species at pH 1, decreasing sharply to insignificant concentrations at pH 4. $Th(SO_4)_3^{2-}$ increases in concentration from pH 1 and has a predicted maximum concentration at pH 2, where its makes up 39% of the thorium in the system. The positively charged sulphate species, $ThSO_4^{2+}$, also exists in significant concentration in this pH region, decreasing in concentration gradually between pH 1 and 3, where its concentration becomes insignificant in the chemistry of thorium.

In the pH region 3-4.5 there are two species that control the chemistry of thorium. These species were not predicted by the Visual Minteq modelling facility, which predicted that the sulphate species will still be controlling the chemistry of thorium in this pH region under the set of prevailing conditions. JESS on the other hand predicts that hydrogen phosphate species will start to dominate the chemistry of thorium in this pH region. The species $ThH_3(PO_4)_3^{2-}$ starts to occur in the AMD in significant concentrations at pH 3, having a maximum concentration at pH 4 (34%). The concentration of this species is predicted to decrease sharply between pH 4 and 5. The species $ThH_2(PO_4)_2^{0}$ is the most dominant species in this pH region, having its maximum concentration at pH 4 (58%). This species is also not predicted to occur in significant concentrations in the AMD under reducing conditions by Visual Minteq.

In the pH region 4.5-14, there are only three species that are important in the chemistry of thorium. $ThH_6(PO_4)_6^{8-}$ is the predominant species between pH 4.5 and 9.5 and it is almost the only species that is predicted to exist in the system in the pH range 5-9. This species makes it almost impossible to remove thorium from the AMD using cation exchange resin in this pH region. Therefore according to the prediction by JESS model, this pH region cannot be used in the removal of thorium from AMD using cation exchange resin. The species $ThH_5(PO_4)_5^{6-}$ also exists in significant concentrations

between pH 4 and 6 but does not have a big influence in the chemistry at any pH level. Above pH 9.5 the neutral hydroxy species, $Th(OH)_{4(aq)}$ is the only species that is predicted to exist in the AMD by JESS.

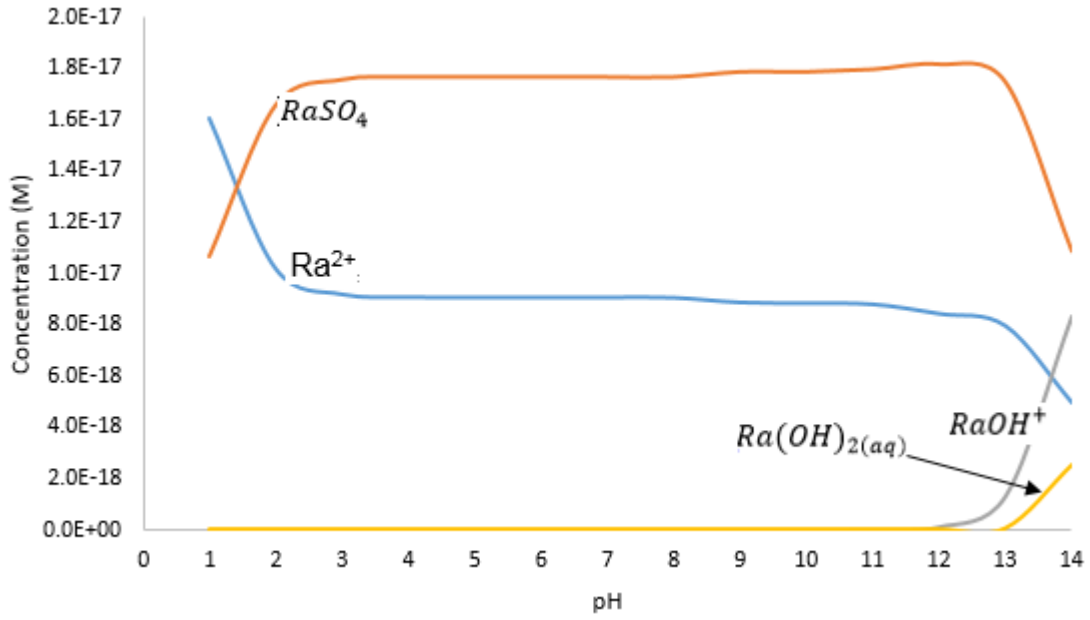

Figure 42: Radium speciation under reducing conditions

As seen in Figure 42 the speciation of the radionuclide radium is not influenced by the redox potential of the AMD that much. The same four species exist under both oxidising and reducing conditions, albeit in slightly different proportions.

4.8 Treatment methodologies results

4.8.1 Reverse osmosis

Table 20 presents the gross alpha and gross beta activity concentration in mine shaft AMD after treatment using reverse osmosis method. The gross alpha activity concentrations are mostly below 1 Bq/L, with the exception of two sampling points considered. Three treated samples had a gross alpha activity concentration that was below the detection limit of the liquid scintillation counting system. In terms of the WHO guidance level the gross alpha activity is still above the 0.5 Bq/L and would therefore still require radionuclide specific analytical considerations to determine its potential risk as portable water. In terms of the gross beta activity concentration, the mine shaft AMD is below the WHO guidance level of 1 Bq/L. Therefore the gross beta activity is not a concern even if the water was to be used as portable water.

Table 20: Gross alpha and gross beta activity concentrations in mine shaft AMD after reverse osmosis treatment

Sample ID	Alpha activity (Bq/L)	Beta activity (Bq/L)
G1	1.477±0.337	<0.026
G2	<0.029	<0.026
G3	0.786±0.327	<0.026
G5	0.663±0.325	0.293±0.144
G9	<0.029	<0.026
G12	0.341±0.320	0.275±0.144
G16	<0.029	<0.026
G17	1.212±0.333	<0.026
G19	<0.029	<0.026
G WASTE	0.407±0.321	0.558±0.153

In terms of release into the environment the mine shaft AMD treated using reverse osmosis is safe. The concentration of alpha active radionuclides combined is at most 1.48 Bq/L. The activity concentration of both gross alpha and gross beta in the rejection stream (G WASTE) is also not high. This means that most of the radioactivity that is removed remains in the reverse osmosis membrane.

Table 21: Gross alpha and gross beta removal rate using reverse osmosis for mine shaft AMD

Sample	Gross alpha removal	Gross beta removal
G1	31.20%	97.86%
G2	98.69%	97.90%
G3	62.32%	99.15%
G5	66.32%	78.33%
G9	98.75%	98.18%
G12	87.12%	90.89%
G16	98.93%	99.26%
G17	58.40%	99.29%
G19	99.05%	99.36%
Average	77.87%	95.58%

The ability of reverse osmosis as a method to remove radioactivity from AMD is demonstrated in Figure 43 and Figure 44. Table 21 presents the removal percentage of gross alpha and gross beta activity for mine shaft AMD using reverse osmosis. A maximum removal of 99% and a minimum of 31% with an average removal of 78% is achieved. The removal of 31% in sample G1 was most likely due to an error in pH adjustment, which affected the chemistry of the radionuclides. If G1 is not considered the average removal increases to 83%. The gross beta removal for this treatment method is very good, showing an average removal of over 95%.

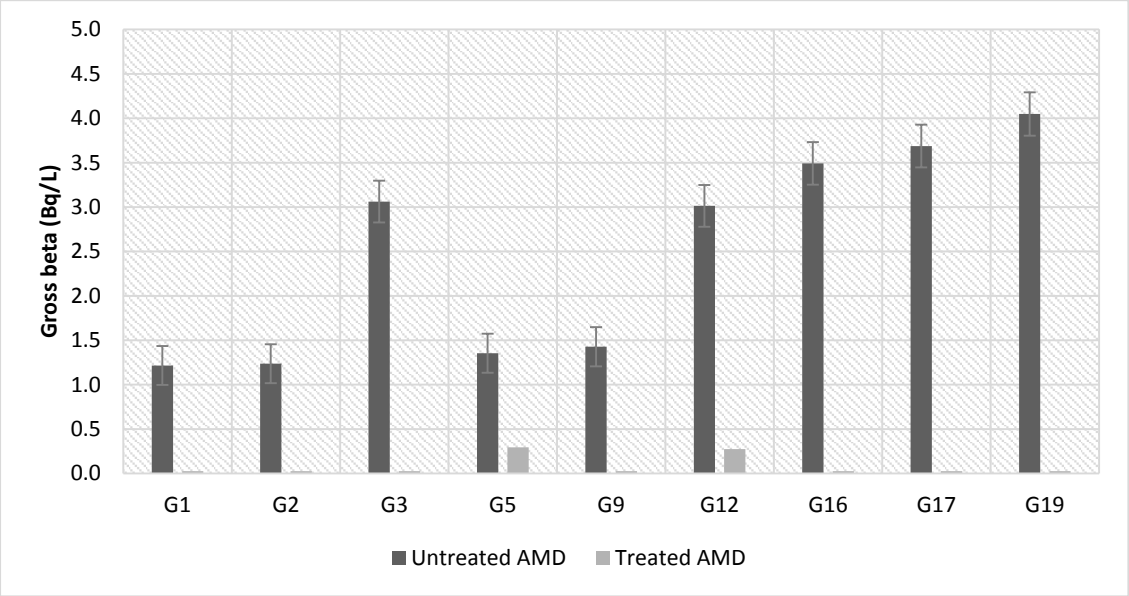

Figure 43: Graphical presentation of gross beta activity before and after treatment using reverse osmosis.

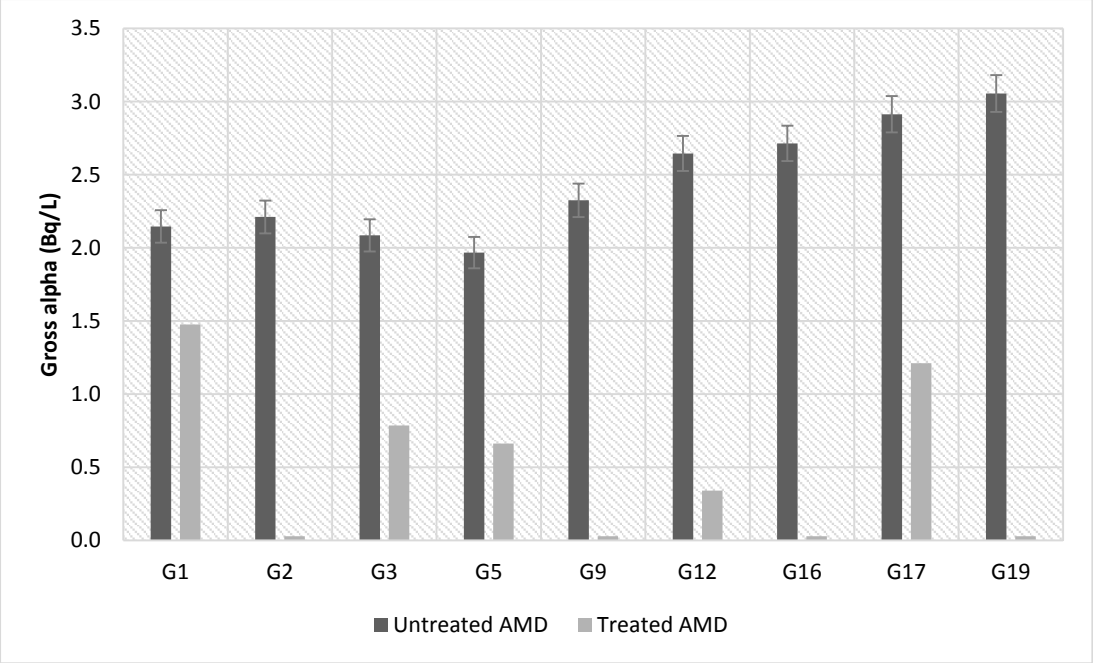

Figure 44: Graphical presentation of gross alpha activity of mine shaft AMD before and after treatment using reverse osmosis.

Table 22*:* Gross alpha and gross beta activity concentrations in surface AMD after reverse osmosis treatment

Sample ID	Alpha activity (Bq/L)	Beta activity (Bq/L)
L5	2.319±0.348	0.435±0.149
L6	2.755±0.354	<0.026
L7	2.111±0.345	<0.026
L8	3.143±0.359	0.312±0.145
L9	0.379±0.321	<0.026
L10	2.802±0.355	0.256±0.143
L11	3.067±0.358	<0.026
L12	2.546±0.351	0.369±0.147
L18	2.158±0.346	<0.026
L20	2.177±0.346	0.360±0.147
L WASTE	5.547±0.390	6.039±0.274

Table 22 presents the gross alpha and gross beta activity concentrations in reverse osmosis treated surface AMD. In all but one of the treated samples, the gross alpha

activity concentration is above 2 Bq/L. This follows from the fact that the initial gross alpha concentration in surface AMD was high. The treated AMD is still above the WHO guidance level of 0.5 Bq/L for portable water. The gross beta activity on the other hand is low after reverse osmosis treatment. All of the treated samples show a gross beta activity concentration below 1 Bq/L, which is the guidance level set by the WHO for gross beta activity in portable water. The waste stream of the reverse osmosis treatment method produces slightly radioactive waste. Even though the waste stream shows higher activity concentrations compared to the treated stream, the activities are still only 10% of the activity concentrations found in the untreated surface AMD. This leaves most of the radioactivity trapped in the reverse osmosis membrane.

The removal of gross alpha activity from surface AMD using reverse osmosis method is high as shown inTable 23. The average removal rate is 96% of gross alpha activity, with one sample showing as high as 99% removal rate. The gross alpha removal percentage is higher than that observed in mine shaft AMD even though the final activity concentration is still higher in the surface AMD.

Table 23: Percentage removal of gross alpha and gross beta activities from surface AMD using reverse osmosis

Sample ID	**Gross alpha removal**	**Gross beta removal**
L5	96.33%	99.24%
L6	95.56%	99.95%
L7	96.51%	99.95%
L8	95.03%	99.47%
L9	99.39%	99.96%
L10	95.50%	99.56%
L11	95.08%	99.96%
L12	95.85%	99.37%
L18	96.57%	99.96%
L20	96.55%	99.39%
Average	96.24%	99.68%

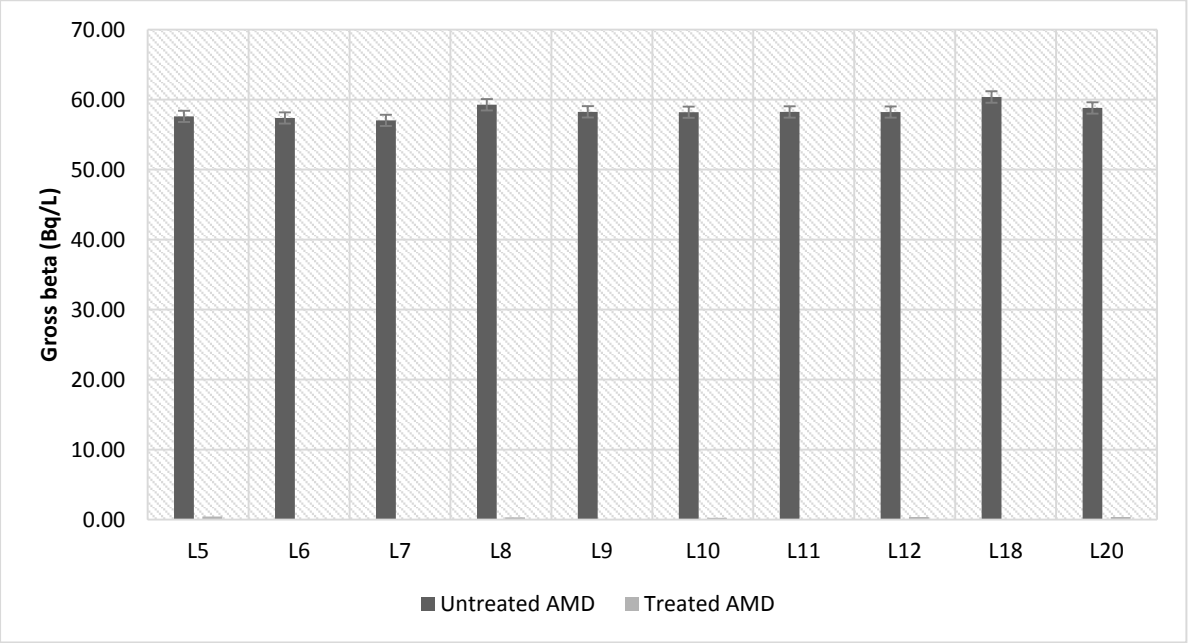

Figure 45: Gross beta activity concentration for surface AMD before and after reverse osmosis treatment.

The difference in removal rates is down to the difference in chemistry of the two types of AMD. The gross beta activity removal is as good for surface AMD as it is for mine shaft AMD, showing an average removal rate of 99.7%. Figure 45 and Figure 46 demonstrate the change in both the gross alpha and gross beta activity concentrations after treatment.

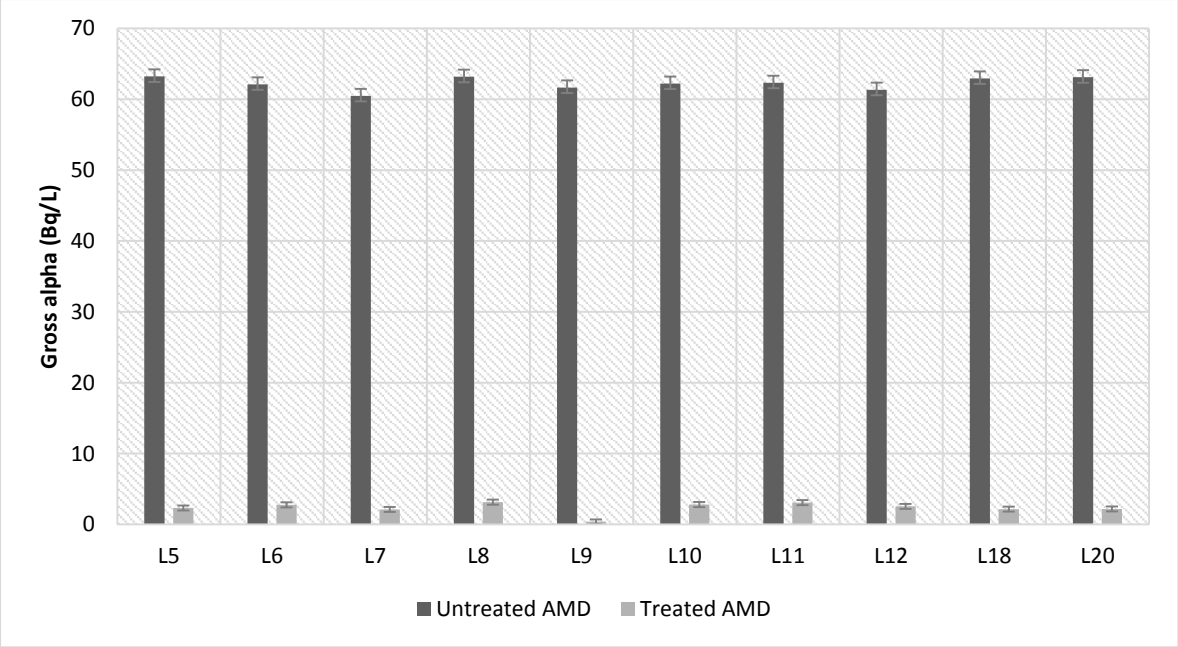

Figure 46: Gross alpha activity concentrations of samples before (untreated) and after (treated) treatment using reverse osmosis.

4.8.2 Ion Exchange

Table 24: Gross alpha and gross beta activity concentration in mine shaft AMD samples after treatment using ion exchange

Sample ID	Alpha activity (Bq/L)	Beta activity (Bq/L)
G1	<0.029	0.134±0.074
G2	<0.029	0.065±0.007
G3	0.164±0.087	0.222±0.086
G5	<0.029	<0.026
G9	<0.029	0.129±0.073
G12	<0.029	<0.026
G16	<0.029	0.391±0.091
G17	0.040±0.0346	<0.026
G19	<0.029	<0.026

The gross alpha and gross beta activity concentration of the mine shaft AMD is reduced drastically after treatment with ion exchange method. In most samples that were treated, the gross alpha activity falls below the detection limit of the Quantulus LSC detector. When the AMD was treated with reverse osmosis method, the gross

alpha activity was still above the WHO guidance level. The highest activity concentration, as can be seen in Table 24, falls to 0.164 Bq/L. This activity concentration is below the WHO guidance level for portable water. The gross beta activity concentration also falls well within the WHO gross beta guidance level for portable water. The highest gross beta activity concentration for ion exchange treated mine shaft AMD is just 0.391 Bq/L.

Table 25: Gross alpha and gross beta removal rate from mine shaft AMD after ion exchange treatment

Sample	Gross alpha removal	Gross beta removal
G1	98.65%	88.96%
G2	98.69%	94.73%
G3	92.15%	92.74%
G5	98.53%	98.08%
G9	98.75%	90.97%
G12	98.90%	99.14%
G16	98.93%	88.81%
G17	98.62%	99.29%
G19	99.05%	99.36%
Average	98.03%	94.68%

The ability of ion exchange treatment method to remove radioactivity from AMD is tremendous. An average gross alpha activity removal of 98% is observed, with only one treated sample showing a removal rate of 92%. The gross alpha removal rate is slightly higher compared to the gross beta removal rate as can be seen in Table 25. This removal ability is demonstrated in Figure 47 and Figure 48. The scenario in AMD treatment where the gross alpha removal is better than the gross beta removal is a better outcome than a lower gross alpha removal. The reason for this is because from Annexure 1 and Annexure 2, it can be seen that from the ^{238}U series only ^{210}Pb is a long lived beta emitter and ^{228}Ra is the only long lived beta emitter in the ^{232}Th decay series. Therefore most of the beta emitters in both series will decay fast when their long-lived alpha emitting parents are removed. The opposite is true when the alpha emitters are not removed efficiently from the AMD. The activity of the AMD will actually

increase over time, as the daughter nuclides of the long-lived alpha emitters start to grow in.

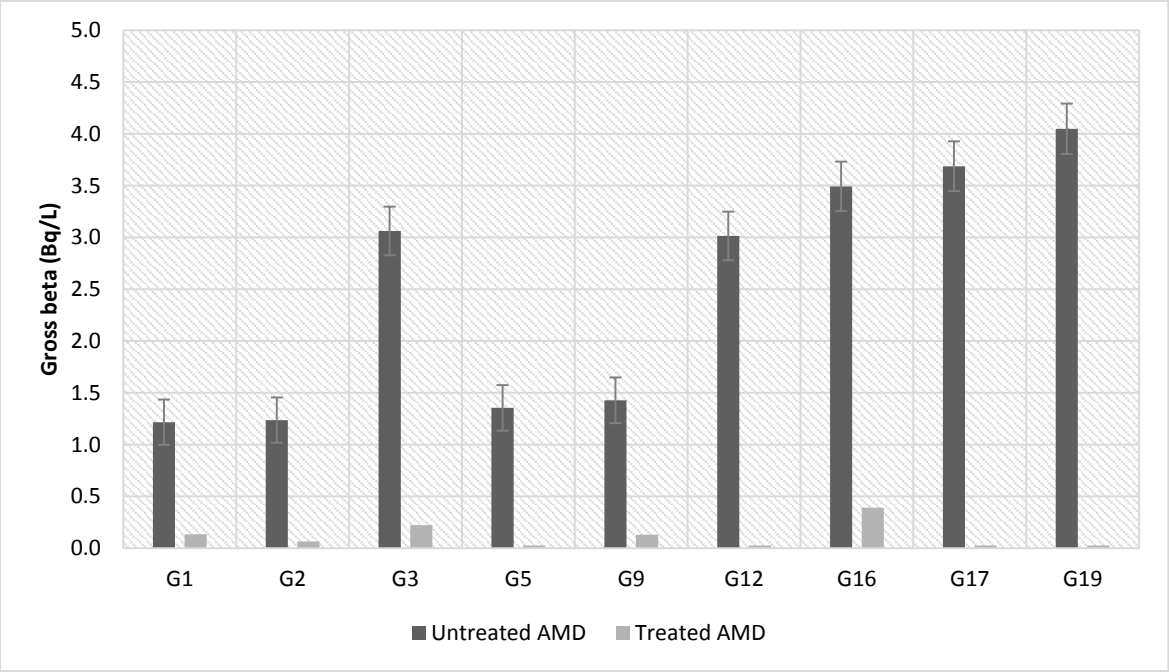

Figure 47: Gross beta removal in mine shaft AMD after ion exchange treatment.

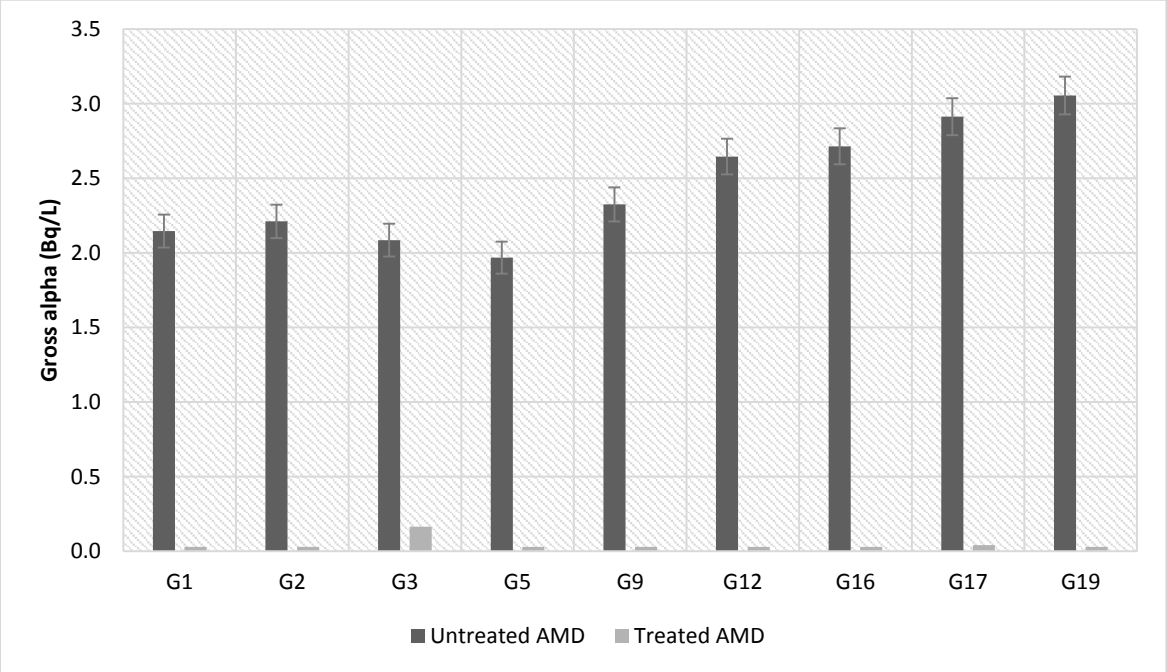

Figure 48: Gross alpha removal in mine shaft AMD after ion exchange treatment.

The activity concentration of surface AMD samples after ion exchange treatment is presented in Table 26. The gross alpha activity concentration in the treated samples

falls below the detection limit for 70% of treated samples. The maximum gross alpha activity concentration is 0.211 Bq/L. This maximum value is less than the WHO guidance level for gross alpha activity in portable water. The gross beta activity removal is not as good as the gross alpha activity removal. The treated samples still have gross beta activities that are above the guidance level for gross beta activity. The maximum gross beta activity is 8.32 Bq/L and the minimum is 1.61 Bq/L.

Table 26: Gross alpha and gross beta activity concentration of surface AMD after treatment using ion exchange

Sample ID	Alpha activity (Bq/L)	Beta activity (Bq/L)
L5	0.211±0.012	8.32±0.47
L6	<0.029	4.54±0.22
L7	<0.029	3.50±0.21
L8	<0.029	2.04±0.24
L9	<0.029	4.20±0.22
L10	0.183±0.010	4.36±0.22
L11	<0.029	3.32±0.21
L12	<0.029	3.20±0.21
L18	<0.029	2.89±0.21
L20	0.050±0.002	1.61±0.20

The removal rate of radioactivity from surface AMD is presented in Table 27. The gross alpha activity removal using this method of treatment is 99.9%. This is an excellent removal rate, leaving the water good enough to be used even as portable water. The gross beta removal rate is also good, reaching an average removal rate of almost 94%. As discussed earlier this is not a bad situation since the beta activity of AMD water will gradually decrease if the long-lived alpha emitting parent nuclides are removed.

Table 27: Gross alpha and gross beta removal rate from surface AMD using ion exchange

Sample ID	Gross alpha removal	Gross beta removal
L5	99.67%	85.56%
L6	99.95%	92.08%
L7	99.95%	93.86%
L8	99.95%	92.65%
L9	99.70%	94.29%
L10	99.95%	94.50%
L11	99.95%	95.04%
L12	99.95%	97.23%
L18	99.92%	96.61%
L20	99.95%	96.52%
Average	99.90%	93.84%

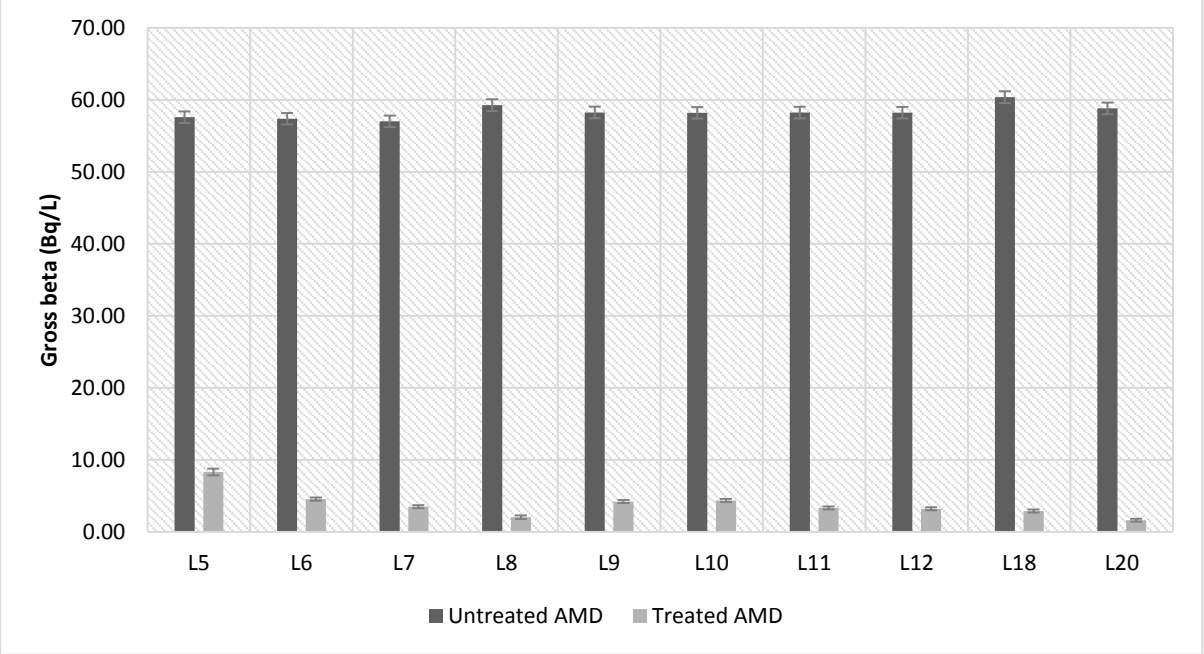

Figure 49: Gross beta activity concentration of surface AMD before and after ion exchange treatment.

Figure 49 shows the difference in the beta activity concentration in surface AMD before and after treatment using ion exchange. The difference in alpha activity concentration

before and after treatment could not be demonstrated due to the extremely low activity concentration after treatment.

4.8.3 Coagulation/flocculation and filtration

Table 28: Gross alpha and gross beta activity concentrations in mine shaft AMD after treatment using coagulation/flocculation and filtration

Sample ID	Alpha activity (Bq/L)	Beta activity (Bq/L)
G1	0.341±0.069	0.420±0.107
G2	0.313±0.068	0.422±0.097
G3	0.412±0.071	1.170±0.107
G5	0.171±0.062	0.449±0.096
G9	0.114±0.060	0.459±0.906
G12	0.199±0.069	0.791±0.107
G16	0.384±0.063	0.760±0.106
G17	0.355±0.070	0.853±0.207
G19	0.497±0.074	0.944±0.107

Table 28 presents the gross alpha and the gross beta activity concentrations of coagulation/flocculation and filtration treated mine shaft AMD. The gross alpha activity concentration in all treated samples is below the WHO guidance level for portable water. The maximum activity concentration is 0.497 Bq/L, which is close to the guidance level but still below. The gross beta activity in most treated samples is also below the guidance level recommended by WHO, with only one sample showing an activity concentration above the guidance level.

The removal rate for both gross alpha and gross beta for this treatment method is not as good as the other treatment methods. The average gross alpha removal rate is just above 87%. The initial activity in mine shaft AMD is low and therefore such a removal percentage is sufficient to reduce the activity to levels below regulation limits. If the gross alpha activity was to get higher though, the method would struggle to reduce the gross alpha activity to the required levels.

Table 29: Gross alpha and gross beta removal rate from mine shaft AMD after coagulation/flocculation and filtration treatment

Sample	Gross alpha removal	Gross beta removal
G1	84.10%	65.47%
G2	85.85%	65.85%
G3	80.23%	61.77%
G5	91.32%	66.86%
G9	95.09%	67.87%
G12	92.47%	73.76%
G16	85.86%	78.24%
G17	87.80%	76.86%
G19	83.72%	76.67%
Average	87.38%	70.37%

The gross beta activity removal rate is worse than the gross alpha removal rate, with an average of just over 70% removal. The method is not good for the removal of gross beta activity from AMD, especially AMD that is formed under the reducing conditions of the mining shaft. Figure 50 and Figure 51 demonstrate the difference in the untreated and the treated AMD water. It is easy to note from these figures that even though the activity concentration gets reduced to levels below guidance levels, the method is not so good.

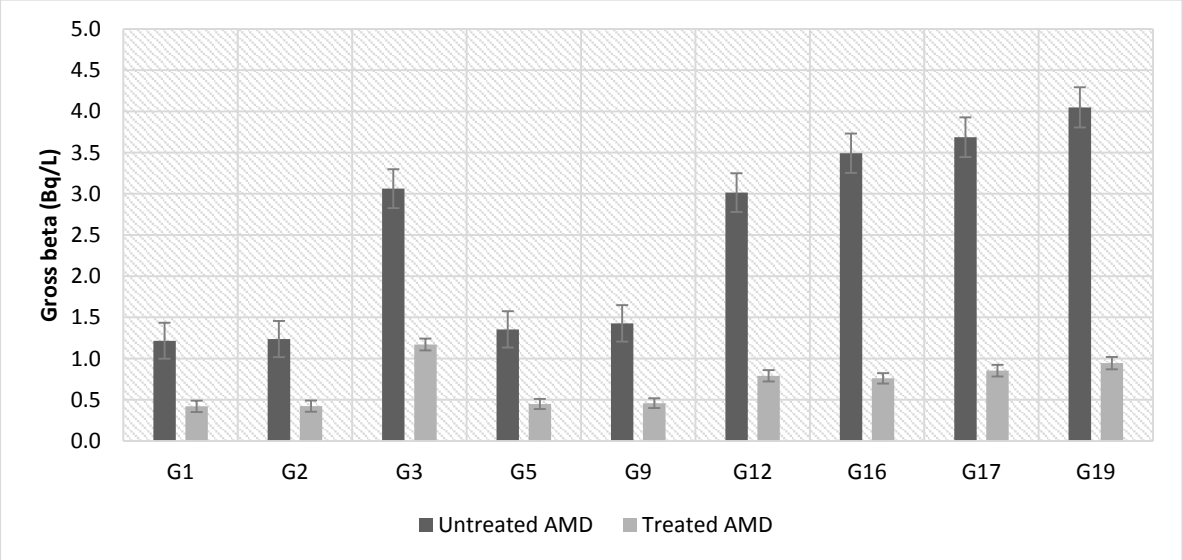

Figure 50: Gross beta activity in mine shaft AMD before and after coagulation/flocculation and filtration treatment.

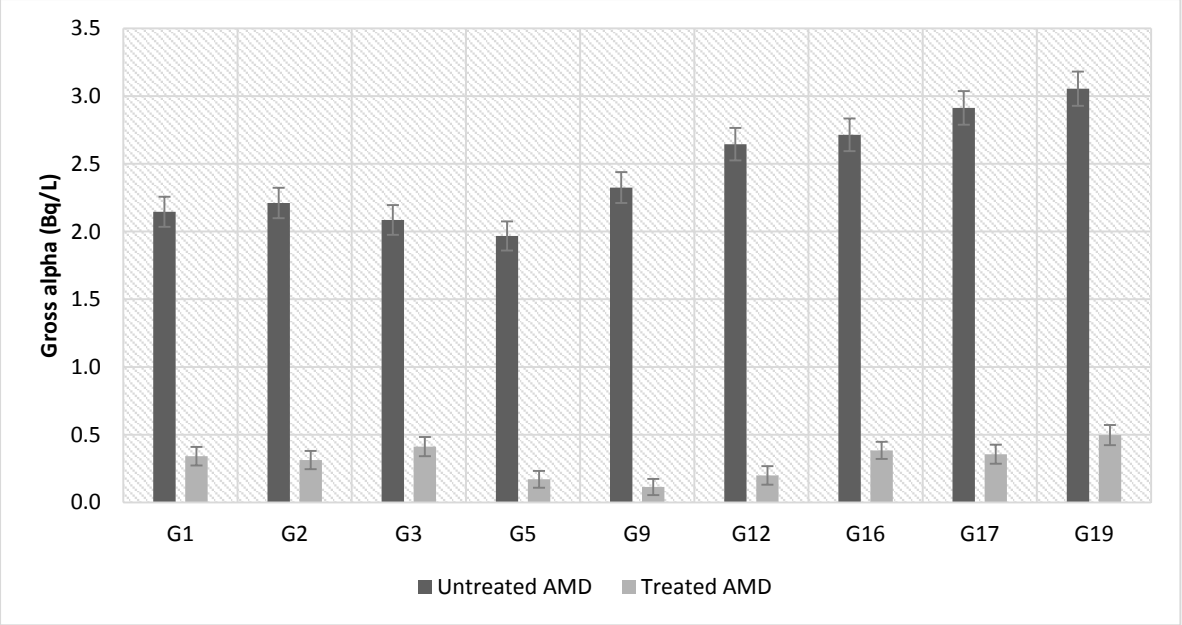

Figure 51: Gross alpha activity in mine shaft AMD before and after coagulation/flocculation and filtration treatment.

Table 30: Gross alpha and gross beta activity concentration in coagulation/flocculation and filtration treated surface AMD

Sample ID	Alpha activity (Bq/L)	Beta activity (Bq/L)
L5	0.36±0.14	5.88±0.15
L6	1.34±0.15	5.31±0.25
L7	2.78±0.12	5.10±0.22
L8	2.29±0.16	5.82±0.26
L9	0.29±0.15	5.68±0.25
L10	2.86±0.10	6.02±0.25
L11	1.33±0.19	5.13±0.29
L12	6.37±0.15	4.40±0.25
L18	4.57±0.15	6.28±0.25
L20	4.98±0.17	8.85±0.27

The initial activity concentration in mine shaft AMD was low, and therefore the treatment method was able to reduce the radioactivity to a level that is below the WHO guidance level. However, surface AMD had a high initial activity concentration for both gross alpha and gross beta. Therefore, as seen in Table 30, the gross alpha activity,

even though reduced by a large percentage is still above the WHO guidance level or portable water. Only two samples that were treated showed a value below the guidance level. The rest of the treated samples had activity concentrations above the 0.5 Bq/L WHO guidance level for gross alpha. The maximum activity concentration observed in treated samples was 6.37 Bq/L. The same is observed with the gross beta activity concentration. All treated samples had a gross beta activity concentration above the WHO guidance level for portable water.

Table 31: Gross alpha and gross beta removal rate for coagulation/flocculation and filtration treatment of surface AMD

Sample ID	Gross alpha removal	Gross beta removal
L5	99.43%	89.79%
L6	97.84%	90.74%
L7	95.41%	91.06%
L8	96.37%	90.18%
L9	99.53%	90.25%
L10	95.40%	89.65%
L11	97.87%	91.20%
L12	89.62%	92.44%
L18	92.75%	89.60%
L20	92.11%	84.96%
Average	95.63%	89.99%

The average removal rate for coagulation/flocculation and filtration was better for surface AMD than mine shaft AMD. The reason for the difference is most likely due to the difference in chemistry of the two types of AMD. The average gross alpha removal rate was just above 95%, with some samples showing a removal rate higher than 99%. The gross beta activity removal rate was lower than the gross alpha removal rate, with average removal of 90%. Due to the high initial concentration of both gross alpha and gross beta activity, the treated samples still showed activities above the WHO guidance level. Figure 52 and Figure 53 demonstrate the difference in the activity before and after treatment. From the figures it can be seen that the method does remove a large percentage of the initial activity.

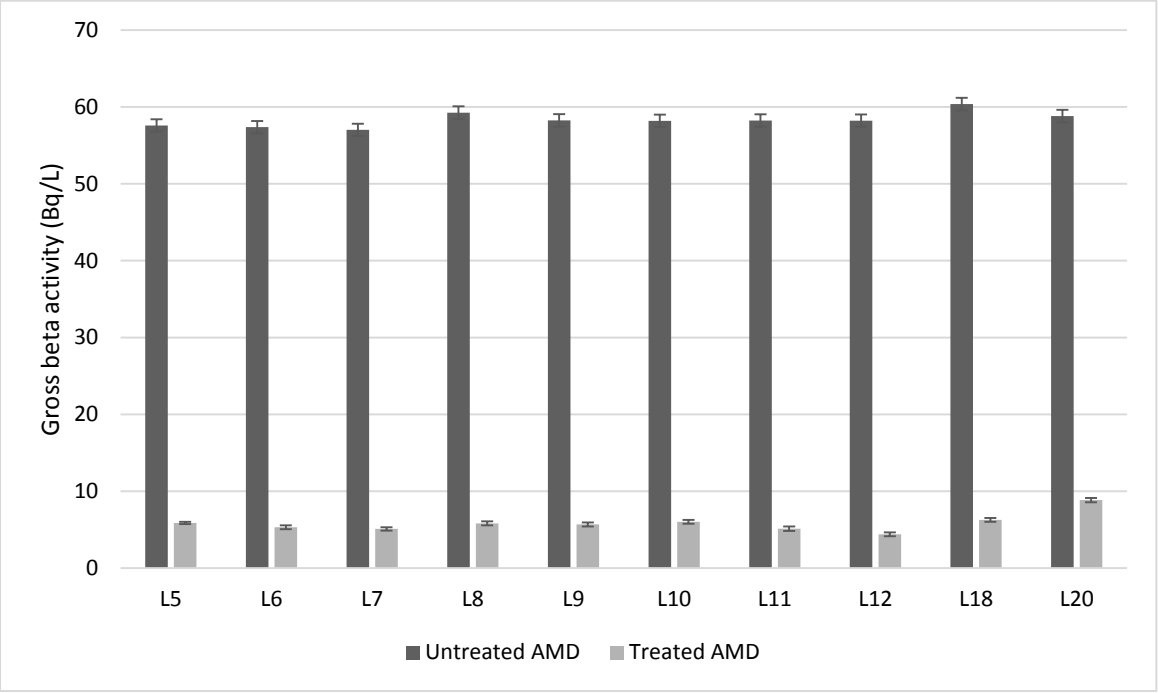

Figure 52: Gross beta activity before and after treatment using coagulation/flocculation and filtration.

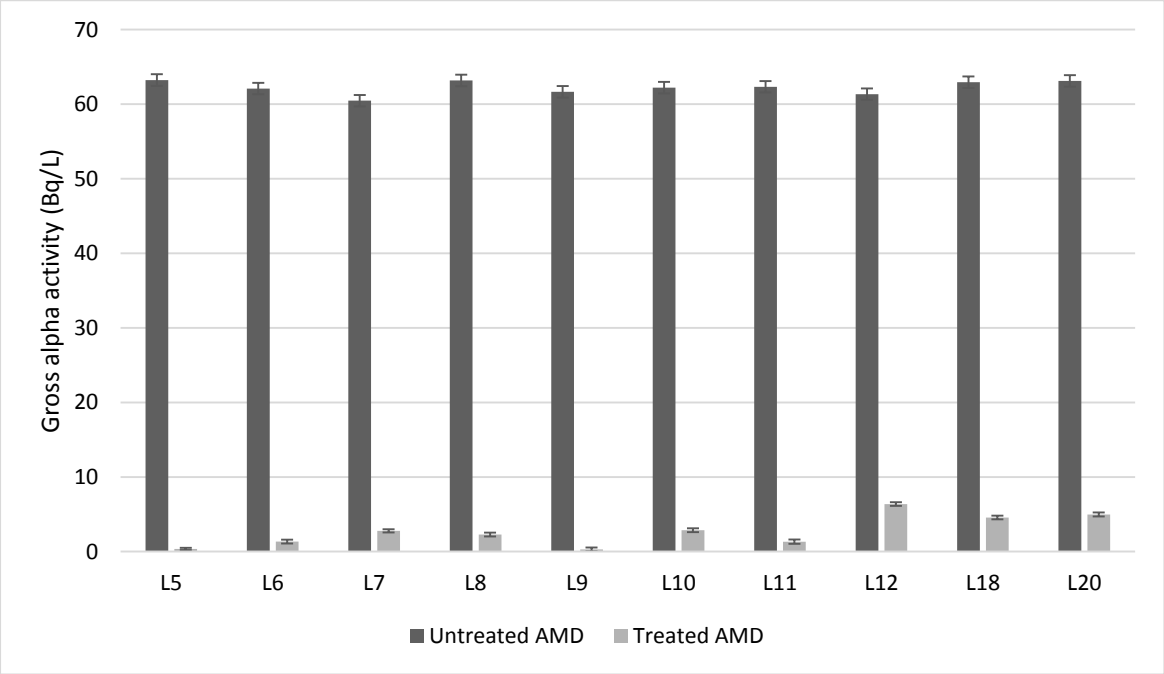

Figure 53: Gross alpha activity before and after coagulation/flocculation and filtration treatment of surface AMD.

4.9 Individual metal removal rates for different treatment methods

4.9.1 Reverse osmosis

Table 32: Concentration of metals in reverse osmosis treated mine shaft AMD

Element	Elemental concentration in mg/L										
	G1 ($\times10^{-3}$)	**G2 ($\times10^{-3}$)**	**G3 ($\times10^{-3}$)**	**G5 ($\times10^{-3}$)**	**G9 ($\times10^{-3}$)**	**G10 ($\times10^{-3}$)**	**G11 ($\times10^{-3}$)**	**G16 ($\times10^{-3}$)**	**G17 ($\times10^{-3}$)**	**G19 ($\times10^{-3}$)**	**Mean ($\times10^{-3}$)**
Be	0.0234	0.124	0.0287	0.0298	0.148	0.0341	0.0319	0.0180	0.0448	0.0191	0.0501
Al	ND	ND	ND	ND	ND	ND	ND	ND	ND	ND	ND
Cr	ND	ND	77.3	ND	ND	ND	ND	ND	ND	ND	77.3
Mn	1640	10400	1750	1990	6020	1430	10900	3270	6980	2860	4720
Mg	8980	75100	10100	12800	44400	8540	79300	22200	32800	18300	31300
K	10400	4900	4490	10100	3210	11200	6470	4840	5710	4300	6560
Fe	ND	63.1	ND	ND	57.7	ND	8.14	ND	ND	ND	43.0
Co	200	777	202	193	403	153	675	249	910	248	401
Ni	192.1	800.4	195	192	432	154	727	256	878	254	408
Cu	22.8	33.3	23.3	20.6	65.3	20.7	23.6	20.3	33.5	38.2	30.1
Zn	484	1380	530	458	745	363	1050	443	2210	516	817
As	1.28	2.95	1.13	0.727	1.99	0.798	1.89	0.910	3.76	1.05	1.65
Se	1.26	3.34	0.809	0.377	1.92	1.02	1.85	1.56	2.07	0.755	1.50
Sr	123	566	130	131	323	100	535	186	562	170	282
Ag	11.5	18.6	10.4	12.2	10.8	14.2	11.5	10.0	12.4	11.7	12.3
Cd	1.01	3.72	0.966	1.06	2.07	0.862	3.29	1.30	4.89	1.25	2.04
Pb	3.56	3.02	2.82	2.75	7.04	2.76	2.89	3.45	2.87	3.43	3.46
Th	ND	ND	ND	ND	ND	ND	ND	ND	ND	ND	ND
U	0.502	1.99	0.685	0.482	2.71	0.694	0.521	0.399	0.512	0.390	0.888

The concentration of metals, including toxic heavy metals in treated mine shaft AMD is presented in Table 32. The concentration of most of the metals is below the WHO guidance levels shown in Table 15. The only metals that are above guidance levels are cadmium and nickel. With chromium, only one sample showed a concentration that is above the guidance level, with all other treated samples having values below the detection limit of the ICP-MS. Zinc doesn't have a guidance level as per the WHO guideline, but the concentration of the metal in all treated samples is above the normal occurrence in surface water. The concentration of radionuclide, ^{232}Th has been reduced to a level below 1.04×10^{-6} ppm. Uranium is a toxic and radioactive heavy metal. In terms of the chemical toxicity, the concentration is below the WHO guidance level of 0.03 mg/L.

Table 33 shows the concentrations of some potentially toxic metals and toxic heavy metals in surface AMD after treatment using reverse osmosis. All metals except nickel, including heavy metals have concentrations below their respective WHO guidance levels. The concentration of zinc is also elevated when compared to the normal occurrence range in surface water. The concentration of toxic and radiotoxic heavy metal uranium is also below the regulation limit of 0.03 mg/L.

Table 33: Concentration of metals in reverse osmosis treated surface AMD

Element	Elemental concentration in mg/L									
	L5 ($\times10^{-3}$)	**L6 ($\times10^{-3}$)**	**L7 ($\times10^{-3}$)**	**L8 ($\times10^{-3}$)**	**L9 ($\times10^{-3}$)**	**L10 ($\times10^{-3}$)**	**L11 ($\times10^{-3}$)**	**L12 ($\times10^{-3}$)**	**L18 ($\times10^{-3}$)**	**Mean ($\times10^{-3}$)**
Be	0.341	0.600	0.547	0.565	0.368	0.995	0.779	0.972	ND	0.712
Al	2700	ND	2540	1870	ND	4280	1970	3460	ND	2950
Cr	ND	ND	ND	ND	ND	ND	ND	ND	ND	ND
Mn	279	756	807	1150	67.1	2320	2250	3400	1060	2030
Mg	4500	6580	6140	7980	5110	13600	11900	16500	68500	18100
K	4300	3730	3540	5400	4010	4090	4880	28600	6170	6550
Fe	288	1690	1370	1290	914	2480	1710	2460	ND	1670
Co	35.7	106	107	144	10	291	270	414	33	250
Ni	46.9	149	140	179	15.4	347	302	429	27.4	269
Cu	20.3	22.0	15.0	39.4	28.2	27.3	24.4	20.5	16.6	31.5
Zn	207	402	369	472	284	881	801	1160	35	757
As	1.58	3.08	2.11	2.19	6.32	3.45	2.95	4.18	1.73	3.55
Se	1.04	1.20	1.42	1.83	0.0539	2.57	3.06	3.52	0.126	2.28
Sr	87.3	140	125	141	109	244	196	275	661	263
Ag	13.0	10.5	10.7	12.7	10.9	10.7	10.6	12.7	11.4	11.6
Cd	0.280	0.605	0.658	0.890	0.128	1.80	1.77	2.93	0.126	1.57
Pb	5.31	6.26	4.16	4.65	8.87	5.32	4.05	4.51	3.07	5.30
Th	ND	ND	ND	ND	ND	ND	ND	ND	ND	ND
U	2.17	3.14	3.02	3.98	0.409	7.55	8.46	12.4	1.14	5.74

4.9.2 Ion exchange

The concentrations of metals, including heavy metals in mine shaft AMD treated using the ion exchange method are presented in Table 34. All analysed metals show very low concentrations in the treated AMD, with concentrations that are lower than their respective WHO portable water guidance levels. The concentration of iron which is a major contributor to the generation of AMD is reduced to levels that are below the

normal occurrence in surface water. The average concentration of zinc in the samples is above the normal occurrence level in surface water, but only slightly.

Table 34: Concentration of metals in ion exchange treated mine shaft AMD

Element	Elemental concentration in mg/L										
	G1 ($\times10^{-3}$)	**G2 ($\times10^{-3}$)**	**G3 ($\times10^{-3}$)**	**G5 ($\times10^{-3}$)**	**G9 ($\times10^{-3}$)**	**G10 ($\times10^{-3}$)**	**G11 ($\times10^{-3}$)**	**G16 ($\times10^{-3}$)**	**G17 ($\times10^{-3}$)**	**G19 ($\times10^{-3}$)**	**Mean ($\times10^{-3}$)**
Be	0.109	0.0416	0.0191	0.00841	0.0159	0.00412	ND	ND	ND	ND	0.0330
Al	ND	ND	ND	ND	ND	ND	ND	ND	ND	ND	19.4
Cr	ND	10.4	ND	ND	0.0909	ND	ND	ND	ND	ND	18.65
Mn	141	28.4	59.1	13.2	18.0	26.9	410	75.4	113	19.7	149
Mg	2270	309	320	298	1300	462	16500	1190	4190	272	5240
Fe	585	188	463	37.8	45.6	297	1320	323	306	208	467
Co	4.77	1.51	1.46	1.22	1.20	1.27	14.1	1.58	6.78	1.21	5.96
Ni	2.52	3.92	1.19	0.945	4.24	1.15	7.71	1.04	3.49	0.817	5.94
Cu	83.3	20.3	16.3	28.0	84.2	16.4	59.4	22.4	31.3	18.8	39.5
Zn	43.8	33.8	28.8	37.5	163.0	37.1	47.5	42.6	33.7	57.1	52.3
As	4.49	0.750	1.83	0.236	0.431	0.349	3.86	2.00	4.36	0.620	2.09
Se	5.48	2.25	1.26	1.24	0.773	1.40	3.83	1.76	1.92	1.11	2.32
Sr	ND	ND	ND	ND	5.37	0.096	0.303	0.836	ND	ND	1.42
Ag	17.4	12.4	13.5	13.2	11.1	13.2	11.4	10.6	17.9	14.5	13.3
Cd	0.401	0.147	0.116	0.128	0.364	0.174	0.135	0.201	0.118	0.147	0.184
Pb	3.30	3.23	3.08	3.42	15.39	3.65	3.49	6.57	2.14	3.72	4.65
Th	ND	ND	ND	ND	ND	ND	ND	ND	ND	ND	ND
U	0.147	0.0637	0.132	0.03	28.8	0.0297	0.0264	0.0101	0.0361	0.0293	2.71

The concentrations of most of the metals analysed and considered in this study were well within the WHO guidance levels for portable water. The only metal that was above its guidance level was arsenic, with an average concentration of 0.016 mg/kg, which is just over the WHO guidance limit of 0.01 mg/kg.

Table 35: Concentrations (mg/L) of metals in ion exchange treated surface AMD

Element	Elemental concentration in mg/L									
	L5 ($\times10^{-3}$)	**L6 ($\times10^{-3}$)**	**L7 ($\times10^{-3}$)**	**L8 ($\times10^{-3}$)**	**L9 ($\times10^{-3}$)**	**L10 ($\times10^{-3}$)**	**L11 ($\times10^{-3}$)**	**L12 ($\times10^{-3}$)**	**L18 ($\times10^{-3}$)**	**Mean ($\times10^{-3}$)**
Be	0.00624	0.0212	0.0191	0.0137	0.0234	0.0234	0.0159	0.0116	0.0180	0.0169
Al	39.0		45.4	27.9		83.0	6.44	110	161	67.6
Cr	1.04	3.59	1.50		0.541	0.856	1.42	0.461	1.42	1.35
Mn	3686	5778	8266	104	8055	7636	8756	7548	9478	6590
Mg	143000	246000	256000	1840	269000	299000	248000	283000	239000	220000
Fe	6950	10800	11800	384	12200	13400	11400	12400	10800	10000
Co	85.5	136	131	10	136	161	122	151	114	116
Ni	56.7	72.5	74.0	16.1	75.2	89.6	67.6	109	69.2	69.9
Cu	53.1	100.7	53.3	27.8	52.8	55.6	48.5	52.1	46.5	54.5
Zn	62.2	68.9	60.6	80.7	51.6	65.3	47.7	60.0	49.6	60.7
As	11.9	17.7	21.1	0.325	19.7	15.2	20.8	17.7	21.0	16.2
Se	8.95	6.99	6.29	1.89	6.15	4.40	3.90	4.08	4.57	5.25
Sr	6.41	11.1	31.9	2.1	27.8	19.8	36.4	23.3	49.4	23.1
Ag	9.17	11.1	10.2	12.1	13.7	9.57	9.76	9.35	11.5	10.7
Cd	0.291	0.497	0.676	0.217	0.618	0.634	0.773	0.582	0.860	0.579
Pb	2.64	5.83	2.30	3.85	2.48	4.40	2.35	2.89	2.09	3.21
Th	ND	ND	ND	ND	ND	ND	ND	ND	ND	ND
U	0.633	0.374	0.571	1.02	0.455	0.618	0.420	0.827	0.633	0.616

4.9.3 Coagulation and filtration

Coagulation/flocculation and filtration is one of the most common treatment methods for portable water in the world, especially in developing countries. The method requires little specialist skill and is not very expensive. Table 36 shows the concentration of metals in mine shaft AMD that has been treated using this method. All metals analysed except for nickel are below their respective regulation limits for portable water.

Table 36: Concentrations of metal elements in mine shaft AMD treated using coagulation and filtration treatment method

Element	Elemental concentration in mg/L										
	G1 ($\times10^{-3}$)	**G2 ($\times10^{-3}$)**	**G3 ($\times10^{-3}$)**	**G5 ($\times10^{-3}$)**	**G9 ($\times10^{-3}$)**	**G10 ($\times10^{-3}$)**	**G11 ($\times10^{-3}$)**	**G16 ($\times10^{-3}$)**	**G17 ($\times10^{-3}$)**	**G19 ($\times10^{-3}$)**	**Mean ($\times10^{-3}$)**
Be	0.0334	ND	ND	0.339	0.0712	ND	ND	ND	ND	ND	0.148
Al	265000	266000	252000	247000	252000	241000	233000	238000	228000	230000	245000
Mg	2591	2171	4253	4287	2078	2148	9081	9255	8301	7961	5213
K	21500	22500	21100	21600	21100	22800	20800	20800	20600	20600	21300
Cr	ND	ND	ND	ND	ND	ND	ND	ND	ND	ND	ND
Mn	20600	18500	19100	20300	19500	16900	17500	19100	17600	18700	18800
Fe	2200	1060	498	945	606	1150	51400	35700	28900	49400	17200
Cd	ND	0.389	ND	0.114	0.0245	ND	ND	ND	0.0114	0.117	0.134
Co	239	195	200	255	198	182	69.4	42.5	37.2	59.3	148
Ni	582	469	483	614	499	446	147	85.9	76.0	127	353
Cu	33.4	31.3	30.2	26.1	27.2	30.6	27.1	32.8	29.5	31.5	30.0
Zn	124	97.8	66.1	96.7	66.8	101	28.7	16.5	27.5	24.5	65.0
As	1.52	1.63	1.70	3.66	2.09	1.80	1.44	1.25	1.66	1.23	1.80
Se	6.09	5.22	5.49	7.65	4.56	4.29	4.43	3.80	3.41	3.75	4.87
Sr	454	444	432	430	433	423	422	426	414	418	430
Ag	44.8	31.8	19.9	34.7	46.1	25.3	49.4	20.1	25.1	66.0	36.3
Pb	ND	0.0514	0.0188	1.17	0.485	8.99	1.87	3.18	2.40	0.840	2.11
Th	ND	ND	ND	0.117	0.0115	ND	ND	ND	ND	ND	0.0641
U	4.78	4.17	1.42	2.66	1.46	1.80	0.106	0.0862	0.0393	0.0652	1.66

Table 37: Concentration (mg/L) of metals in coagulation and filtration treated surface AMD samples

Element	Elemental concentration in mg/L									
	L5 ($\times10^{-3}$)	**L6 ($\times10^{-3}$)**	**L7 ($\times10^{-3}$)**	**L8 ($\times10^{-3}$)**	**L9 ($\times10^{-3}$)**	**L10 ($\times10^{-3}$)**	**L11 ($\times10^{-3}$)**	**L12 ($\times10^{-3}$)**	**L18 ($\times10^{-3}$)**	**Mean ($\times10^{-3}$)**
Be	ND	0.0558	0.436	0.395	ND	0.276	ND	0.197	0.613	0.329
Al	121000	166000	163000	167000	130000	168000	167000	166000	165000	158000
Mg	6320	8100	7150	7380	2310	4960	2940	3990	5860	5210
K	1760	1588	2270	3490	2136	2545	3066	2622	1950	2352
Cr	ND	ND	ND	ND	ND	ND	ND	ND	ND	ND
Mn	14000	45900	44400	46800	15100	45800	44900	45600	45200	39200
Fe	416	489	423	459	382	459	452	423	426	446
Cd	2.67	26.6	26.7	30.8	2.82	30.8	25.7	33.2	38.1	25.7
Co	178	3690	3680	4650	174	4690	3620	4830	4680	3430
Ni	172	6330	6370	8160	159	8080	6080	8400	7940	5870
Cu	61.5	80.8	110	91.5	63.6	119	68.0	98.3	123	89.7
Zn	142	3420	4750	4810	119	5060	2420	5110	6070	3550
As	16.3	12.0	15.2	12.8	15.3	15.9	9.68	14.6	17.6	14.1
Se	4.31	6.51	8.27	7.39	2.94	7.74	4.33	7.23	10.7	6.47
Sr	693	751	751	764	705	767	755	749	736	741
Ag	23.9	35.8	39.8	21.8	54.9	50.5	54.6	18.7	29.4	35.0
Pb	1.70	0.966	0.546	1.27	1.07	2.56	0.709	0.956	1.09	1.16
Th	ND	ND	ND	ND	ND	ND	ND	ND	ND	ND
U	5.81	44.6	106	63.3	7.39	81.9	19.7	70.1	133	56.9

The concentrations of different metals in surface AMD samples that have been treated using coagulation and filtration method are shown in Table 37. Concentrations of arsenic, cadmium, nickel and uranium all exceed their respective WHO guidance limits for portable water. This suggests that this method is not good enough to produce portable water from AMD that has been oxidized through decant or has been formed on the surface.

Chapter 5: Conclusions and recommendations

The aim of this study was to assess ion exchange, reverse osmosis and coagulation filtration, three of the best available treatment methods in the removal of radionuclides and heavy metals from Acid Mine Drainage water and make recommendations on the most appropriate method among the three that South Africa can employ in the treatment of Acid Mine Drainage. South Africa has a problem of AMD that has developed from over a century of gold mining. The South African problem is made worse due to the uranium that is associated with gold in the Witwatersrand basin. There is AMD that is still deep inside the old mining shafts as well as AMD that is decanting or has been formed on the surface. These two types of AMD differ a lot in terms of their chemistry due to the anoxic conditions in the mining shafts and the oxidizing conditions on the surface. This study revealed the significance of this difference in chemistry.

AMD that is on the surface, either through decant or formation, has higher concentrations of heavy metals and radionuclides than AMD that is being pumped directly from the mining shafts. As the AMD gets to the surface, it is oxidized and its ability to dissolve metals into solution increases. Therefore AMD decanting or forming on the surface should be avoided at all costs because not only is it detrimental to the environment but the AMD becomes even more damaging as it oxidizes.

The main radionuclide contaminant in AMD is uranium. The average activity concentration in surface AMD for ^{238}U is 30.7 Bq/L, ^{234}U is 31.5 Bq/L and ^{235}U is 1.4 Bq/L. These makes up the bulk of the average gross alpha activity concentration of 64.1 Bq/L. The activity concentrations of ^{232}Th and ^{226}Ra are very low, with ^{232}Th having an average activity concentration of 0.32 Bq/L and 0.33 Bq/L for ^{226}Ra. Due to the high concentrations of sulphate in the AMD, the radium exists as $RaSO_4$ which is not very soluble and therefore most of the radium is never dissolved into the AMD even though it might present in the contaminating matrix. It takes approximately 241 days to establish this secular equilibrium and the period for which the AMD has been formed is longer than that. Therefore the immediate daughters of ^{238}U, ^{234}Th and ^{234}Pa are the most likely contributors to the gross beta activity of the AMD. Removal of beta

radioactivity from AMD depends mainly on the removal of these radionuclides in this study.

The reverse osmosis treatment method produces water with a gross alpha activity that is largely above the WHO guidance limit of 0.5 Bq/L (Edition, 2011), from both mine shaft and surface AMD. The gross beta activity is below the WHO guidance limit of 1 Bq/L (Edition, 2011) for water produced by this treatment method. Only cadmium and nickel amongst the heavy metals is above the regulation limit in the treated AMD.

The concentrations of some potentially toxic metals and toxic heavy metals in surface AMD after treatment using reverse osmosis were observed in this study. All metals except nickel, including heavy metals have concentrations below their respective WHO guidance levels. The concentration of zinc is also elevated when compared to the normal occurrence range in surface water. The concentration of toxic and radiotoxic heavy metal uranium is also below the regulation limit of 0.03 mg/L.

This makes the treated water very close to being good enough for use as portable water and definitely good enough for use in irrigation and industrial processes. The treated water is also completely safe for disposal into the general environment. However, the method produces a rejection stream of water as waste, with a high concentration of heavy metals and radioactivity and in large scale treatment facilities its volume will also be high. Production of so much toxic and radioactive waste is a huge problem and will make the treatment process expensive.

Ion exchange as a treatment method for AMD shows great removal rates for heavy metals and radioactivity. The average gross alpha activity in treated water for both surface and mine shaft AMD is below the WHO gross alpha guidance limit. Gross beta activity is below 1 Bq/L in treated mine shaft AMD but above that level for surface AMD. A higher gross beta activity is not a big problem for this AMD because the major contributors will decay to insignificant levels over time in the environment. For both surface and mine shaft AMD the treated water had heavy metals concentrations that are below regulation limits. Only arsenic in treated surface AMD had a concentration above its guidance level and even it was just above the limit. This treatment does not produce large volumes of liquid waste like reverse osmosis. The only waste that is produced is the ion exchange resin. This is solid waste and it can be dealt with without

escalating the operation costs since it can be incinerated into much smaller volume and sent to radioactive waste storage facilities.

The last treatment method to consider is coagulation and filtration using alum as a coagulant. This is a standard, well understood and cheap treatment method that is widely used to treat water. The treated water from both mine shaft AMD and surface AMD had gross alpha and gross beta activities which were above the WHO guidance limits for portable water. After treatment the concentration of heavy metals such as arsenic, cadmium, nickel and uranium all remained above their respective WHO guidance limits for portable water. The water that is produced is not good for any use and is not safe for disposal in the general environment.

The performance of coagulation and filtration treatment method in this study for removal of radioactivity in AMD was poor and therefore it is not recommended for use in the treatment of AMD from the Witwatersrand basin. Reverse osmosis is a good treatment method, producing water that can be useful and safe for disposal into the environment. However, the method produces large volumes of radioactive and toxic waste that will be expensive to deal with. On that basis it is also not recommended as the best method for AMD treatment. According to this study ion exchange is the best method for the removal of both radioactivity and heavy metals from AMD, producing small amounts of solid waste and is recommended for AMD treatment.

Further studies are suggested including studies for coagulation and filtration method using other coagulants such as poly-aluminium chloride (PACl), ferric sulphate, ferric chloride, ferrous sulphate and aluminium chlorohydrate (ACH). A broader study using samples collected from all the mining shafts and AMD decant sites in the Witwatersrand basin is also recommended, as the chemistry of the AMD from other sites might differ from the AMD that was used in this study. .

References

ADLER, R. & RASCHER, J. 2007. A strategy for the management of acid mine drainage from gold mines in Gauteng. *Contract Report for Thutuka (Pty) Ltd. Submitted by the Water Resource Governance Systems Research Group, CSIR: Pretoria. Report No. CSIR/NRE/PW/ER/2007/0053/C.*

ADLER, R. A., CLAASSEN, M., GODFREY, L. & TURTON, A. R. 2007. Water, mining, and waste: an historical and economic perspective on conflict management in South Africa*. The economics of peace and security journal, 2.*

AICHINGER, H., DIERKER, J., JOITE-BARFUß, S. & SÄBEL, M. 2012. Interaction of Photons with Matter. Radiation Exposure and Image Quality in X-Ray *Diagnostic Radiology. Springer.*

AIETA, E. M., SINGLEY, J. E., TRUSSELL, A. R., THORBJARNARSON, K. W. & MCGUIRE, M. J. 1987. Radionuclides in drinking water: an overview. *Journal (American Water Works Association)***,** 144-152.

AKCIL, A. & KOLDAS, S. 2006. Acid Mine Drainage (AMD): causes, treatment and case studies. *Journal of Cleaner Production,* 14**,** 1139-1145.

BEAVON, K. 2017. Johannesburg.

BENES, P. 1982. Physico-chemical forms and migration in continental waters of radium from uranium mining and milling. *Environmental migration of long-lived radionuclides.*

BERG, D. 2004. Radionuclides in the Environment. Man-Made and Natural Radioactivity in Environmental Pollution and Radiochronology. Springer.

BIRKS, J. B. 2013. The Theory and Practice of Scintillation Counting: International Series of Monographs in Electronics and Instrumentation, Elsevier.

BLOWES, D., PTACEK, C., JAMBOR, J. & WEISENER, C. 2003. The geochemistry of acid mine drainage. Treatise on geochemistry, 9, 612.

BOUKHENFOUF, W. & BOUCENNA, A. 2011. The radioactivity measurements in soils and fertilizers using gamma spectrometry technique. Journal of environmental radioactivity, 102, 336-339.

BRATBY, J. 1980. Coagulation and flocculation. England: Uplands.

BRODA, R., CASSETTE, P. & KOSSERT, K. 2007. Radionuclide metrology using liquid scintillation counting. Metrologia, 44, S36.

BURCHAM, W. E. 1973. *Nuclear Physics: An Introduction (A Longman text)* Prentice Hall Press.

CARDEN, K. & ARMITAGE, N. 2013. Assessing urban water sustainability in South Africa–not just performance measurement. *Water SA,* 39**,** 345-350.

CARVALHO, F., CHAMBERS, D., FERNANDES, S., FESENKO, S., GOULET, R., HOWARD, B., KIM, C., MARTIN, P., MOORE, W. & PHANEUF, M. 2014. The environmental behaviour of radium: revised edition. International Atomic Energy Agency.

CEMBER, H. & JOHNSON, T. E. 2009. *Introduction to Health Physics,* New York, McGraw-Hill.

CHOPPIN, G. R. 2006. Actinide speciation in aquatic systems. *Marine Chemistry,* 99**,** 83-92.

CIFFROY, P., GARNIER, J.-M. & PHAM, M. K. 2001. Kinetics of the adsorption and desorption of radionuclides of Co, Mn, Cs, Fe, Ag and Cd in freshwater systems: experimental and modelling approaches. Journal of Environmental Radioactivity, 55, 71-91.

COBUT, V., CIRIONI, L. & PATAU, J. 2004. Accurate transport simulation of electron tracks in the energy range 1 keV–4 MeV. *Nuclear Instruments and Methods in Physics Research Section B: Beam Interactions with Materials and Atoms,* 215**,** 57-68.

COETZEE, H., HOBBS, P., BURGESS, J., THOMAS, A., KEET, M., YIBAS, B., VAN TONDER, D., NETILI, F., RUST, V. & WADE, P. 2010. Mine water management in the Witwatersrand Gold Fields with special emphasis on acid mine drainage. *Report to the Inter-Ministerial Committee on Acid Mine Drainage***,** 146.

COETZEE, H., VAN TONDER, D., WADE, P., ESTERHUYSE, S., VAN WYK, N., NDENGU, S., VENTER, J. & KOTOANE, M. 2007. Acid Mine Drainage in the Witwatersrand: Department of Minerals and Energy. Council for Geoscience, Pretoria. Report.

COETZEE, H., WINDE, F. & WADE, P. 2006. *An Assessment of Sources, Pathways, Mechanisms and Risks of Current and Potential Future Pollution of Water and Sediments in Gold-mining Areas of the Wonderfonteinspruit Catchment: Report to the Water Research Commission*, Water Research Comission.

COHEN-TANNOUDJI, C., DUPONT-ROC, J. & GRYNBERG, G. 1998. Atom-photon interactions: basic processes and applications. Atom-Photon Interactions: Basic Processes and Applications, by Claude Cohen-Tannoudji, Jacques Dupont-Roc, Gilbert Grynberg, pp. 678. ISBN 0-471-29336-9. Wiley-VCH, March 1998., 678.

CRITTENDEN, J. C., HOWE, K. J., HAND, D. W., TCHOBANOGLOUS, G. & TRUSSELL, R. R. 2012. Principles of water treatment, Wiley.

DAWSON, M. C. 2008. Social movements in contemporary South Africa: the anti-privatisation forum and struggles around access to water in Johannesburg. University of Oxford.

DEBERTIN, K. & HELMER, R. G. 1988. Gamma-and X-ray spectrometry with semiconductor detectors.

DEVANATHAN, R., CORRALES, L. R., GAO, F. & WEBER, W. J. 2006. Signal variance in gamma-ray detectors—A review. *Nuclear Instruments and Methods in Physics Research Section A: Accelerators, Spectrometers, Detectors and Associated Equipment,* 565**,** 637-649.

DICKSON, B. 1990. Radium in groundwater. *The environmental behaviour of radium,* 1**,** 335-372.

ECKERMAN, K., HARRISON, J., MENZEL, H. & CLEMENT, C. 2013. ICRP publication 119: compendium of dose coefficients based on ICRP publication 60. *Annals of the ICRP,* 42**,** e1-e130.

EDITION, F. 2011. Guidelines for drinking-water quality. WHO chronicle, 38, 104-8.

EISENBUD, M. & GESELL, T. F. 1997. *Environmental Radioactivity from Natural, Industrial and Military Sources: From Natural, Industrial and Military Sources*, Academic press.

ELECTRICAL4U. 2017. *PN Jucntion diode and its characteristics* [Online]. Available: https://www.electrical4u.com/p-n-junction-diode/ [Accessed 29/03 2017].

FAIRES, R. A. & BOSWELL, G. G. J. 1981. *Radioisotope Laboratory Techniques,* London, Butterworth & Co. Ltd.

FANO, U. 1946. On the theory of ionization yield of radiations in different substances. *Physical Review,* 70**,** 44.

FANO, U. 1947. Ionization yield of radiations. II. The fluctuations of the number of ions. *Physical Review,* 72**,** 26.

FEATHER, C. & KOEN, G. 1975. Mineralogy of the Witwatersrand reefs. Anglo American Research Labs., Crown Mines, S. Afr.

FELMLEE, J. K. & CADIGAN, R. A. 1979. Radium and uranium concentrations and associated hydrogeochemistry in ground water in southwestern Pueblo County, Colorado. US Geological Survey.

FORD, M. 1993. Uranium in South Africa. *Journal of the Southern African Institute of Mining and Metallurgy,* 93**,** 37-58.

FRASER, G., ABBEY, A., HOLLAND, A., MCCARTHY, K., OWENS, A. & WELLS, A. 1994. The X-ray energy response of silicon Part A. Theory. *Nuclear Instruments and Methods in Physics Research Section A: Accelerators, Spectrometers, Detectors and Associated Equipment,* 350**,** 368-378.

GIBSON, J. & LALLY, A. 1971. Liquid scintillation counting as an analytical tool. A review. Analyst, 96, 681-688.

GÓMEZ, P., GARRALÓN, A., BUIL, B., TURRERO, M. J., SÁNCHEZ, L. & DE LA CRUZ, B. 2006. Modeling of geochemical processes related to uranium mobilization in the groundwater of a uranium mine. *Science of The Total Environment,* 366**,** 295-309.

GREENLEE, L. F., LAWLER, D. F., FREEMAN, B. D., MARROT, B. & MOULIN, P. 2009. Reverse osmosis desalination: water sources, technology, and today's challenges. Water research, 43, 2317-2348.

GRENTHE, I. & LAGERMAN, B. 1991. Studies on metal carbonate equilibria. 23. Complex Formation in the Th (IV)-H 2 O-CO 2 (g) System. *Acta Chem Scand,* 45**,** 231-238.

HALLER, E. E. 2006. Germanium: From its discovery to SiGe devices. *Materials Science in Semiconductor Processing,* 9**,** 408-422.

HASSAN, M. A. A., LI, T. P. & NOOR, Z. Z. 2009. Coagulation and flocculation treatment of wastewater in textile industry using chitosan. Journal of Chemical and Natural Resources Engineering, 4, 43-53.

HOBBS, P. & COBBING, J. 2007. Hydrogeological assessment of acid mine drainage impacts in the West Rand Basin, Gauteng Province.

HOLTZHAUSEN, L. 2006. Gauteng: save water or pay the price: water resources management. *Water Wheel,* 5**,** 10-13.

HORROCKS, D. 2012a. Applications of liquid scintillation counting, Elsevier.

HORROCKS, D. 2012b. Organic Scintillators and Scintillation Counting, Elsevier.

HU, Q.-H., WENG, J.-Q. & WANG, J.-S. 2010. Sources of anthropogenic radionuclides in the environment: a review. Journal of environmental radioactivity, 101, 426-437.

HUSSAIN, N. & KRISHNASWAMI, S. 1980. U-238 series radioactive disequilibrium in groundwaters: implications to the origin of excess U-234 and fate of reactive pollutants. *Geochimica et Cosmochimica Acta,* 44**,** 1287-1291.

HYDE, E. K. 1960. The Radiochemistry of Thorium. *In:* ENERGY, U. D. O. (ed.). California.

JANISCH, P. R. 1986. Gold in south Africa. *Journal of the Southern African Institute of Mining and Metallurgy,* 86**,** 273-316.

JIA, G. & JIA, J. 2012. Determination of radium isotopes in environmental samples by gamma spectrometry, liquid scintillation counting and alpha spectrometry: a review of analytical methodology. Journal of Environmental Radioactivity, 106, 98-119.

JOHNSON, D. B. & HALLBERG, K. B. 2005. Acid mine drainage remediation options: a review. Science of the total environment, 338, 3-14.

KHANDAKER, M. U. 2011. High purity germanium detector in gamma-ray spectrometry. *International Journal of Fundamental Physical Sciences,* 1**,** 42-46.

KNOLL, G. 2000. Radiation detectors for X-ray and gamma-ray spectroscopy. *Journal of Radioanalytical and Nuclear Chemistry,* 243**,** 125-131.

KNOLL, G. F. 2010. *Radiation detection and measurement*, John Wiley & Sons.

KOPYLOVA, Y., GUSEVA, N., SHESTAKOVA, A., KHVASCHEVSKAYA, A. & ARAKCHAA, K. Uranium and thorium behavior in groundwater of the natural spa area “Choygan mineral water”(East Tuva). IOP Conference Series: Earth and Environmental Science, 2015. IOP Publishing, 012034.

KRESTOU, A. & PANIAS, D. 2004. Uranium (VI) speciation diagrams in the UO 2 2+/CO 3 2-/H 2 O system at 25° C. *European Journal of Mineral Processing & Environmental Protection,* 4.

LANGMUIR, D. & RIESE, A. C. 1985. The thermodynamic properties of radium. *Geochimica et cosmochimica acta,* 49**,** 1593-1601.

LAPP, R. E. & ANDREWS, H. L. 1972. *Nuclear Radiation Physics,* London, Sir Isaac Pitman and Sons Ltd.

LILLEY, J. 2013. *Nuclear physics: principles and applications*, John Wiley & Sons.

MALAEB, L. & AYOUB, G. M. 2011. Reverse osmosis technology for water treatment: state of the art review. Desalination, 267, 1-8.

MANN, W. B., RYTZ, A. & SPERNOL, A. 2012. Radioactivity measurements: principles and practice, Elsevier.

MAREE, J., ADLEM, C., DE BEER, M., VAN TONDER, G. & VAN DIJK, B. 2006. Neutralization of acid mine water and sludge disposal.

MARKICH, S. J. 2002. Uranium speciation and bioavailability in aquatic systems: an overview. The Scientific World Journal, 2, 707-729.

MARSDEN, D. 1986. The current limited impact of Witwatersrand gold-mine residues on water pollution in the Vaal River system. *Journal of the Southern African Institute of Mining and Metallurgy,* 86**,** 481-504.

MARTINEZ, J., MAYOL, R. & SALVAT, F. 1990. Monte Carlo simulation of kilovolt electron transport in solids. *Journal of Applied Physics,* 67**,** 2955-2964.

MATEO, R. & BOSCH-REIG, F. 1998. Classification of Spanish unifloral honeys by discriminant analysis of electrical conductivity, color, water content, sugars, and pH. Journal of Agricultural and Food Chemistry, 46, 393-400.

MAY, P. M. & MURAY, K. 1991. JESS, a joint expert speciation system—II. The thermodynamic database. Talanta, 38, 1419-1426.

MAY, P. M. & MURRAY, K. 1991. JESS, a joint expert speciation system—I. Raison d'être. Talanta, 38, 1409-1417.

MAY, P. M. & MURRAY, K. 1993. JESS, a joint expert speciation system—III. Surrogate functions. Talanta, 40, 819-825.

MAY, P. M. & MURRAY, K. 2001. Database of chemical reactions designed to achieve thermodynamic consistency automatically. Journal of Chemical & Engineering Data, 46, 1035-1040.

MCCARTHY, T. S. 2011. The impact of acid mine drainage in South Africa. *South African Journal of Science,* 107**,** 01-07.

MCDONALD, J. C., COURSEY, B. M. & CARTER, M. 2007. Detecting illicit radioactive sources. *Physics Today*.

MCLEAN, C. 1994. The uranium industry of South Africa. *Journal of the South African Institute of Mining and Metallurgy,* 94**,** 113-122.

MILBRATH, B. D., PEURRUNG, A. J., BLISS, M. & WEBER, W. J. 2008. Radiation detector materials: An overview. *Journal of Materials Research,* 23**,** 2561-2581.

MOMČILOVIĆ, M., KOVAČEVIĆ, J. & DRAGOVIĆ, S. 2010. Population doses from terrestrial exposure in the vicinity of abandoned uranium mines in Serbia. *Radiation Measurements,* 45**,** 225-230.

MONDAL, S. & WICKRAMASINGHE, S. R. 2008. Produced water treatment by nanofiltration and reverse osmosis membranes. Journal of Membrane Science, 322, 162-170.

MOORE, W. S. & REID, D. F. 1973. Extraction of radium from natural waters using manganese-impregnated acrylic fibers. *Journal of Geophysical Research,* 78**,** 8880-8886.

MORRISSEY, C. 2003. Mining's malignant menace. *Review Magazine,* 68**,** 48.

MURPHY, R. J., LENHART, J. J. & HONEYMAN, B. D. 1999. The sorption of thorium (IV) and uranium (VI) to hematite in the presence of natural organic matter. *Colloids and Surfaces A: Physicochemical and Engineering Aspects,* 157**,** 47-62.

MURRAY, A., MARTEN, R., JOHNSTON, A. & MARTIN, P. 1987. Analysis for naturally occuring radionuclides at environmental concentrations by gamma spectrometry. Journal of Radioanalytical and Nuclear Chemistry, 115, 263-288.

MURRAY, K. & MAY, P. 2000. Joint expert speciation system. Jess Primer, Murdoch, Western Australia.

NAICKER, K., CUKROWSKA, E. & MCCARTHY, T. 2003. Acid mine drainage arising from gold mining activity in Johannesburg, South Africa and environs. *Environmental pollution,* 122**,** 29-40.

NING, R. Y. 2002. Arsenic removal by reverse osmosis. Desalination, 143, 237-241.

PENG, C. 1970. A review of methods of quench correction in liquid scintillation counting. Bransome, Jr., editor. Grune & Stratton, IInc., New York, 283.

PEPPAS, A., KOMNITSAS, K. & HALIKIA, I. 2000. Use of organic covers for acid mine drainage control. *Minerals Engineering,* 13**,** 563-574.

PERERA, S. 2005. Gross alpha/beta analyses in water by liquid scintillation counting. Journal of radioanalytical and nuclear chemistry, 264, 357-363.

PERIÁÑEZ, R. 2004. Testing the behaviour of different kinetic models for uptake/release of radionuclides between water and sediments when implemented in a marine dispersion model. Journal of environmental radioactivity, 71, 243-259.

PETERSEN, R. J. 1993. Composite reverse osmosis and nanofiltration membranes. Journal of membrane science, 83, 81-150.

PETERSON, S. 2015. Radiation Interactions & Detection.

PODGORŠAK, E. B. 2009. Interactions of Photons with Matter. Radiation Physics for Medical Physicists. Springer.

POVINEC, P., LA ROSA, J., LEE, S., MULSOW, S., OSVATH, I. & WYSE, E. 2001. Recent developments in radiometric and mass spectrometry methods for marine radioactivity measurements. Journal of Radioanalytical and Nuclear Chemistry, 248, 713-718.

PRINCE, J. R. 1979. Comments on equilibrium, transient equilibrium, and secular equilibrium in serial radioactive decay. *Journal of nuclear medicine: official publication, Society of Nuclear Medicine,* 20**,** 162.

PULLES, W., BANISTER, S. & VAN BILJON, M. 2005. The development of appropriate procedures towards and after closure of underground gold mines from a water management perspective. Water Research Commission Report.

ROBB, L. & ROBB, V. 1998. Gold in the Witwatersrand basin. *The mineral resources of South Africa: Handbook of the Council for Geoscience, South Africa,* 16**,** 294-317.

ROBB, V., ROBB, L., WILSON, M. & ANHAUSSER, C. 1998. Environmental impact of Witwatersrand gold mining. *Mineral Resources of South Africa (1998)*.

ROWLAND, D. & MAY, P. M. 2010. JESS, a Joint Expert Speciation System—V: Approaching thermodynamic property prediction for multicomponent concentrated aqueous electrolyte solutions. *Talanta,* 81**,** 149-155.

SALONEN, L. 2005. Alpha spillover depends on alpha energy: a new finding in alpha/beta liquid scintillation spectrometry. *LSC***,** 135-148.

SANTSCHI, P. H., MURRAY, J. W., BASKARAN, M., BENITEZ-NELSON, C. R., GUO, L., HUNG, C.-C., LAMBORG, C., MORAN, S. B., PASSOW, U. & ROY-BARMAN, M. 2006. Thorium speciation in seawater. *Marine Chemistry,* 100**,** 250-268.

SCHOLZE, F., HENNEKEN, H., KUSCHNERUS, P., RABUS, H., RICHTER, M. & ULM, G. 2000. Determination of the electron–hole pair creation energy for semiconductors from the spectral responsivity of photodiodes. *Nuclear Instruments and Methods in Physics Research Section A: Accelerators, Spectrometers, Detectors and Associated Equipment,* 439**,** 208-215.

SHAHAR, A., EL-HANANY, U., TSIGELMAN, A., KLIER, S. & HALBERTHAL, E. 2001. Semiconductor gamma-ray detector. Google Patents.

SHAMMAS, N. K. 2005. Coagulation and flocculation. Physicochemical treatment processes. Springer.

SICILIANO, E. R., ELY, J. H., KOUZES, R. T., MILBRATH, B. D., SCHWEPPE, J. E. & STROMSWOLD, D. C. 2005. Comparison of PVT and NaI (Tl) scintillators for vehicle portal monitor applications. *Nuclear Instruments and Methods in Physics Research Section A: Accelerators, Spectrometers, Detectors and Associated Equipment,* 550**,** 647-674.

STECHEMESSER, H. & DOBIÁŠ, B. 2005. Coagulation and flocculation, Taylor & Francis.

STOJKOVIĆ, I., TODOROVIĆ, N., NIKOLOV, J. & TENJOVIĆ, B. 2016. PSA discriminator influence on 222Rn efficiency detection in waters by liquid scintillation counting. *Applied Radiation and Isotopes,* 112**,** 80-88.

STUCKER, V., RANVILLE, J., NEWMAN, M., PEACOCK, A., CHO, J. & HATFIELD, K. 2011. Evaluation and application of anion exchange resins to measure groundwater uranium flux at a former uranium mill site. *water research,* 45**,** 4866-4876.

TAVENDALE, A. & EWAN, G. 1963. A high resolution lithium-drift germanium gamma-ray spectrometer. *Nuclear Instruments and Methods,* 25**,** 185-187.

TING, S. C. 1972. Interaction of Photons with Matter. Particles and Nuclei. Springer.

TIPPING, E., LOFTS, S. & LAWLOR, A. 1998. Modelling the chemical speciation of trace metals in the surface waters of the Humber system. Science of the Total Environment, 210, 63-77.

TODOROVIĆ, N., NIKOLOV, J., TENJOVIĆ, B., BIKIT, I. & VESKOVIC, M. 2012. Establishment of a method for measurement of gross alpha/beta activities in water from Vojvodina region. *Radiation Measurements,* 47**,** 1053-1059.

TUREKIAN, K. K. & WEDEPOHL, K. H. 1961. Distribution of the elements in some major units of the earth's crust. *Geological Society of America Bulletin,* 72**,** 175-192.

TURNER, J. E. 2007a. About atomic physics and radiation. *Atoms, Radiation, and Radiation Protection, Third Edition***,** 1-13.

TURNER, J. E. 2007b. Interaction of Photons with Matter. *Atoms, Radiation, and Radiation Protection.* Wiley-VCH Verlag GmbH & Co. KGaA.

TURTON, A. 2010. The politics of water and mining in South Africa. *The Politics of Water: A survey***,** 142-160.

TUTU, H., MCCARTHY, T. & CUKROWSKA, E. 2008. The chemical characteristics of acid mine drainage with particular reference to sources, distribution and remediation: The Witwatersrand Basin, South Africa as a case study. *Applied Geochemistry,* 23**,** 3666-3684.

TYKVA, R. & SABOL, J. 1995. *Low-level environmental radioactivity: sources and evaluation*, CRC Press.

VAN TONDER, D., COETZEE, H., STRACHAN, L., MAFANYA, T., WADE, P., MSEZANE, N., KWATA, M., ROOS, M., SEBAKE, D. & MENGISTU, H. 2008. Regional gold mining closure strategy for the Witwatersrand Basin (Report prepared for the Department of Minerals and Energy). *Sustainable Development through Mining Project Reports, Department of Minerals and Energy, Council for Geoscience Report*.

VARIS, O., BISWAS, A. K., TORTAJADA, C. & LUNDQVIST, J. 2006. Megacities and water management. Water Resources Development, 22, 377-394.

VENTER, I. 2001. South African mining sector facing radiation challenge. *Mining Weekly,* 7**,** 2-3.

WANG, X., NI, S. & SHI, Z. 2014. Uranium distribution in the sediment of the Mianyuan River near a phosphate mining region in China and the related uranium speciation in water. *Chemie der Erde-Geochemistry,* 74**,** 661-669.

WENDLE, G. 1998. Radioactivity in mines and mine water-sources and mechanisms. *Journal of the Southern African Institute of Mining and Metallurgy,* 98**,** 87-92.

WERDMÜLLER, V. 1986. The central rand. *Witwatersrand Gold—100 Years***,** 7-47.

WHO 2006. Guidelines for drinking-water quality [electronic resource]: incorporating first addendum. Vol. 1, Recommendations.

WILSON, M. & ANHAEUSSER, C. 1998. The mineral resources of South Africa(Handbook 16).

WINDE, F. & DE VILLIERS, A. B. 2002. The nature and extent of uranium contamination from tailings dams in the Witwatersrand gold mining area (South Africa). *Uranium in the aquatic environment.* Springer.

WINDE, F., WADE, P. & VAN DER WALT, I. J. 2004. Gold tailings as a source of water-borne uranium contamination of streams-the Koekemoerspruit (South

Africa) as a case study-part III of III: fluctuations of stream chemistry and their impacts on uranium mobility. *Water SA,* 30**,** 233-239.

WU, Y., WANG, Y. & XIE, X. 2014. Occurrence, behavior and distribution of high levels of uranium in shallow groundwater at Datong basin, northern China. *Science of the Total Environment,* 472**,** 809-817.

WYMER, D. 2001. Nuclear regulation of South African mines: an industry perspective. *Impact of new environmental and safety regulations on uranium exploration, mining, milling and management of its waste***,** 73.

YUNOKI, S. & SAITO, M. 2009. A simple method to determine bioethanol content in gasoline using two-step extraction and liquid scintillation counting. Bioresource technology, 100, 6125-6128.

Annexure 1. ^{238}U decay series

Nuclide	Half-life	Major Gamma Radiation Energies (MeV) and Intensities
^{238}U	4.5×10^{9} a	0.04955 (0.0648%)
↓ α		0.1135 (0.013%)
^{234}Th	24.1 d	0.0924 (16.2%)
↓ β		
^{234m}Pa	1.18 min	0.0435 (1.42%)
(99.86%) ↓ β		1.001 (0.856%)
^{234}U	2.38×10^{5} a	0.0532 (28.7%)
↓ α		
^{230}Th	7.52×10^{4} a	**0.068 (0.38%)**
↓ α		
^{226}Ra	1602 a	0.1862 (5.962%)
↓ α		
^{222}Rn	3.825 d	0.511 (0.078%)
↓ α		
^{218}Po	3.05 m	0.837 (0.0011%)
↓ α		
^{214}Pb	26.8 m	0.2952 (27.3%)
↓ β		0.3519 (46.96%)
^{214}Bi	19.7 m	0.609 (46.4%)
(99.98%) ↓ β		1.1203 (15.14%)
^{214}Po	164 μs	0.799 (0.0105%)
↓ α		
^{210}Pb	22,3 a	0.047 (80.2%)
↓ β		
^{210}Bi	5.02 d	0.305 (0.000084%)
↓ β		
^{210}Po	138.3 d	0.803 (0.00124%)
↓ α		
^{206}Pb	stable	

Annexure 2. ^{232}Th decay series

Nuclide	Half-life	Major Gamma Radiation Energies (MeV) and Intensities
^{232}Th	1.39×10^{10} a	0.064 (0.26%)
↓ α		
^{228}Ra	5.75 a	0.0264 (28%)
↓ β		
^{228}Ac	6.13 h	0.0578 (72.5%)
↓ β		0.338 (11.7%)
		0.911 (26.5%)
^{228}Th	1.913 a	0.0844 (26.4%)
↓ α		
^{224}Ra	3.64 d	0.241 (5.26%)
↓ α		
^{220}Rn	55.6 s	0.550 (0.118%)
↓ α		
^{216}Po	0.14 s	0.805 (0.0019%)
↓ α		
^{212}Pb	10.64 h	0.2386 (81.6%)
↓ β		0.3001 (4.66%)
^{212}Bi →(36%)	60.5 m	0.0399 (26.0%)
(64%) ↓ β		0.727 (6.74%)
↓ α	304 ns	No gamma
^{212}Po ↓		
^{208}Tl ↓ α	3.1 m	0.583 (86.7%)
↓ β		2.6145 (100%)
^{208}Pb ←	Stable	